# Dinosaur track assemblages from mid-Cretaceous of Fujian Province, southeastern China : ichnotaxonomic review and faunal comparison (#109629)

First revision

## Guidance from your Editor

Please submit by **6 May 2025** for the benefit of the authors .

**Structure and Criteria**
Please read the 'Structure and Criteria' page for guidance.

**Author notes**
Have you read the author notes on the guidance page?

**Raw data check**
Review the raw data.

**Image check**
Check that figures and images have not been inappropriately manipulated.

If this article is published your review will be made public. You can choose whether to sign your review. If uploading a PDF please remove any identifiable information (if you want to remain anonymous).

## Files
Download and review all files from the materials page.

1 Tracked changes manuscript(s)
1 Rebuttal letter(s)
22 Figure file(s)
8 Table file(s)
2 Raw data file(s)

# Structure and Criteria

## Structure your review

The review form is divided into 5 sections. Please consider these when composing your review:

1. **BASIC REPORTING**
2. **EXPERIMENTAL DESIGN**
3. **VALIDITY OF THE FINDINGS**
4. General comments
5. Confidential notes to the editor

📄 You can also annotate this PDF and upload it as part of your review

When ready submit online.

## Editorial Criteria

Use these criteria points to structure your review. The full detailed editorial criteria is on your guidance page.

**BASIC REPORTING**

- Clear, unambiguous, professional English language used throughout.
- Intro & background to show context. Literature well referenced & relevant.
- Structure conforms to PeerJ standards, discipline norm, or improved for clarity.
- Figures are relevant, high quality, well labelled & described.
- Raw data supplied (see PeerJ policy).

**EXPERIMENTAL DESIGN**

- Original primary research within Scope of the journal.
- Research question well defined, relevant & meaningful. It is stated how the research fills an identified knowledge gap.
- Rigorous investigation performed to a high technical & ethical standard.
- Methods described with sufficient detail & information to replicate.

**VALIDITY OF THE FINDINGS**

- **Impact and novelty is not assessed.** Meaningful replication encouraged where rationale & benefit to literature is clearly stated.
- All underlying data have been provided; they are robust, statistically sound, & controlled.

- Conclusions are well stated, linked to original research question & limited to supporting results.

# Standout reviewing tips

The best reviewers use these techniques

| **Tip** | *Example* |
| --- | --- |
| **Support criticisms with evidence from the text or from other sources** | *Smith et al (J of Methodology, 2005, V3, pp 123) have shown that the analysis you use in Lines 241-250 is not the most appropriate for this situation. Please explain why you used this method.* |
| **Give specific suggestions on how to improve the manuscript** | *Your introduction needs more detail. I suggest that you improve the description at lines 57- 86 to provide more justification for your study (specifically, you should expand upon the knowledge gap being filled).* |
| **Comment on language and grammar issues** | *The English language should be improved to ensure that an international audience can clearly understand your text. Some examples where the language could be improved include lines 23, 77, 121, 128 – the current phrasing makes comprehension difficult. I suggest you have a colleague who is proficient in English and familiar with the subject matter review your manuscript, or contact a professional editing service.* |
| **Organize by importance of the issues, and number your points** | *1. Your most important issue*<br>*2. The next most important item*<br>*3. ...*<br>*4. The least important points* |
| **Please provide constructive criticism, and avoid personal opinions** | *I thank you for providing the raw data, however your supplemental files need more descriptive metadata identifiers to be useful to future readers. Although your results are compelling, the data analysis should be improved in the following ways: AA, BB, CC* |
| **Comment on strengths (as well as weaknesses) of the manuscript** | *I commend the authors for their extensive data set, compiled over many years of detailed fieldwork. In addition, the manuscript is clearly written in professional, unambiguous language. If there is a weakness, it is in the statistical analysis (as I have noted above) which should be improved upon before Acceptance.* |

# Dinosaur track assemblages from mid-Cretaceous of Fujian Province, southeastern China : ichnotaxonomic review and faunal comparison

Lida Xing [Corresp., Equal first author, 1, 2] , Kecheng Niu [Equal first author, 3, 4] , Qiyan Chen [Corresp., 2] , Hendrik Klein [5] , Anthony Romilio [6] , Runsheng Chen [7] , Min Lin [7] , Ke Deng [7] , Jianrong Tang [7]

1 Frontiers Science Center for Deep-time Digital Earth, China University of Geoscience (Beijing), Beijing, China

2 School of the Earth Sciences and Resources, China University of Geoscience (Beijing), Beijing, China

3 State Key Laboratory of Cellular Stress Biology, School of Life Sciences, Xiamen University, Xiamen, Fujian, China

4 Yingliang Stone Natural History Museum, Nan'an, Fujian, China

5 Saurierwelt Paläontologisches Museum, Neumarkt, Bavaria, Germany

6 School of the Veterinary Science, University of Queensland, Gatton, Queensland, Australia

7 Fujian Institute of Geological Survey, Fuzhou, Fujian, China

Corresponding Authors: Lida Xing, Qiyan Chen
Email address: xinglida@gmail.com, qiyan_chen@163.com

Among the the mid-Cretaceous strata in China, considerable dinosaur record are preserved in the southeastern mountainous and arc-related basins. The Shanghang Basin is one of the sporadic red-stratified basins distributed in western Fujian, SE China, and has previously been discovered as the home of an ornithopod-dominaited ichnofauna, which is also characterized by the large troodontid ichnogenera Fujianipus. Include the newly discovered fossils, further confirming that this tracksite is dominated by ornithopods, characterized by a significant proportion (>27%) of large ornithopods, with deinonychosaurians as the possible apex predators. As the only extensive mid-Cretaceous dinosaur tracksite in southeastern China, Longxing offers a temporal comparison with skeletal records from Zhejiang, SE China and other fauna globally. The Longxiang herbivorous assemblage may suggesting limited faunal turnover by aligning more closely with pre-Cenomanian than the contemporaneous faunas in Zhejiang. Besides, unlike South American patterns associated with OAE2, the faunal shifts of SE China are relatively mild and appear more influenced by regional factors—topographic barriers and volcanic activities—rather than global climatic signal affected by marine conditions. Further research is needed to refine faunal chronology and assess the impact of regional environmental factors in shaping Cretaceous ecosystems of SE China.

1

# Dinosaur track assemblages from mid-Cretaceous of Fujian Province, southeastern China: ichnotaxonomic review and faunal comparison

5

6

7  Lida Xing[1, 2, *, #], Kecheng Niu[3, 4, #],  Qiyan Chen[2, *], Hendrik Klein[5], Anthony Romilio[6],
8  Runsheng Chen[7], Min Lin[7], Ke Deng[7], Jianrong Tang[7]

9

10  [1] Frontiers Science Center for Deep-time Digital Earth, China University of Geosciences
11  (Beijing), Beijing, China;
12  [2] School of the Earth Sciences and Resources, China University of Geosciences (Beijing),
13  Beijing, China;
14  [3] State Key Laboratory of Cellular Stress Biology, School of Life Sciences, Xiamen University,
15  Xiamen, China
16  [4] Yingliang Stone Natural History Museum, Nan'an, China
17  [5] Saurierwelt Paläontologisches Museum, Alte Richt 7, Neumarkt, Germany
18  [6] School of the Veterinary Science, The University of Queensland, Gatton, Queensland, 4343,
19  Australia
20  [7] Fujian Institute of Geological Survey, Fuzhou, China

21

22  #These authors contributed to the work equally and should be regarded as co-first authors.

23

24  Corresponding Author:
25  Lida Xing[2] and Qiyan Chen[2]
26  School of the Earth Sciences and Resources, China University of Geosciences (Beijing), Beijing,
27  100083, China
28  Email address: xinglida@gmail.com (L. Xing) and qiyan_chen@163.com (Q. Chen)

29

30

## Abstract

Among the the mid-Cretaceous strata in China, considerable dinosaur record are preserved in the southeastern mountainous and arc-related basins. The Shanghang Basin is one of the sporadic red-stratified basins distributed in western Fujian, SE China, and has previously been discovered as the home of an ornithopod-dominaited ichnofauna, which is also characterized by the large troodontid ichnogenera *Fujianipus*. Include the newly discovered fossils, further confirming that this tracksite is dominated by ornithopods, characterized by a significant proportion (>27%) of large ornithopods, with deinonychosaurians as the possible apex predators.

As the only extensive mid-Cretaceous dinosaur tracksite in southeastern China, Longxing offers a temporal comparison with skeletal records from Zhejiang, SE China and other fauna globally. The Longxiang herbivorous assemblage may suggesting limited faunal turnover by aligning more closely with pre-Cenomanian than the contemporaneous faunas in Zhejiang. Besides, unlike South American patterns associated with OAE2, the faunal shifts of SE China are relatively mild and appear more influenced by regional factors—topographic barriers and volcanic activities—rather than global climatic signal affected by marine conditions. Further research is needed to refine faunal chronology and assess the impact of regional environmental factors in shaping Cretaceous ecosystems of SE China.

## Introduction

Considerable dinosaur records, including fossil skeletons, eggs and tracks, are preserved in the Late Cretaceous reddish-dominated deposits in northeastern China, including Zhejiang, Jiangxi and Guangdong, especially in the Jinqu Basin of Zhejiang (Yu, 2013; Du et al., 2015), the Ganzhou Basin of Jiangxi (Lü et al., 2007, 2016; Xing et al., 2020) and the Nanxiong Basin of Guangdong (Xing et al., 2017, 2020). Among these provices, Fujian has now become one of the emerging hotspots for Mesozoic dinosaur evolutionary studies in recent years, especially which of the bird-line theropods, as the local geological surveys and the excavation of newly discovered fossil fauna continued (Xu et al., 2023; Xing et al., 2024a; Chen et al., 2025).

In November 2020, the Dinosaur Laboratory of China University of Geosciences, Beijing, in cooperation with the Yingliang Stone Natural History Museum, started to search for dinosaur fossils in the red beds of Fujian Province. The preliminary findings from the core area (upper and lower Longxiang site I, LXIU and LXID) and a few scattered specimens (Longxiang site II, LXII) of Kejiayuan Cultural Centre in Longxiang Village, Shanghang Basin is the first time that dinosaur tracks have been identified in Fujian Province (Fig. 1), and was described by Niu and Xing (2023). The largest known specimen of troodontid tracks by far, subsequently named *Fujianipus*, was also found during this fieldwork (Xing et al., 2024a). In January 2021, the lead author of this paper found a third footprint site adjacent to the core area (Longxiang site IN and III, LXIN and LXIII). In April of the same year, a detailed investigation of the site LXIN was carried out. Thereafter, in October 2022, an additional isolated slab was found in eastern Longxiang site I (LXIE) by Kecheng Niu.

This study focuses on describing the discovery of new specimens during fieldworks in 2021

71  and 2022. On this basis, this study will also synthesise the record of the entire Longxiang site
72  and compare its ichnofauna with other skeletal faunas from East and Northeast Asia of the same
73  period, focusing on similarities and differences between the faunas of the region, as well as the
74  possible impact of environmental and preservation differences on the occurrence of distinctive
75  members at the Longxiang site.
76
77  **Geological setting**
78  *The tectonic setting of Fujian Province in early Cretaceous*
79  Southeastern China is situated on the southeastern margin of the Eurasian Plate. During the Late
80  Jurassic to Early Cretaceous, intense volcanism occurred, leading to the formation of a widely
81  distributed, thick terrestrial volcanic-sedimentary rock system in the eastern part of the province
82  (Fig. 2). In the latest Early Cretaceous to Late Cretaceous, the intensity of volcanism decreased,
83  resulting in volcanic or nonvolcanic terrestrial red-bed arc-related basin deposits (Fig. 3; Li,
84  1997; Xi et al., 2019).
85    After the end of the subduction stage on the eastern side of the Cathaysia block in Cretaceous,
86  the tectonic stage in southeastern China shifted from a syn-orogenic shortening stage to a post-
87  orogenic stage (Li et al., 2014). This stage was mainly represented by NW-SE extension in the
88  late Valanginian to early Aptian. Subsequently, the collision of the South China continental crust
89  and the West Philippine Plate transformed the region into an isotropic compressional event in the
90  late Aptian to early Albian (Charvet, 1994; Li et al., 2014). During the compressional phase,
91  tectonic uplift induced by Minchenorogeny (Gu, 2005), the mountains included the area covered
92  by Paleo-Yunmengze Lake and the associated inland river system, i.e. most of Hubei, northern
93  and northwestern Hunan, and part of Henan and southwestern Jiangxi (Chen, 1979, Compilation
94  Committee of Geological Atlas of China, 2002; Wan et al., 2007). The high and wide
95  southeastern coast mountains made it difficult for the paleo-Pacific moisture flow to reach the
96  above regions, causing these areas to develop into tropical-subtropical hot plains, hills and desert
97  landscapes (Chen, 1979), where gypsum and halite were deposited (Wan et al., 2007). To the
98  east and south of this region are dominated by plains and hills belonging to Zhejiang, Fujian,
99  Jiangxi and Guangdong regions, where dinosaurs lived in these small and sporadic intermountain
100 arc-related basins (Chen, 2000; Li et al., 2013).
101   Since the Aptian, SE China began to gradually move out of the dry climate phase, however,
102 the mid- to Upper Cretaceous faulted, red basin composed of brick-red siltstone implies a long
103 warm (or hot)-wet climate phase thereafter (Wang et al., 2022), and also containing gypsum
104 layers, with conglomerates and sandy conglomerates at the base (Zhou, 2007).
105
106 *The of geological background of Longxiang site*
107 In the late Albian to Late Cretaceous, extensive layers of purplish-red beds were developed in
108 west-central Fujian, divided into the lower Shaxian Formation and the upper Chong'an
109 Formation (Li, 1997; Xi et al., 2019), and the latter is dominated by coarser-grained
110 conglomerates (Lü et al., 2019).

111  In western Fujian, there are about 36 red bed-dominated Cretaceous basins spatially
112  distributed in a northeast-trending belt in the west of the Zhenghe-Daipu Rift.The Shanghang
113  Basin is one of the small basins in southwestern Fujian Province, where the Cretaceous red beds
114  are a sequence of purplish-red coarse-fine clastic assemblages. The Shanghang Basin is
115  dominated by the Chishi Group (Junkou, Shaxian and Chong'an Formations), of which the
116  Shaxian Formation is the most widely distributed (Fujian Institute of Geological Survey, 2016).
117  The lithology of the Shaxian Formation consists mainly of purplish-red medium-thick bedded
118  calcareous, fine sandstone and muddy siltstone, interspersed with purplish-red sandstone, and
119  complex-composed conglomerate, while regionally interbedded with tuff, tuff lava, and marl,
120  which is composed of terrestrial red clastic rocks. In Shanghang Basin, the maximum thickness
121  of Shaxian Formation is about 1,913 m.
122  According to the 1:200,000 regional geological survey report of Shanghang Area (G-50-27),
123  the dinosaur tracks from Longxiang Village are preserved in the lower part of the Shaxian
124  Formation (Fig. 3-4).
125  At the Longxiang site, a continuous section is exposed which successively develops the
126  alluvial fan fringe deposits (layers 1-12), the braided river channel and point bar deposits (layers
127  13-17), the shore lake and shallow lake deposits (layers 18-34).  The lacustrine deposits in the
128  Longxiang site are mainly dominated by graywacke, fine sandstones and siltstones, interspersed
129  with thin layers of mudstones, with little gravel content. The grain size of the sediments is
130  generally only about 2 mm-10 mm, with a maximum of 2 cm. The dinosaur tracks are found near
131  the top of this section (layer 31), which is a medium-thin-bedded, light purple-red muddy
132  siltstone. The upper beds are darker, thinly bedded silty claystone.
133  The sediments in the adjacent area also include thin gypsum layers and calcareous clasts, with
134  local occurrences of Cu-bearing sandstones (Chen, 2008).
135  As with many Late Mesozoic terrestrial deposits in China, isotope chronology data for the
136  Shaxian Formation in the Shanghang Basin are limited due to frequent volcanic and tectonic
137  activity. Hu (1990) suggested that the depositional age of the Shaxian Formation in the red bed
138  of Shanghang is between 80 and 105 Ma, based on magnetic stratigraphy. The $^{206}Pb/^{238}U$ dates
139  of the Shaxian Formation in the Shanghang Basin vary from 87 to 101 Ma, with a weighted
140  average of $96.0 \pm 4.1$ Ma (Chen et al., 2020). Therefore, the Shaxian Formation in the
141  Shanghang Basin can be assigned to the latest Early Cretaceous to the early Late Cretaceous,
142  which lies roughly within the Albian to Coniacian, with a weighted average in the Cenomanian.
143  Based on palynology (Zheng and Li, 1986; Liang et al., 1992) and paleosoil evidence (Li et
144  al., 2009; Yin and Li, 2014), the Shaxian Formation is a riverine and lacustrine detrital deposit
145  that formed in an inland arc-related basin under a hot, dry and oxidizing environment (Li, 1997).
146  Based on the evidence of stratigraphic magnetic characterization, Lü et al (2019) suggested that
147  hematite in the red strata of the Shaxian Formation and Chong'an Formation is indicative of a
148  high-temperature climatic environment.
149
150  **Materials & Methods**

**Materials**

151

152    At least three dinosaur tracksites were discovered in Longxiang Village, which are numbered as

153    LXIs ( GPS: 25° 2'15.69"N, 116°23'58.29"E), LXII (GPS: 25° 2'38.20"N, 116°23'35.37"E) and

154    LXIII ( GPS: 25° 1'48.36"N, 116°24'32.25"E) (Fig. 1).

155    Site LXI is the main tracksite, divided into the upper (LXIU), lower (LXID) , northern (LXIN)

156    and eastern (LXIE) parts (Figs. 5-7), with a total area of approximately 1,600 $m^2$. These areas are

157    originally  from the same track surface. However, the connections between these regions were

158    severed during the excavation of the tracksite, and the faults created by the excavation leave

159    these regions with some differences in their current positions on the outcrop. There are currently

160    more than 700 tracks exposed on the site, including 79 trackways and more than 100 isolated

161    tracks (trackways see Table 1). Among the Longxiang tracks, 274 tracks in LXIU abd LXID has

162    been already reported in Niu and Xing (2023).

163    With the exception of the very large didactyl tracks, the vast majority of Longxiang footprints

164    can be confirmed not to be undertracks. Some footprints, especially the more complete tridactyl

165    tracks, show impressions of phalangeal pads or preserve traces left by sediment flow within the

166    tracks. Furthermore, the deformation between these tracks is mostly continuous and can be

167    correlated with one another. Some of these trackways even exhibit characteristics of penetrate

168    tracks, with digit traces significantly narrowing, accompanied by sediment bulging inward from

169    both sides of the footprint.

170    The LXIU site covers an area of about 320 $m^2$, with 17 trackways and eight relatively clear

171    isolated tracks, making a total of about 229 tracks (Fig. 5). Site LXID covers an area of about

172    170 $m^2$, with a large number of root trace, seven trackways and one relatively clear isolated

173    track, totalling about 81 tracks (Fig. 6). The LXIN tracksite covered an area of about 290 $m^2$,

174    with a large number of root trace, 54 trackways and 31 relatively clear isolated tracks, totaling

175    about 398 tracks (Fig. 7). The LXIE site only including one slab (YLSNHM07318), with one

176    trackway of two tracks. Site LXII is located approximately 950 m northwest of Site I and

177    preserves only three isolated tracks (Fig. 8). Site LXIII is located approximately 1250 m

178    southeast of Site I and preserves only six isolated tracks (Fig. 8). The vast majority of the tracks

179    at these sites are relatively well preserved, with only a small number (<10%) preserved in the

180    form of scattered, structurally ambiguous shallow pits. The tracks in very poor preservation

181    condition are not considered in this paper.

182    YLSNHM07318 was found at the site of the landslide on the east side of the previously

183    described Longxiang tracksite (25° 2'13.76"N 116°24'2.70"E), with light purple-red silty

184    claystone. In the early rainy season, the mountain slid down the slope and formed some

185    fragmented rock specimens with preserved dinosaur tracks. This slab is now preserved in

186    Yingliang Stone Natural History Museum, Nan'an, China..

187

**Methods**

188

189    All the exposed footprints were photographed, outlined with chalk, and traced on large sheets of

190    transparent plastics. In addition, a representative area of well-preserved tracks was mapped

191  manually using a simple chalk grid. Latex molds of representative tracks were made. Detailed
192  tracings of selected tracks were made on transparent acetate film. Latex molds, plaster replicas,
193  and most tracings were reposited at China University of Geosciences, Beijing.
194  The entire exposed surface was photographically recorded using a remote controlled four axis
195  quadcopter (DJI Inspire 1: weight: 3400 g; max service ceiling above sea level: 4500 m; max
196  flight time: 15 min; max wind speed resistance: 10 m/s and with DJI GO App, iOS 8.0 or later)
197  with a 12 mega–pixel camera (model X5, with a 15 mm lens). After taking off from the ground,
198  the DJI Inspire 1 was controlled by remote and it provide real–time HD video through a mobile
199  APP (DJI GO version 3.1.23).
200  Digital 3D models were created of the *in situ* track-bearing surface following photogrammetry
201  methods outlined by Romilio (2020). Digital photographs were taken from multiple viewpoints
202  of the in situ tracks with an Apple iPhone XS Max (focal length 4.25 mm). Virtual 3D models
203  were created following the step-by-step process outlined by Romilio (2020), which included
204  adding photographs to Agisoft Metashape Professional (v.1.6.3), repositioning and centering
205  models using Meshlab (Cignoni et al., 2008), and visualising the surface topography using
206  Paraview (v. 2020.06; Ahrens et al. 2005) and CloudCompare (v. 2.10.2;
207  http://www.cloudcompare.org/) filters.
208  Maximum Length, maximum width, pace length, stride length, pace angulation and rotation of
209  tracks were measured according to the standard procedures of Leonardi (1987) and Lockley and
210  Hunt (1995). For the trackways of quadrupeds, gauge (trackway width) was quantified for pes
211  and manus tracks using the ratio WAP/P'ML (Marty et al., 2010). The distance between the pes
212  and manus imprints was measured from the proximal margin of the manus to the distal margin of
213  the pes following the method of Xing et al. (2014a). Hip heights and speed estimations of the
214  theropod, sauropod and ornithopods trackmakers were derived from the trackways following the
215  methods of Alexander (1976), Thulborn (1990), and González Riga (2011) respectively (see
216  below).
217
218  **Abbreviations of measurements:** L, Track Length; W, Track width; PL, pace length; L/W,
219  length/width ratio; II-III, the divarication angle between digit II and III; III-IV, the divarication
220  angle between digit III and IV; II-IV, the divarication angle between digit II and IV; PL, pace
221  length; SL, stride length; PA, pace angulation; R, rotation of tracks (outward rotation as positive);
222  H, Heteropody (=the ratio of the manus/pes track area); P'ML, the distance between the paired
223  pes and manus track; WAP, width of angulation pattern (=Gauge width); WAP/P'ML, the ratio
224  of WAP and P'ML.
225
226  ## Results
227  ### Sauropod tracks
228  *Description*
229  The sauropods trackways at the Longxiang tracksite are mainly distributed in the site LXIU and
230  LXIN (Fig. 5, 7, 9-10; Table 2).

231    The site LXIU contains medium-large sized sauropod trackway, with a specimen number of
232    LXIU-S1, containing 48 tracks in 24 pairs of manus-pes sets (Fig. 5, 9). LXIU-S1 is medium-
233    large in size, with a preservation of 0-1 from Belvedere and Farlow (2016), with distinguishable
234    manus and pes tracks retaining only general outlines. Due to the tight spacing between the manus
235    and pes of LXIU-S1, it is more difficult to accurately recognise the boundaries between the two,
236    so only the general morphology of the two was taken into account when making regular
237    measurements. Their total length was 55.4 cm and the width was 33.2 cm for an elliptical
238    impression, with an L/W ratio of 1.7. Judging from some of the tracks with a relatively clear
239    separation between the manus and pes tracks, the pes tracks averaged 40.8 cm in length, ~74% of
240    the total length, and 33.2 cm in width, with an L/W ratio of 1.2; the manus tracks averaged 16.6
241    cm in length and 25.9 cm in width, with an L/W ratio of 0.7.
242    Once the hindlimb of the trackmaker has left the substrate, the previously deformed sediment
243    undergoes reflux to varying degrees, contingent on the dissimilarities in the nature of the local
244    substrate and the forces exerted on the ground during travel. The relatively elongated pes track
245    (e.g., S1-LP2, RP13) may have originated from the closer proximity of its centroid to that of the
246    relevant manus, or from the deeper depth at which the trackmaker stepped into the sediment. In
247    the adjacent deformations, the deformed sediment undergoes gradual recovery at varying
248    velocities in response to both flow and pressure gradients. In instances where the ridge of
249    sediment separating the two is not sufficiently stable, the lesser deformation will tend to be filled
250    in first in order to reduce the surface energy of the entire depression (Cross and Hohenberg,
251    1993; Israelachvili, 2011). In other words, the partially capped manus track undergoes further
252    shrinkage and shallowing during the restoration of deformation. The degree of shrinkage may be
253    related to the level of overlapping of the manus-pes tracks and the initial depth of the pes.
254    Almost all of the manus tracks of LXIU-S1 lie anterior to the pes, partially overlapped by the
255    pes track but not very likely affected by the deformation rim. Taking the best-preserved
256    examples, S1-LP8/RM8 and S1-RP10/RM10 (Fig. 10C), the manus prints are oval-shaped and
257    the marks of the digit II−IV and metacarpophalangeal regions are indistinct. Digit I and V are
258    observable, but without detailed morphology. The pes tracks are oval-shaped, and the digits I-IV
259    are indistinct, with the smoothly curved metatarsophalangeal region. The rounded to rectangular-
260    shaped heel pads are not well-preserved but rather distinctive in most pes tracks, especially in
261    RP5, RP8, LP9 and RP13 (Fig. 9), and some of which are proximally elongated (e.g. RP8) and
262    related to form a V-shaped posterior rim. The manus and pes impressions are rotated
263    approximately 27° and 26° outwards from the trackway axis. The mean pace angulation of the
264    pes is 127°.
265    Similar to the variation in the footprint outline, poor preservation also results in a large
266    variation in the size of the manus and pes tracks in trackway S1. The heteropody (ratio of manus
267    to pes size) ranges from 1.6 to 13.3, with a mean of 4.4, a median of 3.0, and only 21% reaches
268    5. The range of width of S1 pes tracks reaches 62.2% of the width of the smallest (S1-RP5).
269    Additionally, an isolated left pes track, designated LXIU-SI1, is present on the northernmost
270    side of the LXIU site (Fig. 10C). This sauropod track is located on the periphery of the LXIU site

271  and exhibits superior preservation in comparison to trackway S1 at the same site (level 2 in
272  Belvedere and Farlow, 2016). The LXIU-SI1 is slightly larger than the mean value of the pes
273  track in LXIU-S1, measuring 50.1 cm in length and 38.0 cm in width. In comparison to the
274  tracks in LXIU-S1, LXIU-SI1 did not retain the associated manus track. However, it did retain
275  four more discernible digit traces (I-IV) and a possible rounded, faint digit V trace adjacent to
276  the digit IV posteriorly. The widths of the digit II to digit IV are comparable, but the
277  anteroposterior width of the digit I is comparable to that of the remaining three visible digits, that
278  may link to a highly  twisted position of digit I (including the pes ungual I) during travelling.
279     Site LXIN also contains a medium to large-sized sauropod trackway, LXIN-S1(Fig. 10A). It
280  contains 16 tracks with seven manus-pes sets and two separate pes tracks. The preservation
281  status of the tracks is level 1 on the Belvedere and Farlow (2016) scale. The manus and pes
282  tracks of LXIN-S1 were very loosely combined, with the pes tracks averaging 65.3 cm in length
283  and 51.2 cm in width, and an L/W ratio of 1.3; the manus tracks averaging 36.6 cm in length and
284  48.8 cm in width, and an L/W ratio of 0.8. Almost all the manus tracks in site LXIN are
285  subrounded or horseshoe-shaped, and anteromedial to the pes along the trackway orientation. In
286  the best preserved examples S1-RP2 and RM2, the manus impressions are oval and the knots
287  made by the digits I, II, IV and V are somewhat visible but not clearly defined (Fig. 10B). The
288  metacarpophalangeal regions are distinct. The pes prints are oval and the digits I-IV are
289  indistinct. Both the anterior rim of  metatarsophalangeal and heel region is smoothly curved, in
290  which the latter may suggest  a kidney-shaped pad. RM3 has a well-developed digit V. RP3,
291  corresponding to RM3, has distinct digits I and II. These features are not seen in the other manus
292  impressions, probably because the substrate in this region are wetter and softer, leaving the
293  tracks with more detail. The manus and pes impressions are rotated approximately 61° and 43°
294  outwardly. The pace angulation of the pes is 108°.
295     Almost all LXIN-S1 tracks had distinct outer sediment rims. Including these rims, the length
296  of the pes track is approximately 80.1 cm with an L/W ratio of 1.2, and the length of the manus
297  track is 59.7 cm in length with an L/W ratio of 0.9. The area of the track, including the rims, can
298  be up to 1.5 to 2 times the original area for pes and 2 to 2.5 times the original area for manus.
299  The heteropody is 1.8, reduced to 1.5 if the rims are included.
300     Site LXIII preserves an isolated sauropod pes track LXIII-SI1(Fig. 10D). SI1 is surrounded by
301  very distinct sediment displacement rims. The pes prints are oval, with a length of 34.6 cm and
302  an L/W ratio of 1.1. The marks of digits I-IV are indistinct and the metatarsophalangeal region is
303  smoothly curved. Unlike other sauropod pes tracks in the Longxiang area, the heel of SI1 is quite
304  narrow, with a width of about 1/2 of the digit region. In the absence of other related tracks, it is
305  not possible to determine whether this character is a stable morphological feature or an
306  ectomorphic variation.
307  ***Comparison***
308  Considering both footprint morphology and trackway configurations, both quadruped trackways
309  LXIU-S1 and LXIN-S1are typical of sauropods affinity (Lockley and Hunt, 1995).
310     The diagnostic features of quadruped ichnotaxa usually include the footprint morphology (the

311  number, size, shape and distribution of claw, digit and metatarophalangeal/heel pad), manus-pes
312  set (the distance, relative size and position of manus and pes print), and trackway parameters
313  (stride, footprint rotation and gauge). Track size (length and width) would be taken into account.
314  However, given that sauropod track morphology is distinct from theropod and ornithopod tracks
315  and does not show other variations that correlate with their body size, this parameter, while
316  included in the diagnosis, is not necessarily considered when categorizing by morphology. For
317  sauropod tracks are often only preserved as pits that lack sufficient footprint morphology, the
318  heteropody (size discrepancy between manus and pes print/heteropody) and gauge are the most
319  commonly used as distinguishing features the diagnostic features of sauropod tracks, and the
320  claw trace (number, orientation) are often taken into consider when preserved.
321      The preservation of  both LXIU-S1and LXIN-S1are somewhat limited in the footprint
322  morphology (Figs. 9, 10), especially the former with overlapped manus and pes that is
323  challenging to obtain a independent heteropody. However, subject to the above conditions, the
324  heteropody is relatively stable for both trackways: which of LXIU-S1 falling between 1:2 and
325  1:3. This is slightly lower than the 1:1.8 observed in LXIN-S1, and the overlap may causes
326  higher ratio for the former. Both LXIU-S1 and LXIN-S1 tracks are characterised by distinct
327  outward rotation.
328      The heteropody of both LXIU-S1and LXIN-S1 are lower than the Cretaceous *Brontopodus*, *B.*
329  *birdi* (>1:3; Farlow, 1989) and *B. changlingensis*(~1:2.5; Lockley et al., 2002), and more similar
330  to Jurassic *B. plagnensis* (1:1.86; Mazin et al., 2017) with well-separated manus-pes sets. For
331  other *Brontopodus*-type ichnotaxa with wide gauge and similar outline, heteropody is generally
332  higher than 2, that holotype of *Gyeongsangsauropus* ( "Brontopodus" *pentadactylus*) and
333  *Parvieouspodus* ( "Brontopodus" isp.) from Cretaceous East Asia reach ~1:2 and ~1:3.5
334  respetively (Xing et al., 2024b). The heteropody of previously named *Brontopodus*-type regional
335  ichnotaxa, mid-Cretaceous "Sauropodichnus" from South America (Calvo and Mazzetta, 2004)
336  and "Rotundichnus" from lower Cretaceous of Germany (Hendricks, 1981) are also estimated to
337  be higher than 1: 2.
338      The Jurassic *Parabrontopodus* defined in Laurasia (*P. mcintochi* and *P.* ("Elephantopoides")
339  *barkhausensis*), with which *Brontopodus* is often compared in gauge width, has a generally
340  smaller manus (>1:5 and 1: 3.2; Lockley et al., 1994; Meyer et al., 2021a),  It is clear from the
341  3D depth maps of *P. barkhausensis* (Meyer et al., 2021a) that at least some of the axial flattening
342  of the manus that occurs in its type series is related to pes-induced substrate deformation.
343      For the most refered series of other highly regional sauropod ichnotaxa that vary in gauge,
344  including Jurassic *Breviparopus* from Morroco (1:2.4; Marty et al., 2010) , *Galinhapodus*
345  ("Polyonyx") from Protugal (1:2; Santos et al., 2009, 2024); Jurassic-Cretaceous *Iniestapodus*
346  from Spain ("Polyonyx" assosiated; ~1:2.5; Torcida Fernández-Baldor et al., 2021); Cretaceous
347  *Oobardjidama* from Australia (1: 2.9; Salisbury et al., 2016); *Teratopodus* and *Titanopodus* from
348  different basins of Argentina (1:2.3 and 1:3.1; Gonzalez Riga and Calvo et al., 2009;  Tomaselli
349  et al., 2021), their manus-pes sets are all loosely compacted and have a statistically stable
350  heteropody between 2 and ~3. Of these, *Titanopodus* has a relatively high heteropody ( Gonzalez

351   Riga and Calvo et al., 2009), but this is not the only feature that distinguishes it from most
352   sauropod ichnotaxa. As can be seen from the faint digit trace inside its manus print, its manus
353   track and pes are very far apart, but still subject to compression from the posteromedial direction,
354   resulting in a difference in the degree of deformation in the mediolateral direction in addition to
355   the axial deformation.
356       Only Jurassic *Occitanopodus* from France has *P. mcintochi*-like higher heteropody that can be
357   linked to the distinctly packed manus-pes set (1:4 to 1:6; Moreau et al., 2019), and Cretaceous
358   *Calorckosauripus* from Bolivia that can be compared to *B. plagnensis* in slightly lower
359   heteropody and *B. changlingensis* in axially shortened pes track (1:1.85?; Meyer et al., 2018,
360   2021a). *Titanosaurimanus* from Cretaceous of Croatia (Dalla Vecchia, 2000) and *P. frenki*
361   defined in Chile (Moreno and Benton, 2005), on the other hand, lack sufficient records of manus-
362   pes set.
363       Besides, for the ratio of the WAP/length of the pes (P'ML), a value of 1.0 separates narrow-
364   gauge from medium-gauge trackways, whereas the value 1.2 is arbitrarily fixed to distinguish
365   between medium-gauge and wide gauge trackways (Marty, 2008). Therefore, LXIU-S1 and
366   LXIN-S1 can be catagorized as medium-gauge trackways for their WAP/P'ML are both ~1.0
367   (Table. 2).
368       The outline of both LXIN-S1 fits the *Brontopodus-type* tracks, especially LXIN-S1 is similar
369   to *Gyeongsangsauropus pentadactylus* occur in Cretaceous of East Asia (Kim and Lockley,
370   2012). And the loosely compacted LXIN-S1 manus-pes set can be compared to *B. plagnensis*
371   and *Calorckosauripus* in heteropody and the absence of any claw trace, while the size,
372   recognisable axial elongation (L/W>1), and the degree of outward rotation of pes track is more
373   comparable to morphotype E described in Meyer et al. (2021b).
374       The LXIU-S1 with highly compacted manus-pes set and the more distinctive outward rotation
375   may be more comparable to *Parabrontopodus*-type (Lockley et al., 1994; Moreno and Benton,
376   2005), while the relative width of manus (i.e. potential size of manus) may wider than the former.
377   However, as the compactness of manus-pes set is somewhat associated with the relative speed of
378   trackmaker (Lallensack et al., 2022), we suggest to assign LXIN-S1 with more valid features to
379   the *Brontopodus* -type trackway (or *cf. Gyeongsangsauropus* considering the track size and the
380   similar Albian-Cenomanian age), and LXIU-S1 to an unclassified sauropod track or *cf.*
381   *Brontopodus* comparing to the regional ichnofauna.

382   ***The implication of sauropod ichnotaxonomy***
383   It seems clear from the currently named (or formerly named), well-preserved sauropod ichnotaxa
384   that, given the relative consistency of manus/pes track depth (Table 3), the heteropody in these
385   records more readily reflects the original manus/pes size relationships. As a result, the valid
386   intervals for this character should be confined to a very limited range. Given the extent to which
387   heteropody can reflect differences in support function between manus and pes (Strickson, 2020),
388   this phenomenon may indicate that in the later stages of sauropod divergence, in contrast to the
389   differences brought about by gait (or speed) (Lallensack et al., 2018), differences in the role
390   played by manus and pes in supporting body weight are likely to be relatively small in terms of

391    sauropod morphology (including phylogeny, individual differences and ontogeny). This

392    hypothesis needs to be further explored in a comprehensive comparative study of well-preserved

393    material with low heteropody trackways found to date.

394      Also, the question of whether large angles or significant rotation of manus prints is a valid

395    diagnostic feature needs to be treated with caution, as there are quite a few factors that influence

396    this feature. Lallensack et al. (2018) analyzed sauropod trackways from the global record and

397    found that strong lateral or postero-lateral rotation (supination) of the manus is restricted to

398    trackways of small- and medium-sized individuals (pedal impression length <60 cm), this feature

399    is also correlated with low speed and narrow gauge. Lallensack et al. (2018) also conclude that

400    pronation occurs when the forelimb is actively contributing to the progression, at higher speed or

401    when performing a wider gauge with the center of mass (COM) shifted anteriorly. There may

402    also be relationships between the rotation of the pes and manus in trackways (Xing et al., 2021a).

403      Morover, most sauropod trackways in China are wide- (or medium-) gauge and have been

404    therefore, referred to the ichnogenus *Brontopodus* form lower Cretaceous of Corolado, USA

405    (Farlow, 1989; Lockley et al., 2002), as the palaeofauna and ichnofauna are both considered to

406    be comparable between East Asia and North America during Cretaceous (Matsukawa et al., 2006;

407    Lockley et al., 2014a), rather than a strict correspondence on dianogistic features from different

408    perspectives.

409      Not only in Asia and North America, however, but also in other regions, a similar

410    ichnotaxonomy focusing on the similarity of members of regional faunas (especially skeletal

411    faunas) is used, rather than one dominated by track/trackway morphology. As in South America,

412    one of the centres of sauropod evolution in the Cretaceous, the relative number of ichnotaxa

413    there currently corresponds to the diversity of the sauropod skeletal record (Riga et al., 2015;

414    Tomaselli et al., 2021, 2022; Pol et al., 2022; Carvalho and Leonardi, 2024). It should be noted,

415    however, that not only are there few sauropod records in the region that can be taxonomically

416    classified (Tomaselli et al., 2021), but also those specimens that are theoretically classifiable and

417    were considered to have a distinguishable feature at the time of their discovery, including

418    *Calorckosauripus*, *Titanosaurimanus*, *Titanopodus*, *Teratopodus* and 'Sauropodichnus', all of

419    which are or were once considered valid holotypes of ichnogenera, with the range of

420    comparisons essentially limited to specific basins based on potential maker differences or

421    occurring only in specific tracksites.

422      This is not only due to contrast difficulties associated with differences in preservation

423    (Marchetti et al., 2019), but is also related to the functional limitation of sauropod autopods to

424    weight bearing (Hutchinson, 2021). In contrast, the current diagnostic features used in sauropod

425    tracks are more similar to those of theropods and ornithischians, with an additional emphasis on

426    gauge only in the trackway parameters (see the discussion above). The differences in foot

427    function between the latter two and sauropods are more pronounced. Therefore, it seems

428    appropriate for future studies to incorporate more 3D data and to include additional qualitative

429    characteristics for plantar details other than digits that are statistically different between regions

430    or between epochs within the same region. For example, heel morphology, which was mentioned

431    in Farlow (1989) and has been the focus of some of the subsequent studies (e.g. sauropod
432    morphotypes in Salisbury et al. (2016)), or other features that may be related to weight bearing
433    modality/COM.

### Speed Estimation

435    For sauropods, Alexander (1976) first suggested that hip height be estimated as h=4 × foot
436    length, whereas, later, Thulborn (1990) estimated hip height as h=5.9 × foot length. González
437    Riga (2011) estimated hip height as h=4.586 × foot length. Relative stride length (SL/h) may be
438    used to determine whether an animal was walking (SL/h ≤ 2.0), trotting (2 < SL/h < 2.9), or
439    running (SL/h ≥ 2.9) (Alexander, 1976; Thulborn, 1990). Based on the formula of Thulborn and
440    González Riga, the SL/h ratios of the LXIU-S1 and LXIN-S1 sauropod trackway are between
441    0.67–0.87, 0.49–0.63, and accordingly suggest walking. Using the equation to estimate speed
442    from trackways (Alexander, 1976), the locomotion speed of the trackmaker of LXIU-S1 is
443    between 2.27–3.02 km/h, LXIN-S1 is estimated as 1.66–2.23 km/h, and are consistent with most
444    Chinese *Brontopodus*-type trackways (Xing et al., 2016; Xing and Lockley, 2016), for which
445    speed estimates are always low.
446        It is notable that the relative stride length values of LXIU-S1 are highly consistent with those
447    of BTY-S1 from the Tuchengzi Formation (across the J-K boundary) in western Liaoning (Xing
448    et al., 2021b). In other words, the LXIU-S1 and LXIN-S1 specimens demonstrate that the
449    outward rotation of the manus and pes tracks, as well as the degree of MPL, can exhibit notable
450    differences in the gait during low-velocity movements.

### Trackmaker and the analogy of sauropod quadruped gaits

452    The gleno-acetabular distance (GAD) has been proposed as an independent trackway parameter
453    for estimating the body size of the sauropod trackmaker (trunk length) by Lallensack et al.
454    (2018). This method is adapted for estimating trunk length when the trackmaker is in a stable
455    gait (limb phase) (Lallensack et al., 2022). Ideally, GAD may not be influenced by the limb
456    lengths in the direction of trackway orientation when the gait is known. Furthermore, the actual
457    gait of sauropods has been re-evaluated in order to determine which pair of manus and pes tracks
458    should be selected for GAD measurement (Lallensack and Falkingham, 2022; Stevens et al.,
459    2022).
460        Based on the above study, we selected only the limb phase of 25% and 50% as two plausible
461    gait end members to measure the GAD of the sauropod trackway at sites LXIU and LXIN.
462    Among them, LXIU-S1 has adjacent manus and pes tracks, with strong reduction of the manus
463    track by deformation. Therefore, for LXIU-S1, we only use the more clearly-delimited segment
464    from LXIU-S1-RP9/RM9 to LP13/LM13 in the southwest for estimation. Since the pes tracks of
465    LXIU-S1 cover the correlative manus track, the measured value of this trackway is theoretically
466    smaller than the actual value. It should also be noted that in LXIU-S1 there is a marked change
467    in orientation between RP11 and LP11, so in this case we used two measurement methods for the
468    25% limb phase of LXIU-S1: 1) using RP11 as the boundary, dividing LXIU-S1 into two
469    segments and considering the orientation in each part of the trackway as constant; 2) using the
470    four adjacent manus-pes sets as a cluster to define the orientation of the posterior stride.

471     For LXIU-S1, the interval of its GAD was 1–1.63 m. When estimating the midline of the track
472 using the different methods, the mean of the maximum estimates were all about 1.53 m (limb
473 phase=25%), with a variance of about 0.0080, and the mean of the minimum estimates were all
474 about 1.09 m (limb phase=50%), with a variance of about 0.0035. For the LXIN-S1 trackmaker,
475 the GAD interval was 1.75-3.19 m. The mean of the maximum value was 3.14 m with a variance
476 of about 0.0078- 0.0080, and the mean of the minimum value was 1.83 m with a variance of
477 about 0.0060. The greater variance in the LXIN-S1 data is due to: 1) apparent turning point; 2)
478 increased stride length (RP12/LP13).

479     The wide/medium gauge of the *Brontopodus*/*Gyeongsangsauropus*-type trackways, especially
480 the wide gauged trackways, are commonly attributed to titanosaurian sauropods by their
481 compulsive abducent femur posture (Wilson and Carrano, 1999; Lockley et al., 2002; Henderson,
482 2006; Mannion and Upchurch, 2010). This posture is co-occurred with the ante-displacement
483 with the COM (Henderson, 2006), and is hypothesised to be the consequence of adaptation to
484 gigantism, as opposed to being merely phylogenetic-related in Macronaria (Blazquez et al., 2024
485 (preprint)). Furthermore, the discovery of early medium-sized wide-gauge trackways in the
486 Lower-Middle Jurassic can be attributed to the basal Eusauropoda (Xing and Lockley, 2016).
487 However, it is also probable that these trackways could be the consequence of intense
488 orientation-turning in their path (medium-gauge instead).

489     Both Lallensack and Falkingham (2022) and Stevens et al. (2022) demonstrate a tendency for
490 sauropods to utilise a symmetrical, diagonal-supported walking gait. The diagonal-supporting
491 gait is similar to the wide-gauge, classically hypothesised to be correlated with demand for
492 stability maintaining of gigantic trackmakers (Henderson, 2006).

493     The hippopotamus is the most typical of the extant mammals that can use a torting gait
494 (Hildebrand, 1989). They differ from other extant large-sized quadrupeds, and is the only known
495 compulsory diagonal-supporting quadruped (e.g. elephants and giraffes; see Fig. 1 in Lallensack
496 and Falkingham, 2022). With the exception of hippopotamus, rather than graviportal elephants,
497 which are more commonly analogised with sauropods, rhinoceros are also capable of utilising
498 this gait at low-speed running (Henderson, 2006; Hutchinson, 2021; Lallensack and Falkingham,
499 2022). The body size, body mass and total track area of rhinoceroses are comparable to that of
500 hippopotamuses (the track size estimation is from Van den Heever et al., 2024), yet the overall
501 gait performance differs markedly (Hutchinson, 2021).

502     We hypothesise that this extreme obligate gait in hippopotamus terrestrial locomotion is likely
503 to be related to its significantly shorter limbs relative to body mass (or possibly trunk length), in
504 addition to the gravitational constraints it faces in common with other giant mammals
505 (Hutchinson, 2021). First, the sub-ellipsoidal, elongated trunk is associated with the presence of
506 its amphibius-adapted habit, with a specialisation logic approximating Sauropterygia (Endo et al,
507 2019; Gutarra et al., 2023). For hippopotamus and rhinoceros, which have similar other body
508 parameters, the proportion of trunk length relative to the legs clearly distinguishes the two, and
509 this particular proportion for hippopotamus is also rare in the full range of extant large-sized
510 terrestrial quadrupeds (Christiansen, 1999). Second, given that modern giant mammals all use a

511  narrow-gauge, the simultaneous usage of a diagonal-supporting gait during walking may limit
512  the location of the pes drop point in the presence of a large limb length. To illustrate, narrow-
513  gauged trackways for extant mammal trackmakers have been observed to avoid collisions
514  between the front and hind limbs during walking. This has led to the hypothesis that terrestrial
515  mammal trackmakers with longer hindlimbs are more likely to choose a lateral-supporting gait to
516  ensure walking efficiency. However, the need to maintain trunk stability is not as pronounced in
517  extant mammalian clades (Vermeij, 2016), as it is not as extreme as in the case of titanosaurian
518  sauropods, which have undergone a extreme process of gigantism (the phylogenetic relationship
519  of paraceratheriids to extant rhinoceros see Bai et al., 2020).
520      It can be reasonably deduced that the underlying causes of the disparate trotting gaits observed
521  in sauropods and certain other gigantic mammals are likely to be inconsistent. Sauropods exhibit
522  a distinctive array of intra-clade body plan variations with regard to their mechanical locomotion,
523  when compared to the extant gigantic mammals. For example, large mammals exhibit
524  considerable variation in their relative trunk length (GAD-associated) in comparison to limb
525  length (Hutchinson, 2021), as previously discussed. Conversely, the typical sauropod
526  trackmakers display a notable discrepancy in the relative length of their forelimb and hindlimb
527  along with the antedisplacement of COM (e.g. see the reconstructions of macronarian
528  brachiosaurus and diplodocoids Diplodocus by Henderson, 2006). It is similarly conceivable that
529  these factors facilitated the advent of the hypothetical specialised gaits utilised by the makers of
530  wide-gauged trackways via the disparate COM and hindlimb postural adaptations. However, this
531  hypothesis requires further investigation in the future. However, since the estimation of GAD
532  trunk size is independent of the functional reasons for the generation of torting gait, it does not
533  affect the possibility of using the aforementioned approach to constrain the trackmaker's trunk
534  size.
535      Besides, handful of questionable trackways made by large Paleocene-Eocene mammals shows
536  similar  wide-gauge as sauropods' (e.g., Henderson, 2015; Wroblewski and Gulas-Wroblewski,
537  2021). Wroblewski and Gulas-Wroblewski (2021) argue that some wide-gauge mammal
538  trackways are possible parallel pairs of narrow-gauge ones. However, the relative size of their
539  tracks suggests that the body width of their makers was probably wider than the width of the
540  inner part of their trackways, and also that if they are treated as parallel trackways, their gait
541  angulation does not seem to match the non-cursorial morphology of their trackmaker's autopods.
542  Therefore, we suggest that the wide-gauged trackways of early mammals should be further
543  considered together with sauropods.
544
545  **Tridactyl tracks**
546  The tridactyl tracks at Longxiang Sites are distributed in the three main layers of LXI and LXIII
547  (Figs. 5–9), and can be divided into three different forms. Given that the diagnostic feature of
548  many isolated tracks are not sufficient for classification (e.g. LXIN-TI17 to TI23), only the best
549  preserved tracks were selected for discussion, and the undiscribed tracks can be found in the
550  distribution map.

551

### *Grallatorid morphotype*

552

*Grallator* was originally defined in the Lower Jurassic, and used in a narrow sense for describing a type of small, slender tridactyl biped with possible early theropod affinities (Olsen et al., 1998). It is also characterised by the markedly anterior extension of digit III, tightly packed digit II-IV, and the particularly low divarication angle of digit II-IV, which make it comparable to *Atreipus* in Triassic, which may be related to non-theropod dinosauromorphs (Haubold and Klein, 2000).

Due to the very well-preserved state of the *Grallator* holotype and the detailed comparisons and collations it received early on (Olsen et al., 1998), it has been subsequently frequently cited by researchers from different regions of the world (e.g. Lockley et al, 2011a; Xing et al., 2014b, 2024b; Castanera et al., 2016; Niedźwiedzki and Pieńkowski, 2016; Melchor et al., 2019; Klein et al., 2023) and has defined a group of ichnotaxa produced by small theropods by comparison with *Grallator*. These include some of the regional ichnospecies commonly used under *Grallator*, as well as some of the grallatorid ichnogenera. For example, the former include *G. ssatoi* from the Cretaceous of East Asia (Xing et al., 2024c), while the latter include *Kalohipus* from the Upper Jurassic of Europe (Castanera et al., 2016), *Picunichnus* and *Deferrariischnium* from the Lower Cretaceous of South America (Calvo and Rivera, 2018; Melchor et al., 2019), and *Jialingpus* from the Jurassic-Cretaceous of East Asia (Xing et al., 2014b). As a consequence, grallatorid is currently used in a broad sense to describe a class of small theropod track morphotypes with a rather large morphospace.

Relative to the originally defined *Grallator parallelus*, other grallatorids generally possess a wider size range (up to ~25 cm in *G. ssatoi* and *Picunichnus*), slightly higher divarcation of digit II-IV (up to ~60° when measuring the angle between the midline of digit), stronger digits or more developed digit pads, and more tightly compacted or fused heel region.

However, there are some examples of lower divarcation angles, such as the well-preserved referred specimens of *Picunichnus* with a typical maximum of <45° (Melchor et al., 2019), very close to the definition of <40° in *G. parallelus*. The distinguishable feature of most typical grallatorid in Jurassic-Cretacaous of East Asia (*Jialingpus* and *G. ssatoi*) from other grallatorid likely for statistically lower mesxomy and the developed, rounded metatarsophalangeal pad IV in the well- preserved *Jialingpus* specimen.

Within regions, the use of grallatorid ichnotaxa is often influenced by the morphological continuity of tracks within the same region, as well as the taxonomic perspective of historical studies. As a result, the choice of whether to establish new ichnogenera or new ichnospecies varies considerably. For example, the morphospace of *G. ssatoi*, which is widely distributed in the Lower Cretaceous of China, may be sufficient to establish an ichnogenera by simultaneous comparison with *Jialingpus* and *G. parallelus* under criteria from other regions (Xing et al., 2024c). However, preliminary size statistics (Lockley and Xing, 2021), together with morphological comparisons, indicate that it is difficult to find a stable morphological boundary between the tracks attributed to this morphotype. On this basis, a significant number of tracks are limited by preservation and lack track support to discuss their mode of deformation, hence the

591 aforementioned peculiarities of the grallatorid ichnotaxa in this region. Adjustment for
592 interregional differences in these ichnotaxa will require careful integration of detailed differences
593 in representative tracks and statistical differences in interregional tracks over the same period. As
594 this is not the focus of this paper, we suggest further discussion in conjunction with data from
595 large tracksites where the data are statistically significant.
596     In the Longxiang tracksite, none of the trackways resemble the grallatorid morphotype,
597 although a few isolated tracks and tracks within certain trackways show similarities to it. Among
598 the isolated tracks, only LXIU-TI7, LXIN-TI3 and TI4 are similar to grallatorid morphotype in
599 the extended digit III and the associated L/W ratio and mesxomy (Fig. 11; measurements see the
600 following tables). However, the spindle-shaped digit III and the linear digit II and IV indicate
601 that this footprint has undergone significant distortion, making it uncertain whether its original
602 characteristics truly resembled the grallatorid morphotype. For LXIN-TI3 and TI4, although their
603 preservation is slightly better than that of LXIU-TI7, the lack of well-defined digit traces and the
604 presence of sediment deformation structures indicate that neither represents its original
605 morphology. Additionally, their size (~35 cm in length) is significantly larger than the general
606 range of grallatorids.
607     Furthermore, the LXIN site also contains LXIN-T5-R1, which is part of a robust theropod
608 trackway. This footprint resembles grallatorids in its high length-to-width (L/W) ratio (>1.5) and
609 high mesaxony (~0.66), but its digits II and IV are distinctly medially directed. This suggests that
610 at the Longxiang site, footprints resembling the grallatorid morphotype may have resulted from a
611 robust trackmaker adopting a specific behavior of drawing digits II and IV inward while moving
612 on a soft substrate, combined with substrate deformation, rather than representing a distinct
613 trackmaker.
614

615 ***The comments on the ichnotaxonomy of large theropod track***
616 The large-sized tridactyl tracks (> 30 or > 25 cm in length) are widely distributed across the
617 Jurassic and Cretaceous strata (Foster et al., 2024; Xing et al., 2024b). Excluding the
618 distinguishable *Caririchnium* and *Hadrosauropodus* exhibiting derived ankylopollexian
619 affinities, which characterized by large, rounded metatarsophalangeal pad and short, snout-like
620 digits (Diaz-Martinez et al., 2015), and the typical theropod tracks with slenderer,
621 asymmetrically developed digits and sharper claws, a considerable number of intermediate
622 ornithopod and theropod ichnotaxa with highly comparable morphology are also found
623 (Lallensack et al., 2016, 2020), for example, *Iguanodontipus* with smaller, less separated heel
624 pad than *Caririchnium*.
625     Considering the morphology of known theropod ichnotaxa, generally three roughly defined
626 morphotypes could be used to describe the large tracks with possible theropod affinity. These
627 morphotypes mainly differ in the shape and relative position of the trace of digits II‑IV and the
628 metatarsophalangeal pad IV, including:
629

630    ①The elongated *Eubrontes* morphotype is characterized by a higher length/width ratio,
631    generally evenly developed digit II and IV, typically exhibit a lower divarication angle (<40°).
632    The definition here differs from that of eubrontid, which is used to describe an overly large
633    morphospace of Eubrontidae, which simultaneously includes the widely used *Kayentapus*,
634    *Megalosauripus* and *Eubrontes*. The most typical member of this morphotype is the *Eubrontes*
635    specimens that most closely match the currently recognized diagnostic features (Olsen et al.,
636    1998), such as type ichnospecies *E. giganteus* and the exceptionally well-preserved *E. nobitai*
637    (Fig. 6 in Xing et al., 2021c).
638    Other specimens can be broadly assigned to this morphotype based on the similar
639    development of digits II and IV (i.e., exhibiting a more comparable range of motion) and a more
640    pronounced anterior symmetry, while possess a higher divarication angle. These members with
641    mainly include *Asianopodus*-like tracks (Matsukawa et al., 2006; Xing et al., 2021d; or
642    *Jialingpus*-like), which is characterized by the presence of a significantly developed bulbous
643    metatarsophalangeal IV that is essentially positioned along the central axis of the footprint, and
644    they are statistically more symmetric than the following mentioned *Megalosauripus* morphotype.
645    These tracks are most typical and well-preserved in the Cretaceous of East Asia and include the
646    representative *Asianopodus* and the comparable *Chapus* (Lockley et al., 2018; Xing et al.,
647    2021d), as well as *Changpeipus* from the Jurassic (Xing et al., 2014c; Klein et al., 2023) and the
648    larger *Jialingpus* (Xing et al., 2014b), which lacks a definitive diagnosis based on size.
649    Some Cretaceous specimens previously classified as *Irenesauripus* from North America
650    (Lockley et al., 2014b) also loosely resemble *Eubrontes* morphotype. Gondwana morphotypes
651    appear to be relatively lacking in this category (Salisbury et al., 2016; Melchor et al., 2019;
652    Leonardi and Carvalho, 2021). A previously identified *Irenesauripus* from Argentina is closer to
653    small tracks resembling *T. pandemicus* (Fig. 1 in Melchor et al., 2019).
654
655    Among the *Asianopodus*-like tracks, most non-Asian tracks, in addition to Asian
656    *Changpeipus*, show a slightly lower mesaxony compared to *Asianopodus* and *Jialingpus*, with
657    digit III and metatarsophalangeal IV being more tightly connected. Sometimes, digits II or IV
658    exhibit a larger range of motion (RoM). For example, in Moroccan *Changpeipus* (Klein et al.,
659    2023), the notable asymmetry between digits II and IV, is more similar to *Megalosauripus*.
660    Furthermore, except the indistictive metatarsophalangeal region, non-*Changpeipus* morphotypes
661    (e.g., the aforementioned *Irenesauripus*) often display less posteriorly compacted digits, with
662    digits II and IV being relatively parallel. These tracks are more likely to be associated with
663    ornithischian *Dinehichnus* of similar size (e.g., Castanera et al., 2020), with some specimens
664    possibly belonging to *Iguanodontipus*? ("*Therangospodus*") *oncalensis* (Fig. 6 and 11 in
665    Castanera et al., 2013). However, ornithischian ichnogenera tend to have more robust digits II-IV
666    with indistinct phalangeal pads, and possibly co-occur with manus tracks (Lallensack et al.,
667    2020). Similar digit III connections have been found in smaller emu and possible ornithomimid
668    ichnogenera (*Ornithomimipus* and *Irenichnites*), as well as large bird-like tracks (*Magnoavipes*
669    and *Saurexallopus*). Comparative studies of the Cretaceous theropod fauna in Laurasia (e.g.,

670 Novas et al., 2013) reveal that the East Asian Cretaceous paleoenvironment is largely restricted
671 to terrestrial deposits (e.g., Zhou et al., 2018), potentially suggesting that habitat, rather than
672 phylogeny, strongly influences the foot morphology of possible theropod trackmakers in this
673 morphotype.
674     And the scarcity of *Eubrontes* morphotype, especially *Asianopodus*-like tracks in Gondwana
675 may be linked to the relatively low presence of derived coelurosaurs in that region. The unique
676 arctometatarsal structure in coelurosaurs (Holtz Jr, 1995; Tanaka et al., 2021) and other body
677 plans may have contributed to their bird-like compacted heel (Xing et al., 2014b), and backward-
678 shifted centers of mass (e.g., Farlow et al., 2000), potentially limiting the distribution of
679 *Asianopodus* (or *Jialingpus*)-like morphotypes. Validation of this hypothesis remains beyond the
680 scope of this study and will require further investigation, including more specimens and
681 biomechanical reconstructions in future research.
682
683
684
685     ②The elongated *Megalosauripus* morphotype with moderate length/width ratio, typically
686 have more flexible and well-developed digit II that results in a separated digit trace II with a
687 more sharply defined outline, an asymmetrical divarication angle between II-III and III-IV, and a
688 tendency to exhibit an unstable anterior angle within the trackway.
689     This morphotype is represented by the worldwide-distributed *Therangospodus* (*T.*
690 *pandemicus*) - *Megalosauripus* (*M. transjuranicus* and *M. uzbekistanicus*) (Gierlinski et al.,
691 2001; Barco et al., 2006; theropod morphotype C in Salisbury et al., 2016; Razzolini et al., 2017;
692 Belvedere et al., 2019; Xing et al., 2024b). Some other moderate-preserved ichnogenera,
693 especially many of which defined in Europe, are similar but usually regionally compared,
694 include *Boutakioutichnium* (Nori et al., 2011), *Bueckerburgichnus* (Cobos et al., 2014),
695 "*Hispanosauropus*"(Lockley et al., 2007), *Eutynichnium* (Belvedere et al., 2019) from upper
696 Jurassic and lower Cretaceous of Europe. The Asian ichnogenus *Gigandipus*, on the other hand,
697 is a relatively small (~30 cm in length) and slender representative among the possible members
698 of this group (Xing et al., 2018a).
699     In contrast to other large ichnogenera, the similar but narrower tracks of this type are more
700 commonly found in small theropod tracks, although in the former, the metatarsophalangeal pad
701 is notably more developed with the increasing body size.
702     It is important to note that some other gigantic theropod ichnogenera also exhibit similar
703 asymmetry, such as *Tyrannosauripus* and *Bellatoripes*, which are suggested to have a
704 tyrannosaurid affinity (Fig. 7.31 in Xing et al., 2024b). However, these tracks not only have
705 more developed heel regions, but also display shorter digits and a slightly more parallel
706 alignment compared to typical *Megalosauripus*. Large theropod tracks (~30 cm in width) with
707 similar features are also found in the Jurassic of Europe, including *Hispanosauropus* and
708 *Eutynichnium* (Foster et al., 2024), with *Eutynichnium* being tetradactyl. The differing
709 development and orientation of digit I suggest significant variation in trackmaker.

710

711      According to the aforementioned classification, some morphotypes exhibit intermediate

712  characteristics between the *Eubrontes* and *Megalosauripus* types. These are primarily relatively

713  symmetrical forms with a higher divarication angle and a relatively isolated small heel pad,

714  though the connection between the latter and the digits is not particularly pronounced. The

715  posterior margin of such morphotypes commonly exhibits a V-shape, and they appear to be

716  generally more slender, tending to occur within a smaller size range (30–40 cm in length).

717      One example is *Kayentapus*, which has been widely used but is primarily defined in the

718  Jurassic and is characterized by a less distinct heel region (Lockley et al., 2011b). Among the

719  more slender forms, some specimens, such as those illustrated by Xing et al. (2021e), show a

720  relatively symmetrical morphology and a larger divarication angle, closer to that of bird tracks.

721  In contrast, more robust forms, such as the type specimen of *K. hopii* (Lockley et al., 2011b) and

722  the Asturias specimen (Avanzini et al., 2012), tend to be more asymmetrical, with the latter

723  exhibiting a more separated digit II.

724      The previously mentioned *Irenesauripus* generally exhibits thinner digits II and IV, which are

725  relatively consistent in length and divarication angle compared to other large theropod

726  ichnogenera from the same region. In contrast to the *Megalosauripus* type—where digit IV is

727  more frequently connected to the heel—digit II in *Irenesauripus* is more isolated (McCrea, 2000;

728  Lockley et al., 2014b). By comparison, *Megalosauropus*, which has been redefined exclusively

729  from Australia, more closely resembles the aforementioned *Kayentapus* in both morphology and

730  its relatively smaller size range (Salisbury et al., 2016).

731      Furthermore, it should be noted that the above-mentioned *Eubrontes* and *Megalosauripus* are

732  not well-separated morphotypes by definition. In fact, the distinguishing features in their

733  diagnoses are quite different. The primary difference between them lies in the *Grallator* (-

734  *Anchisauripus*)-*Eubrontes* plexus and the *Megalosauripus-Therangospodus* plexus, and the

735  differences between the two are not purely morphological, but also involve issues such as

736  temporal limits (Lockley et al., 1998a, b). Therefore, it is important to emphasize again that the

737  two morphotypes discussed above are based on distinctive commonalities observed through the

738  re-examination of type specimens and other well-preserved specimens, rather than simply a

739  morphological comparison at the ichnotaxon level.

740

741      ③The stout *Jurabrontes* morphotype with ornithopod track-like (*Dinehichnus* or

742  *Iguanodontipus*) outline that possess short digits, generally low length/width ratio (~1) and

743  mesaxony (~0.5), but with distinctive phalangeal pads, fainter, smaller but often separated

744  metatarsophalangeal pad IV, as well as sharp claw traces. The majority of giant morphotypes

745  (generally >50 cm in length), although differing in the position of digits II and IV and the

746  occurrence of digit I, can largely be classified within this morphotype based on the evenly

747  developed, robust digits II and IV, as well as the higher heel pad length/footprint length ratio

748  (indicating a shorter digit III).

749     This morphotype is well-represented by specimens such as *Jurabrontes* from the Upper
750     Jurassic of Europe (Marty et al., 2018; Belvedere et al., 2019; Antonelli et al., 2023). These
751     tracks show some asymmetry, but to a lesser extent than *M. transjuranicus* (Belvedere et al.,
752     2019).
753     Giant ichnotaxa with similar weight-bearing adaptations include the *Tyrannosauripus* and
754     *Bellatoripes* from the Cretaceous of North America and East Asia, and *Bueckeburgichnus* and
755     "Hispanosauropus" from lower Cretaceous and upper Jurassic of Europe respectively, while all
756     of these morphotypes possess a digit I trace with different length, and develop the somewhat
757     develop *Megalosauripus*-type lateral digits. Some referred specimens of *Iberosauripus* from
758     Upper Jurassic to Cretaceous of Europe represents rather more *Eubrontes* type-like, with unfused
759     heel region, relatively elongated and paralleled digits (Castanera et al., 2015), while the part of
760     the type series represent indistinct heel region that somewhat similar to *Jurabrontes* (Belvedere
761     et al., 2019). However, the latter still differ with the moderate-preserved *J. teutonicus* also
762     without the occurrence of heel pad in the compact arrangement of digits, and there is no
763     tendency for fusion between the metatarsophalangeal pads or a significant enlargement of one of
764     them (Fig. 5 in Belvedere et al., 2019).
765     *Moraesichnium* and *Salfitichnus* from the Cretaceous of South America, comparable to
766     *Jurabrontes* morphotype in track size, have been subject to criticism regarding their original
767     outline interpretations (Masrour et al., 2017; Xing et al., 2024a), making morphological
768     comparisons with morphotype 3 and the aforementioned two types challenging. Notably, the
769     interpretation of *Moraesichnium* seems to differ significantly from the photograph (Fig. 4.71 in
770     Leonardi and Carvalho, 2021). In particular, digit IV in SOPP 2/5 appears to have sunk deeply
771     into the sediment, exhibiting a trace of sediment collision (e.g., Fig. 3 in Campos-Soto et al.,
772     2025). This deformation resembles that seen in Track 1321 from the Piau-Caiçara tracksite (Fig.
773     4.38 in Leonardi and Carvalho, 2021). We recommend further imaging or 3D depth mapping of
774     the specimens associated with *Moraesichnium* before revisiting its morphological interpretation.
775     Compared to these problematic ichnotaxa mentioned by Melchor et al. (2019) and Leonardi and
776     Carvalho (2021), *Jurabrontes*-like tracks are fit more to describe the South American
777     indeterminate bipedal dinosaur footprint fall within this size range.
778     The other large theropod ichnogenera defined in South America, the mid-Cretaceous
779     *Abelichnus,* is slightly smaller in size (40-50 cm in length, possible present smaller in size due to
780     the moderate preservation), but could be compared with the small *Jurabrontes*, *J. melphicticus* in
781     the general outline than the giant *J. curtedulensis* considering the less robust, V-shaped heel.
782     Other large ichnogenera mainly occupy similar size ranges as *Abelichnus* usually have slenderer,
783     longer digit III proportionally than the former, including the European *Boutakioutichnium* and
784     the Asian *Chapus* and *Ordexallopus.* However, compared to the Asian morphotypes,
785     *Boutakioutichnium*, despite preserving the trace of digit I, more closely resembles *Abelichnus*.
786     In Australia, large theropod tracks classified as the Broome Theropod Morphotype B resemble
787     *Jurabrontes*-like tracks (Salisbury et al., 2016). However, due to average preservation, it is

788 unclear whether they are more similar to Broome Theropod Morphotype C, which exhibits a
789 greater degree of asymmetry that more closely resembling the European *Megalosauripus* type.
790
791     Generally, large theropod tracks that resemble *Asianopodus*/ large *Jialingpus*-like
792 morphotypes may be more directly associated with specific theropod clades among the theropod
793 morphotypes. This hypothesis requires further validation through future studies, including
794 posture reconstructions of coelurosaurian and non-coelurosaurian trackmakers. Additionally, the
795 distinct ceratosaurian and megaraptoran-dominated theropod fauna of Cretaceous South America
796 (Novas et al., 2013; Lamanna et al., 2020) urgently requires comparative analysis with the
797 Jurassic records of Laurasia, considering possible deformations and subsequent ichnotaxon
798 revisions
799
800

801 ***Theropod morphotype A***
802 **Description.** The majority of theropod tracks and trackways in Longxinag site belongs to
803 Theropod morphotype A, including five trackways (LXIN-T1 – T5; Figs. 12, 13) and at least 12
804 isolated footprints (LXIN-TI1 – 6, TI10 – 16) are from the LXIN site (Fig. 11), one trackway
805 (LXID-T2; Fig. 13) and one isolated track (LXID-TI1) from LXID site (Fig. 11), one isolated
806 track from LXIU site (LXIU-TI7) and four isolated tracks in LXIII (LXIII-TI1 – 4; Fig. 11)
807 (Tables 4, 5).
808     Five trackways from the LXIN site including LXIN-T1-T5 (Fig. 12E; Table 4). These tracks
809 vary in length due to the erratic occurrence of heel region, however, they exhibit a relatively
810 stable width, concentrated within the range of 25 – 35 cm. Only some of the isolated small tracks
811 (<~20 cm in length) with very similar outlines to the large track from the same site, including
812 LXIN-TI6, LXIU-TI7, LXIII-TI2 to TI4, are also classified in this morphotype,that may
813 represent some small individuals . All the trackways are short but distinguishable, and contains
814 three to eight continuous footprints. In most of the trackways, the footprints are slightly inward-
815 rotated overall.
816     Among these trackways, the three well-preserved tracks in LXIN-T5 (R1, L1, R2) essentially
817 represent the two main deformation patterns within this morphotype (Fig. 13). This further
818 supports that these morphologically diverse yet size-consistent footprints should be classified
819 under the same morphotype. In the Theropod morphotype A, the majority of trackways (LXIN-
820 T1, T2, T4, T5) and a considerable number of isolated tracks (LXIN-TI5?, TI10–11, TI12?,
821 TI14–15; LXIII-TI2–3) exhibit a digitigrade form similar to T5-L1 or R2, preserving only a
822 partial metatarsophalangeal pad.
823     The preservation state of LXIN-T5 corresponds to level 1–2 on the scale of Belvedere and
824 Farlow (2016) (Fig. 12E). The digit imprints are stable in width, possess quite clear and sharp
825 outline, and claw marks and some phalangeal pads can be faintly identified. Trackway LXIN-T5
826 shows functionally tridactyl, digitigrade-like and mesaxonic pes imprints that have an average
827 length of 32.4 cm and length/width ratio of 1.2. Digit II is the shortest and digit III and digit IV

PeerJ

828   are similar lengths. There is a generally wide divarication angle (59°) between digit II and digit
829   IV  and the mean mesaxony of LXIN-T5 is 0.49.. The tracks are rotated slightly outwards
830   towards the axis of the trackway. The average pace angulation is 127°. The T5-R1 is the most
831   complete footprint amontg this trackway(Fig. 13), and as previously mentioned in the section
832   "grallatorid morphotype", it has been radially compacted due to the behavior of trackmaker. The
833   metatarsophalangeal pads of digit II are fairly well-developed in T5-R1, with a size almost as
834   large as the phalangeal pad of digit IV. However, this feature is not preserved in the other two
835   footprints in the trackway. T5-L1 and R2 exhibit a more digitigrade form with radially spread
836   digits II and IV. L1 lacks a prominent metatarsophalangeal pad II, while R2 preserves only
837   distinct digit traces II–IV.
838      The footprints in LXIN-T1 represents the more standard theropod-type semi-digitigrade
839   pattern within this morphotype (Fig. 12B; Table 4). It contains three consecutive tracks with an
840   average length of 31.5 cm and a length/width ratio of 1.2. Distinct external morphological
841   changes can be found in trackway T1-L1, with the curved impression of number IV, possibly
842   signalling its entry and exit. Digits II to IV are sandwiched between the semicircular heel track
843   and have an overall shuttlecock-shape, with a possible large, rounded trace of digit I proximally.
844   The morphologies of T1-R1 and L2 are comparatively conventional (Fig. 13), with a mean
845   mesaxony of 0.54, which is overall quite close to the LXIN-T5 traces. Among other tracks and
846   trackways, excluding size considerations, LXIN-T4, LXID-TI1 and LXIII-TI1 exhibits the
847   greatest morphological difference compared to LXIN-T1.
848      The LXIN-T4 comprises four consecutive tracks(Fig. 12D), with a mean length of 24.3 cm
849   and a mean width of 28.7 cm and mean L/W ratio of 0.9. The LXIN-T4-R1, shows a digitigrade
850   track somewhat simliar to LXIN-T5-R2 with the digit III occupies 80% of the length of the track,
851   while its L/W ratio (0.6) is significantly lower relative to the latter (1.0). Meanwhile, in the
852   relatively well-preserved specimens LXIN-T4-L1, R2 (Fig. 13), and LXID-TI1(Fig. 11), the
853   robust and proportionally shorter digits exhibit a greater resemblance to the more stoutly built
854   *Jurabrontes* or the ornithopod ichnotaxon *Iguanodontipus* than to other theropod tracks from the
855   Longxiang site. However, considering that the proximal portions of digits II and IV in these
856   footprints still display marked asymmetry, and that ornithopod tracks from the Longxiang site
857   are characterized by a distinctly elongated metatarsophalangeal region, an ornithopod affinity is
858   deemed unlikely. Furthermore, given the considerable morphological variation within this
859   morphotype attributable to substrate deformation, and the fact that LXIN-T4-R2 can be
860   morphologically linked to the digitigrade forms represented by LXIN-T2-L2 and LXIN-T5-L1,
861   these footprints are best interpreted as belonging to the same morphotype.
862      The LXID-T3 closely related to the outline represented by LXIN-T4, which consists of three
863   consecutive but highly distorted tridactyl tracks (Fig. 13; Table 4). In this trackway, the digit
864   traces appear disproportionately short and slender due to sediment backflow. This effect also
865   results in a notably enlarged heel region in the deeper tracks, R1 and L1, whereas in the
866   shallower R2, only the anterior outline of the digit traces is preserved. Additionally, T3-R2
867   exhibits a distinct sedimentary ridge between digits III and IV. In LXID-T3-R1 and L1, the large

868  metatarsophalangeal region is well-preserved, displaying a notable degree of development and
869  bearing a resemblance to the tracks of large ornithopods rather than those of theropods. The
870  sedimentary deformation in the interdigit region of L1 suggests a highly fluid substrate that differ
871  from which of LXIN when the track formed. As the sediment becomes more hydrated, the
872  likelihood of the occurrence of the metatarsophalangeal region increases, particularly in birds or
873  bird-footed dinosaurs, such as the extant helmeted guineafowl (*Numida meleagris*; Gatesy et al.,
874  1999).
875      Anomalous and significant deformation is also observed in LXIN-TI5 and TI10 (Fig. 11;
876  Table 5); however, for these isolated track, the deformation occurs based on a more digitigrade
877  form. This results in a larger divarication angle with excessively slender digits, rather than
878  shorter digits combined with a more prominent heel region.
879      As for the remaining trackways and isolated tracks, their morphology generally falls between
880  the aforementioned members:
881      In the LXIN site, the degree of deformation of the footprints is generally lighter compared to
882  the LXIU site, and it preserves more complete trackways relative to the LXIII site.
883      The LXIN-T2 contains four consecutive tracks, of which R1 and L2 are in better preservation
884  (Fig. 12A; Table 4). The average length of T2 tracks is 23.7 cm, with an average L/W ratios of
885  0.8. Three of these tracks have been preserved as tridactyl, and the II-III angles of all three tracks
886  are smaller than those of III-IV. The tracks exhibit a rotation of approximately -15° with respect
887  to the trackway axis. T2-R1 is the most typical among the LXIN-T2 tracks (Fig. 13), yet no
888  phalangeal pads could be identified. All the digits of R1 are connected posteriorly, with deep
889  claw marks, and occupy 62%-74% of the length of the track (N=3). The digit II and III traces of
890  R1 are notably wider than those of digit IV, which are narrow and connected to the posterior
891  margin at a small heel.
892      LXIN-T3-L1 and L2 only preserve digit III and IV, while the former is poorly preserved in
893  R1.The overall L/W ratio of T3 is 1.3, similar to that of L1 and T5 (Fig. 12C).
894      As previously mentioned, LXIN-TI3 and 4, as well as LXIU-TI7 from LXIU site could be
895  compared to LXIN-T5-R1, while LXIU-TI7 is in the size range of small theropod track..And of
896  the other nine isolated tracks from LXIN (excluding TI3–TI5, TI10),  are all comparable to the
897  well-preserved LXIN-T5-L1 or T1-R1 (Fig. 13). These isolated tracks are from 26.4 cm to 36.8
898  cm in length, with mesaxony greater than 0.45 and L/W ratios between 1.1 and 1.6. Distinct
899  external morphological changes can be found in isolated tracks TI1 and TI5, reflected in a
900  pronounced curvature of the digit or a deformity of the heel. There was an overlap between TI6
901  and TI7, with the former destroying the track of the latter.
902      The LXIII site preserves four tridactyl theropod tracks (Fig. 11), of which LXIII-TI1 shows
903  functionally tridactyl, digitigrade and mesaxonic pes imprint that have an average length of 28.9
904  cm and length/width ratio of 1.0. Digit II is the shortest, and digit III is shorter than digit IV.
905  Digit III accounts for 64% of the total length of the footprint. There is a wide divarication angle
906  (76°) between digit II and digit IV. The divarication angle between digits II and III (37°) is
907  almost equal to the one between digits III and IV (39°). Each digit impression ends in a sharp

908    claw mark. The mean mesaxony of LXIII-TI1 is 0.51.
909        The other three tridactyl theropod footprints from site LXIII are all less than 25 cm in length.
910    TI2 lacks the heel but comparable to TI1 in width, TI4 is 15.8 cm in length, has a length/width
911    ratio of 1.1, and a mesaxony of 0.53, and the overall morphology is similar to the the Theropod
912    morphotype A.
913    **Comparison and discussion.** Among the best preserved trackways, LXIN-T1 and T5, the
914    average mesaxony of  is about 0.54 and 0.49 (Fig. 12, Table 4), which is typical for the
915    morphofamily Eubrontidae (Lull, 1953). LXIN-T5-R1 track shows convergent traits with non-
916    *Asianopodus Eubrontes*-type tracks(see the defination in previous section), especially the overall
917    evenly developed digit II and IV,  and the separated metatarsophalangeal pad II and IV. However,
918    the capability of reaching higher divarication angle in the footprints shows higher digitigrade
919    level is also differ from the  most typical *Eubrontes*, such as the holotype AC 151 (Olsen et al.
920    1998) and the Cretaceous *E. nobitai* from East Asia (Xing et al., 2021c)
921        Conversely, their loosely arranged digits, combined with a size range positioned at the lower
922    boundary of large theropods (25–30 cm), suggest an intermediate morphotype between
923    *Eubrontes* and *Megalosauripus*, more closely resembling the *Eubrontes*-type. Examples include
924    *Kayentapus*, particularly the type specimen of *K. hopii* (Lockley et al., 2011b), as well as the
925    typical Cretaceous North American *Eubrontes* from the Mail Station Dinosaur Tracksite
926    (Lockley et al., 2021), which exhibits a larger divarication angle compared to its Jurassic
927    counterparts. The more robust footprints, such as LXIN-T4, LXID-TI1, and LXIII-TI1, resemble
928    the *Kayentapus* Asturias specimen (Avanzini et al., 2012).However, compared to *Eubrontes* and
929    *Kayentapus*, the heel region of the Longxiang Theropod morphotype A is less distinctly
930    preserved, evoking similarities with *Carmelopodus* (Lockley et al., 2014b), which is primarily
931    defined within the small-to-medium size range. Nonetheless, despite some similarities in
932    exhibiting a relatively strict digitigrade posture, the large theropods from the Longxiang site
933    display relatively low mesaxony, distinguishing them from large grallatorid tracks.
934        Besides, the fleshy digits and the large, rounded, posteriorly slightly protruded heel pads in
935    some of the morphotype A tracks are somewhat reminiscent of large neornithischian tracks with
936    fleshly pads for weight-bearing, including basal ankylopollexian mainly from lower Cretaceous
937    of Europe (*Iguanodontipus*), and axially compacted dryosaurid ornithopods or relatively large
938    basal neornithischian tracks mainly record in upper Jurassic of Europe, North America and lower
939    Cretaceous of Europe (*Dinehichnus*) (Diaz-Martinez et al., 2015; Castanera et al., 2020; Foster et
940    al., 2024; Xing et al., 2024b). They are also similar in structure to moa footprints from
941    Newzeland (especially the ornithopod-like *Moapus* and *Dinornipus*; Hunt and Lucas, 2024).
942    However, digit II of T4-R1 preserves slender, sharp claw trace that more comparable to theropod
943    footprints, and they are remarkablely distinguished from the aforementioned ornithopod and moa
944    ichnospecies by the frequent absence of metatarsophalangal pad within a particular trackway.
945        In summary, among the currently established ichnotaxa, *Kayentapus* or *Eubrontes* may be the
946    most appropriate classification for this morphotype. However, given that *Kayentapus* remains
947    primarily defined within the Jurassic, we propose classifying the large-sized and morphologically

948    distinct members of Theropod morphotype A as *Eubrontes isp.*, while the significantly smaller
949    tracks should be assigned to *cf. Eubrontes*, or left unclassified due to the absence of referable
950    trackways.
951        Xing et al. (2021c) reviewed most of the records of *Eubrontes* in China. The Lower
952    Cretaceous of China has yielded a considerable record of theropod tracks of the generalized
953    *Grallator- Eubrontes* plexus type, which are typical in Jurassic formations of North America and
954    China (Xing et al., 2021c). This has extended the stratigraphic and palaeobiogeographic range of
955    these generalized theropod trackmakers into Cretaceous East Asia (Xing et al., 2018b). The
956    records of this morphotype extend this assembly to the early Late Cretaceous.
957    **The primary comments on the validity of *Tridentigerpes*.** It is worth noting that in trackways
958    LXIN-T2, T4, and T5, which comprise a mixture of both semi-digitigrade and digitigrade
959    footprints, the semi-digitigrade forms—characterized by a combination of lower mesaxony, a
960    higher divarication angle, and a reduced proportion of the metatarsophalangeal region (e.g., T2-
961    L2 and T4-R2; Fig. 13)—resemble *Tridentigerpes huashibanleei* from its type series, particularly
962    HSB-T2-R1. Additionally, LXIN-T2-R1 and L2 exhibit morphological consistency with HSB-
963    T2-L1 and R2 (Fig. 3 in Xing et al., 2021f).
964        Within Theropod morphotype A, footprints such as LXIN-TI5 and TI10, which have
965    undergone significant distortion, also show similarities to *T. huashibanleei*. These footprints are
966    characterized by elongated digit traces and an overall robust appearance, with divarication angles
967    ranging from 88° to 135°, which closely aligns with the type series of *T. huashibanleei* (93°–
968    130°). However, they exhibit slightly lower values compared to the large-sized referred
969    specimens of *Tridentigerpes* from the Morrison Formation of Colorado, which reach a maximum
970    of approximately 150° (Fig. 6 and Table 1 in Xing et al., 2021f). Regarding the relatively low
971    mesaxony observed in large *Tridentigerpes* specimens (ranging from 0.26 to 0.34 in the
972    Huashiban specimens and 0.38 to 0.51 in the Colorado specimens), the footprints assigned to
973    Theropod morphotype A at the Longxiang site exhibit a comparable range (0.29–0.5) despite
974    their relatively elongated digit lengths. The co-occurrence of *Tridentigerpes-like* and *Eubrontes-*
975    *type* non-avian dinosaur tracks within the same area, and even within the same trackway at the
976    Longxiang site, preliminarily suggests that these two morphotypes may be linked through
977    transient variations in digitigrade levels during locomotion. Furthermore, all referred specimens
978    of large *Tridentigerpes* exhibit significant distortion, with no known examples displaying the
979    less-deformed morphology observed in the type series.
980        Although Theropod morphotype A does not entirely match the type series of *Tridentigerpes*,
981    the findings suggest that, rather than resembling *Carmelopodus*, the distinctive "digitigrade"
982    form of large *Tridentigerpes*, characterized by a high divarication angle, is unlikely to result
983    from the trackmaker's intrinsic foot morphology, stable locomotor behavior, or an avian-like
984    trackmaker. Instead, it is more plausibly interpreted as a temporary locomotor adaptation in
985    response to a slippery substrate. This interpretation raises doubts about the ichnotaxonomic
986    validity of *Tridentigerpes*, particularly regarding the relationship between *T. pinuelai*, a smaller
987    morphotype that more closely resembles typical bird ichnotaxa, and *T. huashibanleei*, the type

988   ichnospecies. Consequently, we propose the removal of *T. pinuelai* from *Tridentigerpes*.

989   However, due to the weathering of the in situ specimens of *T. pinuelai*, and the lack of clear

990   reference material beyond the low-quality images provided in Xing et al. (2021f), we refrain

991   from formally reclassifying it in this study. The issue of *Tridentigerpes*' validity will be further

992   examined in the following sections, incorporating additional specimens for a more

993   comprehensive evaluation.

994

995   **Speed estimates.** Thulborn (1990) put forth the proposition that hip height (h) =4.5$\times$track

996   length (Fl) for small theropods (track length < 25 cm), and h=4.9 × FL for large theropods. After

997   this, the stride length/hip height ratios of the LXIN-T1, T2, T4 and T5 trackway are 1.34, 2.32,

998   1.9 and 1.14 respectively, mostly indicating a trotting gait, except T4 shows fast walking gait;

999   the largely distorted LXID-T3 rather show a trotting gait (1.82). The speed of LXIN-T1, T2, T4

1000   and T5 trackmakers are 5.69, 11.92, 8.58, and 4.39 km/h respectively, and which of LXID-T3 is

1001   7.86 km/h.

1002     Given the considerable density of tracks at the LXIN site, it seems reasonable to suggest that

1003   subsequent trackmakers slowed down when confronted with the rugged substrate in the bustling

1004   area. It is important to note, however, the co-existence of the absence of the heel traces, low

1005   divarication angle and the low L/W ratio is correlated with an incomplete estimation of foot

1006   length in LXIN-T2 and T4, by which the estimated velocity would be relatively large when using

1007   the aforementioned methods.

1008

1009   ***Theropod morphotype B***

1010   ***Description.*** The Theropod morphotype B trackways includs LXIU-T2 and LXID-T1 (Table 4),

1011   which are characterized by their large divarication angles of ~100°–110° and the total absence of

1012   distinguishable metatarsophalangeal region. These resulting in exceptionally low L/W ratio of

1013   ~0.5 to 0.6, and the concomitant weak mean mesaxony of <0.3 (Fig. 13).

1014     The LXIU-T2 trackway is representative of the type B from the Longxiang site, comprising

1015   seven consecutive tridactyl tracks (Fig. 13). The preservation condition of the LXIU-T2 is

1016   classified as level 2 on the scale proposed by Belvedere and Farlow (2016). The mean length of

1017   the T2 tracks is 14.7 cm, with a mean width of 29.3 cm. The mean L/W ratio is 0.5, and

1018   mesaxony is 0.29. The digit traces are clearly discernible and distinct, and the claw marks are

1019   readily apparent. The length of digit III occupies between 87% and 92% of the length of the track,

1020   as observed in three specimens. All the tracks exhibit markedly distinct divarication angles

1021   between digits II and IV, with a mean value of 107° and a range of 100° to 114°. The trackway is

1022   notably broad, with a pace angulation of 133° and a stride length of approximately 6.7 times the

1023   track length. The tracks exhibit a rotation of approximately 9° (between -9° and 8°) from the

1024   trackway axis.

1025     LXIU-T2-R1 is the most well-preserved of the LXIU-T2 tracks (Fig. 13). However, no

1026   phalangeal pads can be identified. The trace of digit III is notably broader in comparison to the

1027   traces of digits II and IV, and the posterior margin of the footprint is not distinctly delineated.

1028  The digit III of R2 is distinctly conical in shape, exhibiting the sharpest claw marks; digit II is
1029  subfusiform with the deepest claw marks; digit IV is the smallest and oval in shape, with claw
1030  marks only visible at the anterior margin. Comparatively, L1, L2, and R3 in T2 only preserved
1031  digit II and III, and digit II of them show claw marks tangent to the median axis of the digit, as
1032  an ectomorphological feature as the lifting of digit.
1033      Morphologically, almost all the features and dimensions of track LXID-T1 match those of
1034  LXIU-T2 (Fig. 13). LXID-T1 consists of seven tridactyl footprints with an average length of 14
1035  cm and an average width of 30.7 cm. This gives an average L/W ratio of 0.5. LXID-T1 appears
1036  to have a longer stride length, which is approximately 10.3 times the length of the track. The
1037  tracks have an outward rotation of approximately 28° (with a range of -45° to 24°) from the track
1038  axis.
1039  **Comparison and discussion with *Tridentigerpes*.** Xing et al. (2021f) provided diagnostic
1040  features of *Tridentigerpes* including: weakly mesaxonic tridactyl tracks with unusually wide
1041  digit divarication, averaging from ~107°~135° in three samples, and short digit III giving pes
1042  length width ratios of ~0.5–0.80. Trackway narrow with step typically 4 time track length.
1043  Compared to the aforementioned Theropod morphotype A, the Theropod morphotype B in
1044  Longxiang sites generally more consist with the diagnostic features of *Tridentigerpes*, especially
1045  in the exceptionally low length/width ratio of ~0.5 that separates *Tridentigerpes* from the other
1046  ichnogenera. Specifically, the other detailed characteristics of morphotype B are almost
1047  completely consistent with *T. huashibanleei*, including wide digit divarication angles (both mean
1048  107°), the mesaxony (both are 0.29), and the tendency of the inward rotation of pes (Table. 4).
1049  Minor difference occurrence between overall feature of morphotype B tracks and  *T.
1050  huashibanleei*: the former is higher in the relative speed with an average step length for about 6.7
1051  times footprint length, different from 4 times of *T. huashibanleei*. In addition, *T. huashibanleei*
1052  tracks are rotated approximately 25° inward from the trackway axis, type B tracks rotated inward
1053  and outward with small angles. Among the Longxiang tracks, LXIU-T2-R1 show very similar
1054  outline to HSB-T2-L1, including the similar anterior extension of digit II. However, in LXIU-T2
1055  and LXID-T1, the relative positions of the ungual traces of digits II and IV are inconsistent. For
1056  instance, in LXID-T1-L1 and L2, the degree of distal extension of digit II varies, while in LXIU-
1057  T2, there are significant differences in the abduction of the lateral digits between R2 and L2.
1058  This indicates that for large *Tridentigerpes*, the only remaining diagnostic features are the L/W
1059  ratio and divarication angle, which are more influenced by environmental factors rather than the
1060  trackmaker itself.
1061      In conclusion, this morphotype does not exhibit a stable and distinctive pedal morphology,
1062  consistent kinematic characteristics (e.g., high-digitigrade posture), or significant behavioral
1063  indicators (e.g., swim tracks) that would justify its classification as an independent ichnogenus.
1064  Therefore, we consider *Tridentigerpes* to be a *nomen dubium*. Considering that Theropod
1065  morphotype A and morphotype B coexist at both the LXIN and LXIU sites and share a similar
1066  size range, it is more reasonable to classify morphotype B as *cf. Eubrontes*. However, it is
1067  important to note that, unlike morphotype A, which preserves more complete footprints,

1068  morphotype B lacks sufficient diagnostic features and may correspond to more than one
1069  ichnogenus.
1070     Furthermore, if the claw traces are not sharply defined, the possibility of an ornithischian
1071  affinity should also be considered. This suggests that directly assigning *Tridentigerpes* from the
1072  Huashiban site— which resembles Theropod morphotype B—to *cf. Eubrontes* would be
1073  inappropriate. At the Huashiban site, the tridactyl ichnogenus that coexists with *Tridentigerpes*
1074  within the same tracksite and falls within a similar footprint width range (25–35 cm) is
1075  *Dinehichnus*. The primary differences between *Dinehichnus* and *Eubrontes*-like tracks with a
1076  higher divarication angle (e.g., *Kayentapus*) lie in the connection between the
1077  metatarsophalangeal region and the digits, the clarity of phalangeal pads, and statistically distinct
1078  symmetry patterns. However, these distinguishing features cannot be observed in the Huashiban
1079  *Tridentigerpes*, as only the anterior portions of the digits are preserved. Therefore, following the
1080  classification approach for Longxiang Theropod morphotype B, we propose that the Huashiban
1081  *Tridentigerpes* should be regarded as *cf. Dinehichnus*.
1082  **Speed estimates.** Similar to which applied to morphotype A, hip height (h) $=4.9 \times$ FL for large
1083  theropods from Thulborn (1990) are used to estimate the speed of trackmaker. After this, it is
1084  inferred that the relative stride length (SL/h) of the LXIU-T2 and LXID-T1 are 2.72 and 4.44,
1085  which indicate a trotting (slow running) and scarce running gait, and have estimated speeds of
1086  12.14 and 26.93 km/h, respectively. Also similar to the LXIN-T2 and T4, estimated velocity of
1087  morphotype B would be relatively higher when considering the footprint length of LXIU-T2 and
1088  LXID-T1as the actual length of the pes. Additionally, compared to morphotype A trackways, in
1089  which the metatarsophalangeal region is preserved to varying degrees and track length is
1090  relatively complete, the estimation of speed for morphotype B trackways—where this region is
1091  entirely absent—is more significantly affected by the aforementioned factors. Consequently, the
1092  current speed estimates are likely to be considerably higher than the trackmaker's actual speed
1093  and should be interpreted as representing only the upper limit.
1094  **The formation of morphotype B.** The short, pointed tracks with extremely low mesaxony,  can
1095  also be seen in buoyancy-related punting tracks (Romilio et al., 2013; Navarro-Lorbés et al.,
1096  2023). It may be hypothesized that the morphology resembling morphotype B and the "T.
1097  huashibanleei" may be formed in a swimming-like state with the pes in a distinctly oblique
1098  position to the ground. However. the specific genesis of this state is not unique and may be
1099  behavioural (McAllister and Kirby, 1998) or by substrate condition (Milàn, 2006). Both of these
1100  can be manifested as the distal end of digit III moving relatively proximally in the plane. With
1101  regard to the large divarication angle, it may be a consequence of the oblique intersection with
1102  the ground during footfall (Milàn, 2006). However, in purely substrate-related speculation, the
1103  large divarication angle is only observed on the upper surface of muddy substrate that is
1104  sufficiently wet and soft to retain plastic deformation at the track (Milàn, 2006). The presence or
1105  absence of heel traces on the upper surface of the substrate is indicative of the degree of
1106  weathering. In lower surfaces where heel traces are absent, the divarication angle is not
1107  significantly larger than that of conventional tracks (Falkingham and Gatesy, 2014; Turner et al.,

1108  2020).

1109  In conclusion, it suggests that the digit-only morphology of Theropod morphotype B may have
1110  a behavioural genesis that approximates swimming. Further speculation is contingent upon
1111  further observation and comparison of both referred trackways of morphotype B and HSB-T2
1112  from Hushiban site..

1113

1114  **Caririchnium *morphotype***

1115  *Description*

1116  The ornithopods left the most abundant footprints in the Longxiang area, which spreading
1117  through all the LXI, LXIII sites (Figs. 5-7; Table 6), and the size of the tracks exhibited
1118  considerable variation. The size variation in LXI sites can be divided into five intervals: less than
1119  10 cm, 10–20 cm (20 cm excluded), 20–30 cm (30 cm excluded), 30–40 cm (30 cm excluded),
1120  and ≥ 40 cm. The number of preserved tracks within each interval is as follows: 2, 31, 21, 6, and
1121  6, respectively. Although the length appears to be continuous, a relatively clustered area of track
1122  lengths between 12 and 26 cm can be observed in the box plots (Fig. 14). However, the
1123  preservation condition of ornithopod tracks in this area is quite limited, with the majority being
1124  at level 1. These tracks are shallow, blurred, or deformed, yet still recognisable as digit traces.
1125  Some claw traces were also present; the manus and pes tracks are distinguishable, with the
1126  former retaining only a rough outline. Of the 66 ornithopod trackways, 14 (21%) preserved
1127  manus tracks.

1128  Four ornithopod trackways are preserved in LXID site, numbered LXID-O1–O4, with track
1129  lengths ranging from 20.8 cm to 33.1 cm (Figs. 15, 16).

1130  Eight pes tracks are preserved in LXID-O1. The pes tracks of LXID-O1 are mesaxonic and
1131  functionally tridactyl, with a mean length of 33.1 cm and an average length/width ratio of 1.2
1132  (Fig. 15; Supplementary Information 2; Table 6). The mean mesaxony is 0.32. In the better-
1133  preserved O1-R3 and L5, digit III is observed to project the farthest anteriorly, followed by digits
1134  IV and II. Each digit trace exhibits a pronounced ungual or claw mark. A distinct border is
1135  absent between the heel and the three digits. The O1-R2 and L3 specimens exhibit an extended
1136  heel, which may be part of the metatarsal impression. This is potentially caused by the deeper
1137  deposition of the metatarsal. The mean interdigital divarication II–IV is 49°. The average pace
1138  angulation of LXID-O1 trackway is 161°. The pes traces show outward and inward rotation
1139  mean 7° from the trackway axis.

1140  The LXID-O2, 3 and 4 trackways preserved approximately 15, 10 and 14 tracks respectively.
1141  All tracks were very similar in length, ranging from 20.8 cm to 22.8 cm (Fig. 16; Supplementary
1142  Information 2; Table 6). Out of a total of 39 tracks, only about 4 had better preserved
1143  morphological characteristics. For example, of the 10 tracks in O3, only L4 shows a distinct
1144  tridactyl pattern, the length is 19.4 cm, the length/width ratio is 1.2 and the mesaxony is 0.44.
1145  The other tracks in O3 are irregularly elliptical, but the L/W ratios are essentially in the range of
1146  1.1 to 1.4. O2 preserves two possible manus tracks: R9m and R10m are located in the outer part
1147  of digit IV of the pes, with an average length of 5.2 cm and an L/W ratio of 0.7. Due to the poor

1148  preservation of the individual tracks, the information on the trackways is remarkable. The pace
1149  angulation of LXID-O2, 3 and 4 are 154°, 144° and 146° in average, respectively. The tracks are
1150  predominantly outwardly rotated, being 10°, 11° and 12° from the track axis in the three
1151  trackways respectively.
1152  LXIU site preserves 13 ornithopod trackways and a number of isolated tracks, the former
1153  numbered LXIU-O1-O13, with tracks ranging from 10 cm to 44.5 cm in length (Figs. 15-17. 13-
1154  14).
1155  LXIU-O3, O6, O9 and O13 represent the smallest ornithopod trackways (10 cm to 12.2 cm in
1156  length) at the LXIU site (Fig. 16; Supplementary Information 2; Table 6).
1157  LXIU-O3 preserved nine pes tracks that are mesaxonic, functionally tridactyl with an average
1158  length of 10 cm, an average length/width ratio of 1.2 and an average mesaxony of 0.25 (Fig. 16).
1159  In the better preserved O3-R4, digit III projects most anteriorly, followed by digits IV and II.
1160  The digits II and IV are almost equal in length. Each digit trace has a strong and blunt claw or
1161  ungual mark. There is no distinct border between the heel and the three digits. The average
1162  interdigital divarication II-IV is 55°. The average toe angulation of the LXIU-O3 trace is 153°.
1163  The pes traces show an average outward rotation of 6° from the trackway axis.
1164  LXIU-O6, O9 preserved five and four pes traces respectively (Fig. 16). Both trackways had
1165  limited preservation, with tridactyl morphology discernible in O6-L3, and numbers II and IV
1166  discernible in O9, the other tracks representing oval pits.
1167  LXIU-O13 has preserved five pes tracks (Fig. 16). All except O13-L1 have very pronounced
1168  ectomorphological distortions, most likely due to highly fluid sediments. O13-L1 is mesaxonic,
1169  functionally tridactyl with a length of 8.2 cm, and the mean length/width ratio is 0.6, the mean
1170  mesaxony is 0.18, representing very broad contours and extremely low mesaxony.
1171  LXIU-O1, O4, O5 and O7 represent medium sized ornithopod tracks ranging from 18 cm to
1172  27.5 cm from the LXIU site (Figs. 15-17; Supplementary Information 2; Table 6).
1173  LXIU-O1 has only a single step, R1 is well preserved, functionally tridactyl with a mean
1174  length of 31.6 cm, with a mean length/width ratio of 0.9 and a mean mesaxony of 0.31. The
1175  interdigital divarication of digits II-IV is 69°. The three digits are almost equal in width and
1176  length from the hypex, while the claws of digit III are more acute than those of digits II and IV.
1177  LXIU-O4 is probably the best preserved ornithopod trackway on the LXIU site (Fig. 15). It
1178  contains 5 tracks. All tracks are functionally tridactyl with an average length of 26 cm, the
1179  average length/width ratio is 0.8, the average mesaxony is 0.14, the interdigital divarication of
1180  digit II-IV is 51°. There is a distinct border between the heel and the three digits. The digits II
1181  and IV are almost the same length. Each digit has a strong and blunt claw or ungual mark. The
1182  average pace angulation of LXIU-O4 trackway is 141°. The pes traces show inward rotation, on
1183  average 12° from the trackway axis. LXIU-O4-R1 has a slightly smaller digit III than II and IV,
1184  and its heel is quite large, almost twice the size of the individual digits. This feature is not
1185  present on the other tracks. The mesaxony of O4-L1 is significantly above average at 0.35. The
1186  heel of R3 has a drag mark and preserves a large manus track located between digits III and IV,
1187  the track is wider than long, measuring 8.6 cm in length, with a L/W ratio of 0.7, and the track is

1188    rotated outwardly by 43°, relative to the axis of the pes. The ratio between the area of the manus
1189    track and the pes track is 0.22. Overall, the average length of the right track is 24.1 cm, which is
1190    less than that of the left track at 28.7 cm, and may be the result of a large difference between the
1191    left and right foot sizes of this trackmaker. Even when well preserved, where each track is clearly
1192    quartered, the features of LXIU-O4 are unstable, which is an ectomorphological distortion
1193    caused by slippery substrates.
1194       LXIU-O5 preserved nine tracks of which three were incomplete (Fig. 15). The mean length of
1195    the tridactyl tracks is 27 cm, with an average length/width ratio of 0.8 and a mean mesaxony of
1196    0.21. The interdigital divarication of digit II–IV is 51°. A clear delineation between the heel and
1197    the three digits is absent. The length of digits II and IV is approximately equal. Each digit trace
1198    has a strong and blunt claw or ungual mark. The mean pace angulation of the LXIU-O5 trackway
1199    is 160°. The pes traces exhibit outward and inward rotation, with a mean deviation of 5° from the
1200    trackway axis. O5-L2, R2, L3 and R3 are particularly well-preserved, with clear claw marks
1201    visible on digit IV of L2 and on digits II-IV of R3 (Fig. 17). The claw marks on R3 are the most
1202    well-preserved, with a clearly defined boundary. However, other areas of the internal deposition
1203    have not been completely removed, which impedes further observation. O5-L1 has a large heel
1204    that is twice the length of the other tracks in the same trackway, which may be the result of
1205    metatarsals being involved in the formation of the impression, or it may have been formed by the
1206    fragmentation of the track layer.
1207       LXIU-O7 is the longest ornithopod trackway at the Longxiang site, with a length of 23 m and
1208    preserving about 43 tracks, which is probably the longest ornithopod trackway in China (Fig. 16).
1209    It commences with an orientation to the northwest and then turns 90° to the southwest after ~13
1210    metres, subsequently extending progressively in a southward direction. The pes tracks of LXIU-
1211    O7 are mesaxonic and functionally tridactyl, with a mean length of 18.3 cm (Fig. 17). The
1212    average length/width ratio is 1.1, and the mean mesaxony is 0.24. In the well-preserved R6 and
1213    R13, it can be clearly observed that Digit III projects the farthest anteriorly, followed by digits II
1214    and IV. Each digit trace has a strong and blunt claw or ungual mark. A clear border between the
1215    heel and the three digits is absent; however, at times, the boundaries between digits or between
1216    digits and the heel area can be discerned . The mean interdigital divarication II–IV is 55°. The
1217    mean pace angulation of the LXIU-O7 trackway is 161°. The pes tracks predominantly exhibit
1218    outward rotation, with an average deviation of 23° from the trackway axis. Within the trackway,
1219    O7-R11, L12, R12, and L13 represent the location of the change of direction, and the outward
1220    rotation angles of them were 17°, -58°, 25°, and -8° separately. From R11, there is a notable
1221    decrease in stride length from 114.8 cm to 86.8 cm, followed by a further decrease to 66.8 cm,
1222    after which it gradually recovers. From L12, pace angulation decreases from 154° to 102°, before
1223    recovering to 166°. In the aforementioned process, the trends of the track rotation angle and pace
1224    angulation were found to be largely consistent. These observations indicate a reduction in the
1225    speed of the trackmaker during changes in direction.
1226       The trackways LXIU-O2, O8, O10, O11, and O12 comprise the largest tracks observed on the
1227    same track layer (Figs. 15, 17; Supplementary Information 2; Table 6). Of these, O8 is the largest,

1228 with an average track length of 44.5 cm, while the other trackways range from 31.1 to 39.5 cm in
1229 length.
1230 The LXIU-O2 trackway preserves only two tracks, forming a single step (Fig. 15). The mean
1231 length of these tracks is 31.1 cm, with an average length/width ratio of 0.9 and a mean mesaxony
1232 of 0.24. The interdigital divarication of digit II-IV is 59°. Among them, L1 contains a manus
1233 track on the lateral side of digits III and IV, which represents about 6 cm in length, with a L/W
1234 ratio of 0.4. However, as the sediment filled L1, forming a unweathered natural cast, the true
1235 morphology of the specimen remains uncertain.
1236 The preservation of LXIU-O8 is rather limited (Fig. 15). Although the average length is
1237 known to be 44.5 cm, a considerable number of ectomorphic distortions affect this measurement.
1238 The average pace angulation of the LXIU-O8 trackway is 160°. The best preserved track in O8 is
1239 O8-L3, with a length of 36.9 cm, which can be assumed to represent the true size of LXIU-O8.
1240 The length/width ratio of L3 is 1.2, and the mean mesaxony is ~0.3. O8-L1 preserves a manus
1241 track on the lateral side of digits III and IV, which is ~7.6 cm in length, with the L/W ratio of 0.6.
1242 Given the similarity of the pace angulation to that observed in other ornithopod trackways and
1243 the presence of a manus track, it can be posited that this rather limited preserved trackway still
1244 has strong ornithopod affinities. The L/W ratio of R7 and R8 reaches 1.8-1.9, which is a
1245 relatively uncommon elongation-related distortion observed in ornithopod tracks. This may have
1246 resulted from either sliding due to slippery sediments or as partial metatarsal impressions.
1247 The large heel traces are also evident in LXIU-O11 and can be classified into two categories:
1248 wide and narrow (Fig. 15). The type with wider heels is exemplified by O11-L1 and L7, both of
1249 which exhibit a L/W ratio of 2.1. The elongated heel of L7 is approximately three times as long
1250 as the anterior part of the track, and the proximal section is similar in width to the distal end. The
1251 distal end preserves recognisable tridactyls. The presence of triple elongated digit traces with
1252 identifiable claw traces anteriorly is indicative of a substrate that is slippery. This can be
1253 observed in the case of the theropod track from the Middle Jurassic of the Turpan Basin,
1254 Xinjiang (Xing et al., 2014c). Nevertheless, the digits of LXIU-O11-L7 have not been separated
1255 as in theropod tracks. The type with narrower heels includes O11-R1, L2 and R6. These tracks
1256 exhibit a markedly constricted heel, with the proximal end measuring between one-half to one-
1257 third the width of the distal end. These morphologies are comparable to those observed in
1258 metatarsal impressions commonly associated with tridactyl theropod tracks or basal ornithischian
1259 tracks.
1260 LXIU-O10 trackway preserved 20 footprints, and tridactyl morphology was observed in 90%
1261 of the footprints (Figs. 15, 17). These tracks are functionally tridactyl, with a mean length of 35.9
1262 cm and an average length/width ratio of 1.1. The mean mesaxony is 0.28, and interdigital
1263 divarication II–IV is 53°. There is no clear boundary between the heel and the three digits. The
1264 digits II and IV are almost equal in length. Each digit trace features a prominent and blunt claw
1265 or ungual mark. The average pace angulation of the LXIU-O10 trackway is 155°. The pes traces
1266 demonstrate outward and inward rotation, with an average deviation of 8° from the trackway axis.
1267

1268     The LXIN site preserves 48 ornithopod tracks and a number of isolated tracks (Figs. 18, 19;
1269 Supplementary Information 3; Table 6), the former including LXIN-O1-O48, ranging in length
1270 from 9 cm to 48.8 cm. The preservation of the ~296 tracks is rather limited, and most of them
1271 can only be identified by trackway features. Only a few tracks have clear diagnostic features.
1272     Some of the better preserved tracks and specific trackways are described below (Fig. 18).
1273     LXIN-O1 consists of six tracks, and only LXIN-O1-R3 has identifying features (Fig. 18A). R3
1274 has a length of 33.9 cm, with an L/W ratio of 1.2 and a mesaxony of 0.42. The interdigital
1275 divarication of digits II-IV is 50°, and there is a distinct border between the heel and the three
1276 digits. The digits II-IV are almost equal in length. Each digit has a strong and blunt claw or
1277 ungual mark. The average angulation of the LXIN-O1 tracks is 167°.
1278     LXIN-O2 consists of nine tracks and only LXIN-O2-R7 has the diagnostic characteristics (Fig.
1279 18B). O2-R7 is 18.7 cm long, with an L/W ratio of 0.8 and a mesaxony of 0.23. The interdigital
1280 divarication of digits II-IV is 67° and there is a very clear border between the heel and the three
1281 digits. Digits II and IV are almost equal in length, digit III is about 1/2 the length of the two
1282 lateral digits. Each digit has a strong and blunt claw or ungual mark. The average pace
1283 angulation of LXIN-O2 is 131°, which is the lowest for that track point, which may represent a
1284 very slow walking gait.
1285     LXIN-O11 and O48 are very close together and intersect to form a single very short pseudo-
1286 trackway (Fig. 18C). Only O11-L2 has some valid features, such as the presence of three
1287 relatively well defined toes with a heel. This interlaced trackway requires special care in
1288 identification. Overall, the group activity trackways are relatively consistent in their track lengths
1289 and step/stride length ratios.
1290     LXIN-O12 is a poorly preserved turning trackway (Fig. 18D), and the trackmaker of this
1291 trackway was probably influenced by the large ornithopod LXIN-O13, which began to turn as it
1292 approached O13-L1 (detailed figure see Supplementary Information 3). From O12-L3 the
1293 trackway turns about 90°. In contrast to the usual decrease in stride length during the change of
1294 direction, the stride length of LXIN-O12 shows an increasing trend, gradually increasing from
1295 53.7 cm at L1 to 83.6 cm at L3 and decreasing to 68.8 cm at the end of the turn. Due to poor
1296 preservation of the tracks, the rotation angles could not be confirmed.
1297     LXIN-O28 contains six tracks forming a discontinuous trackway with one missing in the
1298 middle (Fig. 18F). R2 and L2 are fairly well preserved with typical tridactyl morphology (Fig.
1299 19). These two functionally tridactyl tracks with a mean length at 19.3 cm, with the average
1300 length/width ratio of 1.0 and the mean mesaxony of 0.30. The interdigital divarication of digits
1301 II–IV is 50°. There is a clear boundary between the digits, whereas the boundary between the
1302 digits and the heel is blurred. The digits II and IV are almost the same length. Each digit has a
1303 strong and blunt claw or ungual mark. The average pace angulation of LXIN-O28 trackway is
1304 149°. The pes traces show an average outward rotation of 16° from the trackway axis.
1305     LXIN-O41 contains eight tracks with an average length of 25 cm, an L/W ratio of 1.2 and a
1306 mesaxony of 0.42, with no clear boundary between the heel and the three digits (Fig. 18E). The
1307 average pace angulation of LXIN-O41 trackway is 164°. Superimposed tracks are probably

1308 present in both the manus track of L1 and the pes tracks of R1 and R2. The superimposed manus
1309 tracks were displaced laterally, while the superimposed pes tracks moved towards the centre of
1310 the trackway. Tracks of almost equal size appeared over a distance considerably smaller than the
1311 track width. This indicates a high frequency of trampling and may suggest that the trackmaker
1312 may have been injured. The latter possibility is more likely than the slipperiness of the ground, as
1313 neither LXIN-O41 nor the other nearby trackways showed sliding tracks or metatarsal marks.
1314     Only two well-preserved tracks can be found on the slab from LXIE site (Fig. 19), which are
1315 in the similar orientation and forming a short trackway LXIE-O1. In which only O1-R1 is
1316 complete, with 21.5 cm in length,14.7 cm in length, and forming L/W ratio of 1.5. The
1317 divarication angle of digit II–IV is 46°, with a mesaxony of 0.27. The incomplete L1 with only
1318 the anterior part can compare to R1 in width and mesaxony.

### *Comparison and discussion*

1320 After the revisions by Lockley et al. (2014c) and Díaz-Martínez et al. (2015) and Xing et al.
1321 (2024b), the number of ichnogenera belonging to Iguanodontipodidae is quite reduced. The most
1322 controversial is "Ornithopodichnus" (Kim et al., 2009), which was originally defined in Korea
1323 and has been used to describe the transversely elongated ornithopod tracks with particularly
1324 flattened anterior triangle from NE Asia exclusively. The latest view considered that
1325 "Ornithopodichnus" is a *nomen dubium* (Xing et al. 2024b), but this does not rule out whether
1326 some of the well-preserved tracks from "Ornithopodichnus" can be considered as a valid
1327 ichnospecies in *Caririchnium*.
1328     *Caririchnium* (Leonardi, 1984) is widely distributed in Berriasian–Albian sediments in Brazil,
1329 Portugal, Spain, England, Switzerland, South Korea, Canada, Japan, China, and the USA, with
1330 the upper limit of this geological period slightly earlier than the Longxiang age (Cenomanian).
1331 The Longxiang specimens fit the diagnosis of *Caririchnium*: pes tracks belonging to
1332 Iguanodontipodidae, with a large heel impression that is rounded, centered and wide (wider than
1333 the width of the proximal part of the digit III impression); short, wide digit impressions (Díaz-
1334 Martínez et al., 2015). Longxiang specimens have a wide range of sizes, which is common in the
1335 *Caririchnium*. The ratio between the length and width of the "heel" pad varies between
1336 ichnospecies. In general, pes tracks are as wide as or wider than long. The size is highly variable,
1337 with common pes tracks between 30 and 60 cm long (Leonardi, 1987; Meyer and Thuring, 2003;
1338 Xing et al., 2007; Razzolini et al., 2017), but there may be smaller or larger examples (e.g.
1339 Lockwood et al., 2014; Xing and Lockley, 2016; Xing et al., 2018c; Lee et al., 2023).
1340     *Caririchnium* currently includes *C. magnificum* (Leonardi, 1984), *C. kortmeyeri* (Currie and
1341 Sarjeant, 1979), *C. billsarjeanti* (Meyer and Thüring, 2003), *C. lotus* (Xing et al., 2007, 2015),
1342 and *C. yeongdongensis* (Kim et al., 2016), a total of five ichnospecies. Among these
1343 ichnospecies, the morphology of the manus tracks is very distinctive and useful to differentiate
1344 between ichnospecies: elliptical, rectangular, and cloverleaf-like subtriangular (Leonardi, 1987;
1345 Meyer and Thuring, 2003; Xing et al., 2007; Kim et al., 2016). There is limited information on
1346 the morphology of the manus tracks in the Longxiang specimens, but they are essentially
1347 elliptical, making them similar to *C. lotus* as a whole (Xing et al., 2007, 2015).

1348    The *Caririchnium* lotus in the Longxiang tracksite extends the chronological range of this
1349    ichnogenus into the early Late Cretaceous.
1350    The abundance of Longxiang *Caririchinium* illustrates a diverse range of ectomorphological
1351    distortion, which is likely caused by the presence of muddy or watery sediments. In this case,
1352    only a small proportion of tracks result in distinctly quartered tracks when the substrate is
1353    moderately strengthed. Such slippery substrate condition also causes the aformentioned
1354    elongated 'heels' in the tracks, and these additional traces can be devided into both wide and
1355    narrow patterns, possibly caused by sliding or as metatarsal impressions, as in LXIU-O11 (Fig.
1356    15). Additionally, some manus tracks are situated medially to the pes track, rather than laterally
1357    to the midpoint of digits III-IV (e.g., LXIN-O33-R2), which may also be indicative of the
1358    influence of a slippery substrate.
1359    It is also noteworthy that some specific behaviour-related features are present, including the
1360    occurrence of a large number of tracks in a limited area, forming a pattern similar to that of the
1361    manus pes-sets of quadruped trackways (e.g. LXIN-O17-L2 and O18-L1 in Fig. 19; Stevens et
1362    al., 2016). Some special trackways can also be observed, including LXIU-O4 (Fig. 16), which
1363    features a difference in the size of the right and left pes tracks; LXIU-O7 and LXIN-O12, which
1364    exhibit directional changes in the midst (Fig. 16); and LXIN-O41, which contains overlapping
1365    tracks that may have been left by injured individuals (Fig. 18E). Meanwhile, in the northwestern
1366    part of the LXIN site, the orientation of the small *Caririchnium* trackways is notably distinct,
1367    forming an assemblage that extends in an east-west direction. This observation aligns with the
1368    commonly documented hypothesis that the smaller trackmakers within this ichnogenus exhibit
1369    gregarious behaviour (e.g. Xing et al., 2015).
1370    ***Trackmaker***
1371    The trackmaker of *Caririchinium* is typically referred to the basal ornithopod, especially the
1372    basal ankylopollexian or styracosternan, that are comparable in sizes, and shares comparable
1373    temporal and spatial interval locally (Díaz-Martínez et al., 2015). For example, the early large
1374    *Caririchinium* from Upper Jurassic of Iberian Peninsula can be linked to *Oblitosaurus* with 6–7
1375    m in length (Sánchez-Fenollosa et al., 2023). However, the distribution of ornithopod tracks is
1376    much more extensive than their trackmakers (Noè et al., 2020; Sánchez-Fenollosa et al., 2023).
1377    For example, there is a paucity of large quadrupedal ornithopod skeletal remains, while large *C.*
1378    *magnificum* have been defined in Brazil (Bandeira et al., 2024). Although southeastern China
1379    also lacks contemporaneous ankylopollexian trackmakers (Xu et al., 2018), however, complete
1380    geographic barriers did not exist between South and North China during the Cretaceous
1381    theoretically (Ke and Meng, 2009). There are large basal ankylopollexian in China that are
1382    contemporaneous with or earlier than the Longxiang *Caririchinium*, including *Lanzhousaurus*
1383    from Gansu (NW; You et al., 2005), and *Bayannurosaurus* from Inner Mongolia (NW; Xu et al.,
1384    2018); basal hadrosaurids including *Bolong* from Liaoning (NE; Wu and Godefroit, 2012) and
1385    *Equijubus* from Gansu (You et al., 2003). At the same time, given that the pes track compared in
1386    size to *Camptosaurus* (~5 m) pes is more than 20 cm (~25 cm in estimation) in length, and which
1387    to *Brachylophosaurus* (~10 m) pes may reach 60 cm in length (Gierliński and Karol, 2008; Paul,

1388    2024), it can thus be postulated that the large trackmaker of Longxiang *Caririchnium* may be

1389    similar in size to the above taxa from lower Cretaceous in China, especially the basal

1390    ankylopollexians among them.

1391    ***Speed Estimates***

1392    For estimating hip height (h), Thulborn (1990) suggests that for large ornithopods (track

1393    length >25 cm) h=5.9 × foot length, and for small ornithopods (track length <25 cm) h=4.8 ×

1394    foot length. The velocity of the trackmakers are estimated by the formula of Alexander (1976),

1395    and the relative speed (gait) are represented by stride length (SL)/h. For the large Longxiang

1396    ornithopods, the relative speed range from 0.67 to 1.48, suggesting a walking gait, and the speed

1397    of the trackmakers is estimated to be between 2.12 and 6.73 km/h (Table 7). For the smaller

1398    trackmakers, the relative speed range from 0.6 to 2.17, suggesting a walking to slow-running gait,

1399    and the speed of the trackmakers is estimated to be between 1.26-10.44 km/h. The evidence

1400    suggests that smaller ornithopods display a greater degree of bipedalism in their locomotory

1401    behaviour, which is relatively independent of factors such as body weight and limb proportions.

1402    This allows them to achieve higher speeds, as evidenced by the skeletal records (Maidment et al.,

1403    2014; Barrett and Maidment, 2017).

1404    Furthermore, among the Longxiang large *Caririchnium* trackways, three of them indicate a

1405    relatively greater speed of slightly over 2 (2.06-2.17), including LXIU-O9, LXIN-O6 and LXIN-

1406    O22 (Supplementary Information 3). These constitute 7% of the total 45 large ornithopod

1407    trackways. This particular slow-running gait is uncommon among *Caririchnium* and other large

1408    ornithopod ichnogenera. On the contrary, two other tracksites that also preserve a substantial

1409    number of *Caririchnium* tracks in China, including the Lower Cretaceous Zhaojue site (Xing et

1410    al., 2014a) and the Mid-Cretaceous Lotus site from Sichuan (Xing et al., 2015). In these cases,

1411    the related trackways all exhibit a walking gait.

1412    With regard to the track layer of the LXIU site, it can be posited that the relative speed of the

1413    trackways with clearly quartered tracks would have been slightly higher than that of the other

1414    poorly preserved trackways. This may indicate that substrate condition (e.g. water content)

1415    affected the speed of the trackmakers, as previously mentioned. However, on the track layer of

1416    the LXIU site, the majority of tracks are poorly preserved, and the trackmakers can still reach

1417    slow-running gait, thereby indicating that there is no prominent positive correlation between the

1418    speed of the trackmakers and the moderately featured or hardened substrate.

1419

1420    ***Didactyl tracks***

1421    The LXIU-T1 and T3 trackways in the LXIU site are didactyl trackways, which are typically

1422    interpreted as deinonychosaurian trackways (Fig. 20).

1423    The average length of LXIU-T1 is approximately 11 cm, and it can be classified within the

1424    ichnogenus *Velociraptorichnus* (Niu and Xing, 2023). The T3 tracks are markedly larger,

1425    measuring ~36 cm in length. They have been classified as a new ichnotaxon, *Fujianipus*, and

1426    represent the largest troodontid deinonychosaurian track documented to date (Xing et al., 2024a).

1427    These two trackways will not be discussed further in this paper. Some isolated tracks, such as

1428 LXIU-TI10 could be compared to LXIU-T1 in track size and the snout, paralleled digit III-IV

1429 and the pointed mark of digit II, and can also suggest an *cf. Velociraptorichnus* affinity.

1430     It is interesting to note that, this kind of reliable didactyl morphotype only exist in LXUI site,

1431 even the LXI sites share the similar track surface. This phenomenon is difficult to attribute

1432 entirely to preservation bias related to the trackmaker's body size. After all, the LXIN site

1433 contains a greater number of tiny (<10 cm) ornithopod trackways and also features isolated small

1434 tridactyl theropod tracks (grallatorid). In contrast, large-sized tridactyl theropod tracks are

1435 noticeably less common at the LXIU site compared to the LXIN site. This may suggest that the

1436 activity ranges of the two major types of theropod trackmakers were either non-overlapping or

1437 had only limited overlap. At the very least, smaller didactyl theropods may have actively avoided

1438 entering the activity range of the numerous larger tridactyl trackmakers with stronger pes.

1439

1440 ### *Possible large didactyl tracks*

1441 **Description and comparison.** In the site LXID, the trackway LXID-T2 comprises four

1442 consecutive tracks and exhibits a distinctive feature among theropod tracks (Fig. 21; Table 8).

1443 The depth of the T2 tracks is notably shallower than that of the majority of tracks in the same

1444 layer. This may indicate that the T2 tracks are likely to be undertracks, yet they still exhibit some

1445 discernible morphological and trackway characteristics. The trackway LXID-T2 comprises

1446 functionally didactyl, digitigrade pes tracks. The average length of the tracks is 53.4 cm, with an

1447 L/W ratio of 3.8. The trace of digit II is either absent or present as an oval imprint proximally. In

1448 contrast, the traces of digits III and IV are essentially parallel (with a divarication angle of

1449 approximately 15°), and their lengths are similar, resulting in low mesaxony. The anterior

1450 margin of each digit trace exhibits sharp claw marks. The tracks exhibit minimal rotation from

1451 the trackway axis, with an average pace angulation of 179°.

1452     In the most well-preserved track in the LXID-T2, T2-R1, can be observed that digit III has

1453 four phalangeal pads, or three phalangeal pads and one rounded clow mark. The length of digit

1454 III is 51.9 cm, while which of digit IV measures 52.1 cm. The proximal ends of digits III and IV

1455 exhibit a minimal metatarsophalangeal area. The L1 only preserves the impressions of digit III

1456 and digit IV, which have a length of 50.8 and 53.6 cm, respectively. It is possible that the R2

1457 may preserve the impression of digit II, which is ~17.6 cm in length, and the impressions of digit

1458 III and digit IV are ~50.3 and 45.5 cm in length, respectively. The digit II trace is isolated, with

1459 the digit II depression situated posteromedial to the margin of digit III. The L2 has only one

1460 overall oval impression.

1461     LXID-T2 is comparable to typical deinonychosaur tracks, which are currently classified into

1462 six ichnogenera (*Velociraptorichnus, Dromaeopodus, Dromaeosauripus, Menglongipus,*

1463 *Sarmientichnus* and *Fujianipus*) (Xing et al., 2024a). The length of 53.4 cm in LXID-T2 is

1464 undoubtedly significantly larger than all current ichnogenera and unclassified species. In a recent

1465 review, the largest and most conclusive didactyl track was identified as *Fujianipus* (36.4 cm),

1466 while the probable isolated didactyl troodontid track from Nanxiong (Guangdong, China) was

1467 found to be 39 cm in length. Among the didactyl morphotypes represent deinonychosaurian

1468    affinities, it is noteworthy that both the *Fujianipus* and Nanxiong tracks exhibit clear troodontid
1469    affinities with relatively short, laterally extended digit IV (Xing et al., 2024a). In contrast, the
1470    largest record of typical dromaeosaur-type tracks is that of *cf. Dromaeopodus* (29.8 cm) from the
1471    Mid Cretaceous, Gulin (Sichuan, China; Xing et al., 2016). The R1 and L1 tracks of LXID-T2
1472    exhibit morphological similarities to digit-only *Dromaeosauripus hamanensis* (Kim et al., 2008)
1473    and *D. jinjuensis* from Korea (Kim et al., 2012), with strong, elongated, parallel, and almost
1474    equal lengths of digit III and IV.
1475        The insufficiency in the details of LXID-T2 is somewhat reminiscent of specially preserved
1476    tracks, such as the possibility as flattened tracks of large *cf. Dromaeopodus* (Xing et al., 2013;
1477    Lockley and Xing 2015). It is also possible that the vague margins indicate that the tracks may be
1478    undertracks. Furthermore, while the LXID-T2 tracks lack sufficient detail to provide definitive
1479    morphological traits, their large size is also reminiscent of bipedal ornithopod tracks from the
1480    same site. Nevertheless, the LXID-O1 tracks, which are approximately 40 cm in length, do not
1481    exhibit the parallel and nearly equal lengths of the digits observed in the LXID-T2 tracks; the
1482    almost straight trackway of LXID-T2 tracks (pace angulation=179°) is also larger than that of the
1483    aforementioned LXID-O1 (pace angulation=161°), which is more akin to a theropod-type
1484    trackway.
1485        It is notable that, though lacking the signs of kick-of scours in classic swimming tracks
1486    (McAllister and Kirby, 1998), the feature of low divarication angle, the lack of heel, and the
1487    combination of rounded posterior region and awl-shaped anterior part could also be referred to
1488    non-pointed punting-related swimming tracks (Romilo et al., 2013; Navarro-Lorbés et al., 2023).
1489    The absence of digit II and the proximal linkage of digit III and IV may related to the lateral
1490    rotation of the hip/pelvic girdle (Milàn, 2006; Tanaka, 2021). However, like previously discussed
1491    in 4.2.3, the complete absence of heel traces (including the posteriorly supporting digit I in the
1492    bird-like tracks, see Tanaka (2021)) can be hardly interpreted by certain origin, so we merely
1493    retain the possibility of a *cf. Dromaeopodus* affinity of LXID-T2.
1494    **Speed Estimates.** Under the assumption that LXID-T2 is of deinonychosaurian trackmaker
1495    origin, the ratio based on hip-height/foot-length (h/Fl) ratio is 4.32 for dromaeosaurids as
1496    proposed by Tsukiji et al. (2021). In contrast, the standard equation for estimating hip height in
1497    small/medium theropods is $h = 3.06 FL^{1.14}$ (Weems, 2006). In the case of the LXID-T2 tracks,
1498    the estimated average hip height could be 2.3 m or 2.85 m, depending on the equation used. Xing
1499    et al. (2024a) proposed that the length of digit III and deinonychosaurian body length is 5.11%
1500    on average, and the body length of LXID-T2 track maker would be estimated as at least 9.98 m.
1501    **Trackmaker.** The estimated size of LXID-T2 trackmaker is not only dramatically larger than
1502    which of the troodontid *Fujianipus* (~5 m), but also than the skeletal records of large members
1503    from Dromaeosauridae, including *Utahraptor ostrommaysorum* from Utah (Molina-Peréz and
1504    Larramendi, 2016), measuring 4.65 to 6 m in length and 1.5 m in hip height; *Dakotaraptor steini*
1505    from Dakota (DePalma et al. 2015), measuring 4.35 to 6 m in length and 1.4 m in hip height;
1506    *Austroraptor cabazai* from Argentina (Novas et al., 2009), measuring up to ~6 m and 1.5 m in
1507    hip height; and the asian *Achillobator giganticus* from Mongolia (Perle, 1999), measuring 3.9 to

1508 5 m in length and 1.25 m in hip height. All the end-members of estimated size are from Molina-
1509 Pérez et al. (2019) and Paul (2024), the smaller records are from the former; the hip height
1510 estimations are from Molina-Pérez et al. (2019). Among them, the overlapping of the temporal
1511 range of the Shaxian Formation (*Fujianipus*) and Bayan Shireh Formation (*A. giganticus*)
1512 thereby rendering a biogeographic distribution from Mongolia to southeastern China entirely
1513 feasible for different clades within deinonychosaurians to become such considerable size (Xing
1514 et al., 2024a).
1515 The morphological characteristics of LXID-T2 and *Fujianipus* trackmaker are entirely distinct,
1516 with the former displaying clear dromaeosaur-like,equal and paralleled digits III and IV. The
1517 discovery of additional specimens of the LXID-T2 morphological type would constitute
1518 significant evidence of the gigantism of dromaeosaurid deinonychosaurs, whose body size is
1519 undoubtedly at the top of the local food chain.
1520 It is important to note that, however, the digit III-body length proportion provided by Xing et
1521 al. (2024a) does not encompass the length of the drag mark in the average-preserved footprints,
1522 which occurs in LXID-T2. However, it should be noted that this is not necessarily representative
1523 of the true length of digit III. With regard to track width, LXID-T2 is marginally shorter than that
1524 of *Fujianipus* (Xing et al., 2024a), and longer than those of large *Dromaeopodus*, which measure
1525 ~30 cm in length (Xing et al., 2016). Furthermore, the estimation exclusively considered well-
1526 preserved small deinonychosaurians (Xing et al., 2024a) and lacked a sufficient number of large,
1527 complete, and referable deinonychosaurian specimens. In conclusion, when considered as a
1528 deinonychosaurian, the LXID-T2 trackmakers are likely to be smaller than the aforementioned
1529 estimation, but still fall within the range of large deinonychosaurian, which may reach 5 to 6 m.
1530 Besides, for the speed of the trackmaker, the relatively short stride lengths of LXID-T2
1531 trackway is indicative of a trotting gait, with SL/h ratios between 1.9 and 2.35, which is
1532 consistent with the trackways of *Velociraptorichnus* isp. and *Fujianipus* from the Longxiang site.
1533 According to the formula proposed by Alexander, the estimated speeds of the trackways are
1534 13.93 km/h and 17.86 km/h, respectively.
1535

1536 **Dinosaur tracks indet.**
1537 The LXII site contains three isolated tracks with fairly limited preservation (Fig. 8), with a
1538 preservation status of level 0 on the Belvedere and Farlow (2016) scale. Of the three isolated
1539 tracks, LXII-TI1 is 21.6 cm long with an L/W ratio of 1.4, while the other two tracks are 28.8
1540 and 26.1 cm long with fairly high L/W ratios of 2.0 and 2.3. LXII-TI1 is the first track found in
1541 the Longxiang area, and the edge of the track has a distinctive displacement rim. It is
1542 morphologically a possible tridactyl track, although only one lateral and one median digit have
1543 been preserved. Because of the relatively high L/W ratio, these tracks may have a stronger
1544 affinity to theropod tracks.
1545

1546 **Discussion**
1547 Due to the formation of southeastern coastal mountains and the correlated volcanism (Cao, 2018),

1548   northern Guangdong and southern Jiangxi share more similarities in topography and overall

1549   climatic change with the Fujian region among SE China during mid-Cretaceous (Chen, 2000; Li

1550   et al., 2013; Wang et al., 2022). In contrast, the Zhejiang region, which is relatively close to the

1551   northern part of the mountain range, is more similar, at least during the Cenomanian-Turonian

1552   period, to the more northerly Jiangsu region, which is not covered by the mountain range (Yu,

1553   2013; Wang et al., 2022). ,

1554      In the aforementioned mountainous area, with the exception of the Zhejiang region, which is

1555   less affected by the mountains, only Fujian and Jiangxi have dinosaur records in the mid-

1556   Cretaceous of SE China, specifically in the Shanghang and Ganzhou basins, respectively (Xing

1557   et al., 2019, 2024a; Niu and Xing, 2023). However, the fossil record of Jiangxi is and the mid-

1558   Cretaceous record is limited to one ankylosaurid, *Datai* (Xing et al., 2023), one possible

1559   medium-sized tyrannosaurid track (~7.5 m for the trackmaker; Xing et al., 2019), and some

1560   small-sized tridactyl theropod (?oviraptorosaur) tracks in Ganzhou Basin (LX personal

1561   observation). The relatively scarce of Cenomanian-Turonian dinosaur record make Longxiang

1562   tracksite in Fujian is an important mid-Cretaceous fossil locality.

1563   **The summary of Longxiang sites ichnofauna**

1564   Among the aforementioned morphotypes, small (<40 cm) *Brontopodus*−like tracks from

1565   sauropods; the majority of Theropod morphotype A (*Eubrontes* isp.) from large-sized tridactyle

1566   theropods, and some smaller, isolated tracks similar in outline (*cf. Eubrontes*) may originate from

1567   a small theropod trackmaker with a similar body plan to *Eubrontes*; Theropod morphotype B (*cf.*

1568   *Eubrontes*) very possible from (medium- to) large-sized tridactyle theropods, and *cf.*

1569   *Dromaeosauripus* and *Velociraptorichnu*s from large/small deinonychosaurian; two types of

1570   *Caririchnium* isp. from the medium- to large-sized/small-sized (""Ornithopodichnus""-like)

1571   ornithopods respectively the has been reported by Niu and Xing (2023), while medial- to large

1572   sized *Eubrontes* tracks from LXIN, large (>60 cm) *Brontopodus*−like trackway from LXIN, and

1573   a possible large didactyl trackway from LXID has been newly distinguished in this paper.

1574   Furthermore, additional specimens belong to highly digitigrade *cf. Eubrontes*. from LXIN,

1575   *Caririchnium* isp. from LXID and LXIN has been discovered on the basis of Niu and Xing (2023)

1576   (The distribution of size and morphotype see Supplementary Information 4).

1577      Among these tracksites, ornithopod, sauropod and theropod tracks can be identified in LXIII

1578   sites, but only LXI sites (main track surface) have recognisable trackways. The tracks of all

1579   major dinosaur clades have been found in LXI and LXIII sites, except for the sauropod tracks in

1580   LXID. However, within each clade, despite some degree of size variation, the morphotypes

1581   covered by numerous trackways and isolated footprints remain relatively uniform. This may be

1582   partially attributed to the prevalent deformation observed in the tracks from the Longxiang site,

1583   as well as behavioral variations within the same trackway (e.g., transitions between semi-

1584   digitigrade and digitigrade postures), which hinder further classification based on finer

1585   morphological details. Nevertheless, this also suggests, at least within this region, that aside from

1586   the presence of large deinonychosaurians, the trackmakers within each clade were likely

1587   morphologically homogeneous overall.

1588     Certain ornithopod tracks classified in *Caririchnium* are the most prevalent in all LXI sites,
1589     representing 84% of all trackways and 89%, 57% and 76% of the tracks from LXIN, LXID and
1590     LXIU, respectively. Large trackways (≥25 cm) account for 19%, 25% and 62% of the trackways
1591     from the above three sites within *Caririchnium* morphotype respectively, and very large ones
1592     reaching ~40 cm occurs in LXIN (5) and LXIU (3) (Table 1). The largest ornithopod trackway in
1593     LXIU is even comparable in size to the sauropod trackway in terms of pes length. This suggests
1594     that contemporaneous large consumers in the region were probably concentrated in ornithopods,
1595     i.e., that the relatively cooler (compared to lowland regions at the same latitude), at least
1596     seasonally dry, coastal plateau with mountain ranges acting as barriers during the mid-
1597     Cretaceous period in southeast China was suitable for these ankylopollexian survival (Chen,
1598     2000; Li et al., 2009; Lü et al., 2019; Zhang et al., 2021). Besides, it should be noted that for the
1599     three tracksites in LXI, particularly LXIN and LXIU areas, there is a difference in the size at
1600     which the mutation occurs in the ornithopod trackmaker. For the LXIN site, there is a clear gap
1601     between 32 and 41 cm, whereas for the LXIU site, this gap occurs between 19 and 26 cm. For
1602     the LXIN site, there is a clear gap between 32 and 41 cm, whereas for the LXIU site, this gap
1603     occurs between 19 and 26 cm. For the entire LXI ornithopod trackways, track length
1604     predominantly falls within the small to medium size range, with peaks observed at 10–15 cm and
1605     20–25 cm, while a few tracks exceed 40 cm in length (Fig. 22A). In terms of track width, a
1606     unimodal distribution is evident, centering around 15–20 cm, with a noticeable trough in the 25–
1607     30 cm range (Fig. 22B). Based on statistical comparisons and morphological differences across
1608     different areas, the observed statistical discrepancy between track length and width likely results
1609     from variations in deformation patterns across different regions. Therefore, small- to medium-
1610     sized ornithopod tracks are considered as a single category in this study.
1611     Given that juveniles of large animals can occupy the niche of smaller ones (Lockley and Xing,
1612     2021; Schroeder et al., 2021; Wyenberg-Henzler et al., 2022), it can be posited that the
1613     discrepancy of the two track layers may be due to differences in the ontogenetic stage, rather
1614     than the variation in clade.

**1615 The regional comparison of mid-Cretaceous dinosaur fauna in SE China**

1616     The richest and the most continuous record of the mid-Cretaceous dinosaur fauna in SE China is
1617     found in Zhejiang (Fig. 3; Yu, 2013; Xi et al., 2019), and the timing of its faunal changes aligns
1618     with the sedimentary environment shifts reflected in the palynological records (Yu, 2013).
1619     In Zhejiang region, the skeletal record from the Early Cretaceous is sparse, consisting of only
1620     a few small to medium-sized hadrosaurioids and poorly preserved ankylosaurians. However, by
1621     the onset or early stages of the Cenomanian-Turonian, with a relative decrease in temperature
1622     and an increase in precipitation, a diverse assemblage of herbivorous dinosaurs began to appear
1623     in Zhejiang. Sauropods and possible therizinosaurids were the first to emerge in the region (Qian
1624     et al., 2012). In the later stages, despite a slight temperature rise, continued abundant
1625     precipitation was accompanied by a more diverse record of titanosauriforms and titanosaurs
1626     (Tang et al., 2001; Lü et al., 2008), as well as medium-sized pterosaurs and small turtle tracks
1627     (Wu et al., 2018). Notably, during Cenomanian-Turonian, the only suspected ornithischian

1628    record consists of two poorly detailed large ornithopod trackways (Wu et al., 2018), and

1629    ankylosaurian remains—present in earlier and later intervals—have yet to be identified.

1630    In the post-Turonian, Zhejiang and the neighboring Jiangsu region experienced further

1631    temporary warming and prolonged aridification. During this phase, sauropod skeletal and track

1632    remains disappeared entirely, replaced by a resurgence of ornithischians. This includes abundant

1633    ankylosaurians (Lü et al., 2007; Yu, 2013; Zheng et al., 2018), small basal ornithischians (Zheng

1634    et al., 2012), and possible small hadrosauroids. Among theropods, therizinosaurians and avians

1635    appear in the skeletal record, and fragmentary remains indicate the presence of both carnosaurs

1636    and coelurosaurians across multiple basins (Yu, 2013). Pterosaurs from this interval are also

1637    known from skeletal fossils (Unwin and Lü, 1997). Compared to the relatively scarce track

1638    fossils, post-Turonian strata contain egg fossils attributed to Macroelongatoolithus (up to 43 cm

1639    in length), Longatoolithus (10–17 cm in length), and Prismatoolithidae (size unknown) (Yu,

1640    2013). These oofamily records suggest that a diverse assemblage of maniraptorans, including

1641    troodontids, flourished in the region as arid conditions intensified.

1642    The fossil record from the Zhejiang region suggests that, despite being part of the same

1643    southeastern coastal mountain system, the Shanghang site—located further south and more

1644    strongly influenced by orographic barriers—did not experience a temporary dominance of

1645    sauropods during the Cenomanian-Turonian. Furthermore, it lacks a long-term ankylosaurian

1646    presence, which is consistently recorded in other stages of Zhejiang's fossil record. Notably,

1647    ankylosaurians also appeared in the adjacent Ganzhou Basin during the Turonian–early

1648    Coniacian (Xing et al., 2023).

1649    In comparison to other dinosaurs, including other ornithischians, ornithopods demonstrate a

1650    more pronounced and efficient high-fibre herbivory (Button et al., 2023). Additionally, the dental

1651    texture of this clade has been found to be significantly rougher in the Late Cretaceous period

1652    (Kubo et al., 2023). In the case of hadrosaurids, representatives of the ankylopollexia clade,

1653    which underwent distinct gigantism, the auxiliary abrasive capacity of their teeth has been

1654    further enhanced (Kubo et al., 2023). Concurrently, a comparable herbivorous homogenisation is

1655    observed in the latest Cretaceous global cooling process. During this process, hadrosaurids with

1656    more advantageous border herbivorous diets and larger feeding ranges occupied at least the

1657    ecological space of ankylosaurs and ceratopsians (Condamine et al., 2021). These may be

1658    contributing factors to the distinctive domination of large-sized ornithopod tracks at Longxiang

1659    sites in the Fujian region relative to Zhejiang, as the former experienced a more gradual climate

1660    change (cooling and changes in precipitation levels) during this period.

1661

1662    Another noteworthy feature of the Longxiang tracksite in southeastern China is its distinctive

1663    large didactyl track, which includes the *Fujianipus*. For the large deinonychosaurians record to

1664    date, with the exception of *Utahraptor* from the Hell Creek Formation (Pearson et al., 2002;

1665    DePalma et al., 2015), the remaining fauna lacks large tyrannosaurid or abelisaurid predators,

1666    which large deinonychosaurian all occur as currently discovered apex predators of contemporary

1667    terrestrial fauna (Novas et al., 2009; Tsuihiji et al., 2012; Kirkland et al., 2016; Rolando et al.,

1668  2021; Paul, 2024). Concurrently, the associated fauna also exhibits a paucity of large
1669  marginocephalians and giant (>15 m) macronarians (Paul, 2024).
1670      In terms of chronology and palaeogeography, the ichnofauna from Fujian is more closely
1671  related to the contemporaneous Bayan Shireh skeletal fauna from Mongolia. However,
1672  Longxiang site does not contain definitive large tridactyl theropod tracks as which from the pre-
1673  Albian or pre-CenomanianYanguoxia tracksite in NW China (>40 cm; Xing et al., 2018c,
1674  unpublished manuscript), which posited between Bayan Shireh and Longxiang sites. This may
1675  indicate that large deinonychosaurians dispersed in East Asia during the latest Early Cretaceous
1676  period, or that there was convergence in response to similar environments, including the partly
1677  comparable climate conditions and the lack of pre-existing large apex predators, such as
1678  tyrannosaurids (Brusatte et al., 2010; Xing et al., 2024a). The paucity of definite large theropod
1679  record except deinonychosaurians may be attributed to similar factors to those which led to the
1680  domination of ornithopods compared to Zhejiang fauna.
1681
1682      The absence of ankylosaurians at the Longxiang site may be attributed to the relative scarcity
1683  of contemporaneous tracksites in Fujian, leading to a preservation bias. However, the distinct
1684  proportions of sauropods and ornithischians—particularly ornithopods, and the early presence of
1685  large deinonychosaurian, likely reflect a fundamental difference in the Cenomanian-Turonian
1686  faunal composition between adjacent regions within SE China. This suggests that regional signal
1687  variations, rather than globally comparable climatic or ecological factors, may have had a greater
1688  influence on both the composition of local faunas in SE China and the preservation of their fossil
1689  record. Specifically, this influence appears to stem from the region's topography, with
1690  mountainous terrain playing a role in moderating temperature fluctuations (or creating refugia
1691  with a broader thermal range; Antonelli et al., 2018) and reducing peak precipitation levels. A
1692  detailed discussion of these effects is beyond the scope of this study and warrants further
1693  investigation in future research.
1694
1695  **Brief comparison with other mid-Cretaceous low-latitude dinosaur fauna and the**
1696  **environmental influence**
1697  Globally, the mid-Cretaceous period coincided with two oceanic anoxic events (OAE1 and
1698  OAE2), occurring during the Aptian–Albian and Cenomanian–Turonian periods, respectively
1699  (Schlanger and Jenkyns, 1976). During OAE2, average global temperatures reached their peak
1700  for the entire Cretaceous period (Forster et al., 2007; Jenkyns, 2010), and this interval also
1701  witnessed the Plenus Cold Event, a significant cooling episode evident in globally comparable
1702  carbon isotope records (Forster et al., 2007; O'Connor et al., 2020). During this period of
1703  extreme heat and climatic instability, dinosaur faunas were still widely recorded across low-
1704  latitude regions. In particular, extensive records exist from the northern Gondwanan landmasses,
1705  which dominated the continental deposits of these latitudes at the time. Notable examples include
1706  the Kem Kem Group in Morocco (Mannion and Barrett, 2013; Belvedere et al., 2013), the
1707  Candeleros Formation in Neuquén Basin of Argentina (lower Neuquén Group; Coria and

1708 Salgado, 2005; Tomaselli et al., 2021), and the lower Bauru Group in southern Brazil (Navarro et
1709 al., 2025).

1710 Beyond the Longxiang site, contemporaneous representative dinosaur-bearing formations
1711 from Laurasia include the Dakota Formation (Lockley et al., 1992; Lim et al., 2014) and the
1712 Woodbine Group (Noto et al., 2022) in the eastern and southern United States, and the
1713 Cenomanian－Turonian deposits of the Iberian Peninsula (Csiki-Sava et al., 2015). However,
1714 most dinosaur faunas from North America, Europe, and Africa during this interval are derived
1715 from coastal and island ecosystems that expanded due to the rising sea levels, whereas some of
1716 the South American records originate from fully continental deposits, making them more directly
1717 comparable to those of China.

1718 The most noticeable difference between the South America and East Asia during mid-
1719 Cretaceous lies in the fundamental composition of their Mesozoic faunas. In South America,
1720 which was located along the southwestern margin of Gondwana and had already separated from
1721 Gondwana in its southern part by the Late Cretaceous, small notosuchian mesoeucrocodylians,
1722 which first appeared before the late Early Cretaceous and became highly diverse after OAE2,
1723 played a significant role in the ecosystem (Pol and Leardi, 2015). In contrast, in East Asia, small
1724 dinosaur still occupied the similar niche occupied by notosuchian, with oviraptorosaurian
1725 theropods represented as prosperous herbivores and omnivores (Lü et al., 2016). Additionally, in
1726 terms of traditional herbivores, South America maintained a high degree of sauropod diversity
1727 (Tomaselli et al., 2021), while its ornithopods evolved towards more agile forms, leading to the
1728 emergence of a diverse assemblage of elasmarian ornithopods (Bandeira et al., 2024).
1729 Meanwhile, in East Asia, a substantial radiation of large hadrosaurioids had already begun in the
1730 Early Cretaceous (Xu et al., 2018).

1731 Additionally, there are significant differences between the two regions in terms of altitude,
1732 land-sea positioning, and relative temperature. During the mid-Cretaceous, particularly the
1733 Cenomanian-Turonian, the Fujian region (SE China), where the Longxiang site is located, was
1734 part of the previously mentioned linear mountain chains associated with an Andean-type
1735 subduction system. The overall regional temperature was notably lower than that of the mid-
1736 latitude hotspot regions in central South America (Scotese et al., 2025). However, despite
1737 differences in geological origins, both regions were generally arid (Scotese et al., 2025). It is
1738 important to note that, unlike South America—situated along the newly formed Atlantic Ocean
1739 with limited evaporative moisture supply (Stommel, 1957; Carvalho and Leonardi, 2024)—the
1740 aridity in part of the SE China was largely influenced by the aforementioned orographic barriers
1741 that restricted moisture transport. This likely resulted in variations in precipitation across
1742 different intermontane basins in Zhejiang and Fujian, depending on altitude and proximity to the
1743 ocean during the mid-Cretaceous. Locally sufficient precipitation (Wang et al., 2022), combined
1744 with montane environments that could provide relatively cooler habitats within small areas
1745 (Antonelli et al., 2018), may have facilitated the coexistence of morphologically competitive taxa
1746 capable of adapting to a wider range of ecological conditions.

1747 Returning to the discussion of faunal changes across different environments, the mid-

1748 Cretaceous terrestrial fossil records from South America, represented by the Bauru Group in
1749 Brazil and the Neuquén Basin in Argentina, reveal a strongly regionalized faunal turnover
1750 process during the Cenomanian-Turonian interval, which appears to be correlated with
1751 paleolatitude (Coria and Salgado, 2005; Navarro et al., 2025). At least part of these turnovers
1752 may reflect the impact of global climatic perturbations during OAE2, such as the temporally
1753 corresponding Plenus Cold Event (PCE) (Navarro et al., 2025). However, within the sedimentary
1754 terrestrial arc-related basins of SE China, current palynological evidence suggests that only the
1755 temperature variation records from the Jiangsu-Zhejiang region (e.g., Wang et al., 2022), located
1756 beyond the northern boundary of the mountain range, can be correlated with OAE2-related
1757 marine events.
1758    Besides, from the perspective of dinosaur fauna, the primary herbivorous taxa in the Jiangsu-
1759 Zhejiang region differ significantly from those reported at the Longxiang site in Fujian. Given
1760 that skeletal fossils from Zhejiang prior to the Cenomanian, though limited, still include records
1761 of small- to medium-sized ornithopods—comparable to those at the Longxiang site—it can be
1762 hypothesized that the faunal composition within SE China was relatively consistent before the
1763 Cenomanian. If this assumption holds, the Longxiang site represents a record that did not
1764 undergo a fundamental faunal turnover. While in the Zhejiang region, faunal transitions during
1765 relatively extreme climatic periods were temporary, and groups that had not completely migrated
1766 out of the area would return relatively quickly when climatic conditions became favorable for
1767 their activity.
1768    Moreover, although precise geochronological data for Cretaceous terrestrial strata in China
1769 remain scarce, some patterns can still be observed. At the Cenomanian-Turonian boundary, the
1770 temperature variation trends inferred from palynoflora appear to be the exact opposite of the
1771 overall marine temperature changes associated with OAE2 (Forster et al., 2007; Yu, 2013; Wang
1772 et al., 2022), despite the expected increase in precipitation. Given the currently low precision of
1773 the available data, it can only be speculated that these environmental and faunal differences, if
1774 driven by changes in marine conditions, might result from a delayed response to OAE2 or an
1775 amplification of the Plenus Cold Event (PCE) due to certain regional factors.
1776    The example from the coastal region in SE China provides partial insight into how the
1777 orographic barrier effect of local mountain ranges may have partly reshaped basin conditions on
1778 the leeward side, potentially overriding the influence of global marine-driven events. This
1779 hypothesis requires further validation through high-resolution paleoenvironmental
1780 reconstructions based on palynological and isotopic evidence across the various arc-related
1781 basins of SE China, as discussed earlier.
1782

## Conclusions

1784 New material of dinosaur tracks and trackways form Longxing (LX) tracksites in mid-
1785 Cretaceous of Shanghang Basin, Fujian, China are reported in this paper on the basis of earlier
1786 researches of the similar site. New medial- to large-sized theropod tracks with diverse
1787 ectomorphological variations from LXIN site, large (>60 cm) *Brontopodus*−like trackway from

1788 LXIN site, and a possible large didactyl trackway from LXID site has been newly distinguished,
1789 and *Caririchnium* isp. from LXID, LXIN and LXIE has been newly discovered.

1790 The Longxing tracksite is confirmed to be dominated by ankylopollexian ornithopod
1791 trackways (> 84%), with a proportion of large members within ornithopod (> 27% over 25 cm in
1792 length) , and indicates the flourishing of large ornithopods among the herbivores occurring
1793 within this period. The Longxiang sites also demonstrate the presence of concurrent, distinct,
1794 large didactyl tracks, which diverge from the dominated apex predators in most late Cretaceous
1795 fauna.

1796 The Longxiang tracksite represents the only extensive mid-Cretaceous dinosaur tracksite in
1797 southeastern China, providing a temporal comparison with the mid-Cretaceous skeletal record of
1798 Zhejiang (SE China) and Mongolia in East Asia. Compared to the Zhejiang region, which
1799 belongs to the southeastern coast mountains and exhibits a continuous faunal succession, the
1800 Longxiang site not only differs significantly in the richness of its fossil record but also in its
1801 herbivorous composition. The herbivore assemblage at Longxiang appears more closely aligned
1802 with pre-Cenomanian faunas of Zhejiang that before significant climatic changes.

1803 Globally, among contemporaneous dinosaur faunas, the terrestrial assemblages of central
1804 South America provide a more suitable comparison to those of southeastern China. Based on
1805 current fossil evidence and associated chronological data, faunal turnover in both the Longxiang
1806 site and Zhejiang appears to have been relatively mild, with faunal compositions recovering
1807 rapidly when climatic conditions reverted. Furthermore, the observed changes in faunal
1808 composition and timing do not align directly with the OAE2. Instead, they may correspond to a
1809 mid-OAE2 cooling event followed by the PCE warming phase, lacking records of the initial
1810 warming phase.

1811 These findings suggest that the mid-Cretaceous faunas of southeastern China and the
1812 preservation of their fossil records were shaped primarily by regional factors—such as
1813 topographic barriers created by mountainous landscapes, the correlated diverse habitats, and
1814 volcanic activity in adjacent intervals—rather than by related to changes in marine conditions,
1815 globally climatic or ecological drivers. Further research is necessary to refine the understanding
1816 of these regional influences, and improve the temporal framework of faunal changes in SE
1817 China..

1818

1822

## Data Availability Statement
1824 The supplementary information files (Supplementary information 1-4) including the raw data
1825 that support the findings of this study are openly available in Dryad at
1826 https://doi.org/10.5061/dryad.rjdfn2znd.

1827

## References

Ahrens, J., Geveci, B., Law, C., Hansen, C., Johnson, C., 2005. 36-paraview: An end-user tool for large-data visualization. The visualization handbook, 717, pp.50038-1.

Antonelli, A., Kissling, W.D., Flantua, S.G., Bermúdez, M.A., Mulch, A., Muellner-Riehl, A.N., Kreft, H., Linder, H.P., Badgley, C., Fjeldså, J., Fritz, S.A., 2018. Geological and climatic influences on mountain biodiversity. Nature Geoscience, 11(10), pp.718-725.

Antonelli, M., Petti, F.M., Conti, J., Sacco, E., Petruzzelli, M., Spalluto, L., Wagensommer, A., 2023. Lower Cretaceous dinosaur footprints from the Molfetta tracksite (Apulia, southern Italy). Cretaceous Research, 142, p.105388.

Bai, B., Meng, J., Zhang, C., Gong, Y.X., Wang, Y.Q., 2020. The origin of Rhinocerotoidea., phylogeny of Ceratomorpha (Mammalia, Perissodactyla). Communications Biology, 3(1), p.509.

Bandeira, K.L., Navarro, B.A., Pêgas, R.V., Brilhante, N.S., Brum, A.S., de Souza, L.G., da Silva, R.C., Gallo, V., 2024. A reassessment of the historical fossil findings from Bahia State (Northeast Brazil) reveals a diversified dinosaur fauna in the Lower Cretaceous of South America. Historical Biology, pp.1-42.

Barco, J.L., Canudo, J.I., Ruiz-Omenaca, J.I., 2006. New data on *Therangospodus oncalensis* from the Berriasian Fuentesalvo tracksite (Villar del Río, Soria, Spain): an example of gregarious behaviour in theropod dinosaurs. Ichnos, 13(4), pp.237-248.

Barrett, P.M., Maidment, S.C., 2017. The evolution of ornithischian quadrupedality. Journal of Iberian Geology, 43(3), pp.363-377.

Belvedere, M., Jalil, N.E., Breda, A., Gattolin, G., Bourget, H., Khaldoune, F., Dyke, G.J., 2013. Vertebrate footprints from the Kem Kem beds (Morocco): A novel ichnological approach to faunal reconstruction. Palaeogeography, Palaeoclimatology, Palaeoecology, 383, pp.52-58.

Belvedere, M, Farlow, J.O. 2016. A numerical scale for quantifying the quality of preservation of vertebrate tracks. In: Falkingham PL, Marty D, Richter A, editors. Dinosaur tracks—the next steps. Bloomington and Indianapolis: Indiana University Press; p. 92–98.

Belvedere, M., Castanera, D., Meyer, C.A., Marty, D., Mateus, O., Silva, B.C., Santos, V.F., Cobos, A., 2019. Late Jurassic globetrotters compared: A closer look at large and giant theropod tracks of North Africa and Europe. Journal of African Earth Sciences, 158, p.103547.

Blazquez, A.P., Mocho, P., Escaso, F., Ortega, F., 2024. Evolution of hind limb morphology of Titanosauriformes (Dinosauria, Sauropoda) analyzed via 3D Geometric Morphometrics reveals wide-gauge posture as an exaptation for gigantism. eLife, 13.

Brusatte, S.L., Benson, R.B., Xu, X., 2010. The evolution of large-bodied theropod dinosaurs during the Mesozoic in Asia. Journal of Iberian Geology, 36(2), pp.275-296.

Button, D.J., Porro, L.B., Lautenschlager, S., Jones, M.E., Barrett, P.M., 2023. Multiple pathways to herbivory underpinned deep divergences in ornithischian evolution. Current Biology, 33(3), pp.557-565.

Calvo, J.O., Mazzetta, G.V., 2004. Nuevos hallazgos de huellas de dinosaurios en la Formación

1868    candeleros (albiano-Cenomaniano), Picún leufú, Neuquén, Argentina. Ameghiniana, 41(4),
1869        pp.545-554.
1870    Calvo, J.O., Rivera, C., 2018. Huellas de dinosaurios en la costaoeste del embalse Ezequiel
1871        Ramos Mexía y alrededores (Cretácico Superior, Provincia de Neuquén, República
1872        Argentina). Bol. Soc. Geol. Mex. 70 (2), 449e497.
1873    Campos-Soto, S., Tessier, B., Mouazé, D., Benito, M.I., Quijada, I.E., Suarez-Gonzalez, P., 2025.
1874        Formation and preservation of vertebrate tracks in semi-liquid sediments: Insights from
1875        tidal flats and laboratory experiments. Sedimentology, 72(1), pp.5-33.
1876    Cao, K., 2018. Cretaceous terrestrial deposits in China. China Geology, 1(3), pp.402-414.
1877    Carvalho, I.D.S., Leonardi, G., 2024. Dinosaur Tracks of Mesozoic Basins in Brazil.
1878    Castanera, D., Pascual, C., Razzolini, N.L., Vila, B., Barco, J.L., Canudo, J.I., 2013.
1879        Discriminating between medium-sized tridactyl trackmakers: tracking ornithopod tracks in
1880        the base of the Cretaceous (Berriasian, Spain). PloS one, 8(11), p.e81830.
1881    Castanera, D., Colmenar, J., Sauque, V., Canudo, J.I., 2015. Geometric morphometric analysis
1882        applied to theropod tracks from the Lower Cretaceous (Berriasian) of Spain. Palaeontology,
1883        58(1), pp.183-200.
1884    Castanera, D., Piñuela, L., García-Ramos, J.C., 2016. *Grallator* theropod tracks from the Late
1885        Jurassic of Asturias (Spain): ichnotaxonomic implications. Spanish Journal of
1886        Palaeontology, 31(2), pp.283-296.
1887    Castanera, D., Silva, B.C., Santos, V.F., Malafaia, E., Belvedere, M., 2020. Tracking Late
1888        Jurassic ornithopods in the Lusitanian Basin of Portugal: ichnotaxonomic implications. Acta
1889        Palaeontologica Polonica, 65(2), pp.399-412.
1890    Charvet, J., Lapierre, H., Yu, Y., 1994. Geodynamic significance of the Mesozoic volcanism of
1891        southeastern China. Journal of Southeast Asian Earth Sciences, 9(4), pp.387-396.
1892    Chen, P.J., 1979. An outline of Palaeogeography during the Jurassic and Cretaceous periods of
1893        China-with a discussion on the origin of Yantze River. Acta Scientiarum Naturalium
1894        Universitatis Pekinensis, 3(9), 90-109.
1895    Chen, P.J., 2000. Paleoenvironmental changes during the Cretaceous in eastern China. In
1896        Developments in palaeontology., stratigraphy (Vol. 17, pp. 81-90). Elsevier.
1897    Chen, R., Wang, M., Dong, L., Zhou, G., Xu, X., Deng, K., Xu, L., Zhang, C., Wang, L., Du, H.,
1898        Lin, G., 2025. Earliest short-tailed bird from the Late Jurassic of China. Nature, 638(8050),
1899        pp.441-448.
1900    Chen, S., Lin, C., Xu, W., Zhao, J. 2020. Age and Tectonic Significance of Volcanic Rocks in
1901        Cretaceous Red Beds in Fujian. Editorial Committee of Earth Science-Journal of China
1902        University of Geosciences, 45(7):2508-2523
1903    Chen, Y., 2008. Late Cretaceous sedimentary responses to the "Coast Range" and
1904        Paleoclimatechanges in Southeast China. Chengdu University of Technology. Master
1905        Thesis. 59pp
1906    Christiansen, P., 1999. Scaling of the limb long bones to body mass in terrestrial mammals.
1907        Journal of morphology, 239(2), pp.167-190.

1908 Cignoni, P., Callieri, M., Corsini, M., Dellepiane, M., Ganovelli, F., Ranzuglia, G., 2008.
1909     MeshLab: an Open-Source Mesh Processing Tool. Sixth Eurographics Italian Chapter
1910     Conference; Eds V. Scarano, R. De Chiara, U. Erra. Salerno, Italy; p. 129–136.
1911 Cobos, A., Lockley, M.G., Gasco, F., Royo–Torres, R., Alcala, L., 2014. Megatheropods as apex
1912     predators in the typically Jurassic ecosystems of the Villar del Arzobispo Formation
1913     (Iberian Range, Spain). Palaeogeography, Palaeoclimatology, Palaeoecology, 399, pp.31-41.
1914 Compilation Committee of Geological Atlas of China, 2002. Geological Atlas of China.
1915     Geological publishing house, Beijing, p. 348.
1916 Condamine, F.L., Guinot, G., Benton, M.J., Currie, P.J., 2021. Dinosaur biodiversity declined
1917     well before the asteroid impact, influenced by ecological., environmental pressures. Nature
1918     Communications, 12(1), p.3833.
1919 Coria, R.A., Salgado, L., 2005. Mid-Cretaceous turnover of saurischian dinosaur communities:
1920     evidence from the Neuquén Basin.
1921 Cross, M.C., Hohenberg, P.C., 1993. Pattern formation outside of equilibrium. Reviews of
1922     modern physics, 65(3), p.851.
1923 Csiki-Sava, Z., Buffetaut, E., Ősi, A., Pereda-Suberbiola, X., Brusatte, S.L., 2015. Island life in
1924     the Cretaceous-faunal composition, biogeography, evolution, and extinction of land-living
1925     vertebrates on the Late Cretaceous European archipelago. ZooKeys, (469), p.1.
1926 Dalla Vecchia, F., 2000. New dinosaur track sites in the Albian (Early Cretaceous) of the Istrian
1927     Peninsula (Croatia). Università di Padova.
1928 DePalma, R.A., Burnham, D.A., Martin, L.D., Larson, P.L., Bakker, R.T., 2015. The first giant
1929     raptor (Theropoda: Dromaeosauridae) from the hell creek formation. Paleontological
1930     Contributions, 2015(14), pp.1-16.
1931 Diaz-Martinez, I., Pereda-Suberbiola, X., Perez-Lorente, F., Canudo, J.I., 2015. Ichnotaxonomic
1932     review of large ornithopod dinosaur tracks: temporal and geographic implications. PloS one,
1933     10(2), p.e0115477.
1934 Du, T.M., H. Wu, X.S. Jin, G.Z. Jin, Y.M. Sheng. 2015. The features of footprint fossils from
1935     Guanyintang Village, Yiwu City, Zhejiang Province and the suggestions for protection.
1936     Research of Natural History and Museum 2: 54–60.
1937 Endo, H., Yoshida, M., Nguyen, T.S., Akiba, Y., Takeda, M., Kudo, K., 2019.
1938     Three-dimensional CT examination of the forefoot and hindfoot of the hippopotamus and
1939     tapir during a semiaquatic walking. Anatomia, histologia, embryologia, 48(1), pp.3-11.
1940 Falkingham, P.L., Gatesy, S.M. 2014. The birth of a dinosaur footprint: Subsurface 3D motion
1941     reconstruction and discrete element simulation reveal track ontogeny. PNAS 111(51):
1942     18279–18284
1943 Farlow, J.O., 1989. Brotopodus birdi Lower Cretaceous sauropod footprints from the US Gulf
1944     coastal plain. Dinosaur tracks and traces.
1945 Farlow, J.O., Gatesy, S.M., Holtz Jr, T.R., Hutchinson, J.R., Robinson, J.M., 2000. Theropod
1946     locomotion. American Zoologist, 40(4), pp.640-663.
1947 Forster, A., Schouten, S., Moriya, K., Wilson, P.A., Sinninghe Damsté, J.S., 2007. Tropical

1948      warming and intermittent cooling during the Cenomanian/Turonian oceanic anoxic event 2:
1949      Sea surface temperature records from the equatorial Atlantic. Paleoceanography, 22(1).

1950   Foster, J.R., Harris, J.D., Milner, A.R., Bordy, E.M., Sciscio, L., Castanera, D., Belvedere, M.,
1951      Xing, L., Lockley, M.G., 2024. Jurassic vertebrate tracks and traces. In Vertebrate
1952      Ichnology (pp. 265-478). Elsevier.

1953   Fujian Institute of Geological Survey, 2016. The Regional Geology of China, Fujian Province.
1954      Geological Publishing House, Beijing (in Chinese). 976pp

1955   Gatesy, S.M., Middleton, M.K., Jenkins, Jr.F.A., Shubin, N.H. 1999. Three–dimensional
1956      preservation of foot movements in Triassic theropod dinosaurs. Nature, 399: 141–144.

1957   Gierliński, G., Karol, S., 2008. Stegosaurian footprints from the Morrison Formation of Utah and
1958      their implications for interpreting other ornithischian tracks. Oryctos, 8, p.29.

1959   Gierlinski, G., Niedzwiedzki, G., Pienkowski, G., 2001. Gigantic footprint of a theropod
1960      dinosaur in the Early Jurassic of Poland. Acta Palaeontologica Polonica, 46(3).

1961   Gonzalez Riga, B.J., Calvo, J.O., 2009. A new wide-gauge sauropod track site from the Late
1962      Cretaceous of Mendoza, Neuquén Basin, Argentina. Palaeontology, 52(3), pp.631-640.

1963   Gu, Z., 2005. Conventions of Language. J. Stratigr. 29 (1), 1–48.

1964   Gutarra, S., Stubbs, T.L., Moon, B.C., Heighton, B.H., Benton, M.J., 2023. The locomotor
1965      ecomorphology of Mesozoic marine reptiles. Palaeontology, 66(2), p.e12645.

1966   Haubold, H., Klein, H., 2000. Die dinosauroiden Fährten Parachirotherium–Atreipus–*Grallator*
1967      aus dem unteren Mittelkeuper (Obere Trias: Ladin, Karn,? Nor) in Franken: The
1968      dinosauroid trackways parachirotherium–atreipus–*grallator* from the Lower Middle Keuper
1969      (Upper Triassic: Ladinian, Carnian,? Norian) of Frankonia (Germany). In Hallesches
1970      Jahrbuch für Geowissenschaften. Reihe B, Geologie, Paläontologie, Mineralogie (Vol. 22, p.
1971      59).

1972   Henderson, D.M., 2006. Burly gaits: centers of mass, stability, the trackways of sauropod
1973      dinosaurs. Journal of Vertebrate Paleontology, 26(4), pp.907-921.

1974   Henderson, D.M., 2015. A wide-gauge, large-mammal trackway from the upper Paleocene of
1975      Alberta, Canada. Canadian Journal of Earth Sciences, 52(8), pp.696-700.

1976   Hendricks, A., 1981. Die Saurierfährte von Münchehagen bei Rehburg-Loccum (NW-
1977      Deutschland). Westfälisches Landesmuseum für Naturkunde.

1978   Hildebrand, M., 1989. The quadrupedal gaits of vertebrates. BioScience, 39(11), p.766.

1979   Holtz Jr, T.R., 1995. The arctometatarsalian pes, an unusual structure of the metatarsus of
1980      Cretaceous Theropoda (Dinosauria: Saurischia). Journal of vertebrate Paleontology, 14(4),
1981      pp.480-519.

1982   Hu, L., 1990. A Magnetostratigraphic Study of Cretaceous Red Beds From Shanghang, Western
1983      Fujian.Geology of Fujian, 1: 33-42 (in Chinese with English abstract).

1984   Hunt, A.P., Lucas, S.G., 2024. An Overview of the Ichnology of Moa Tracks and Other Traces
1985      from the Late Cenozoic of New Zealand, In: Taylor,L.H., Raynolds, R.G., Lucas, S.G. eds.,
1986      2024, Vertebrate Paleoichnology: A Tribute to Martin Lockley. New Mexico Museum of
1987      Natural History and Science Bulletin, 95.

1988 Hutchinson, J.R., 2021. The evolutionary biomechanics of locomotor function in giant land
1989     animals. Journal of Experimental Biology, 224(11), p.jeb217463.
1990 Israelachvili, J.N., 2011. Intermolecular and surface forces. Academic press.
1991 Jenkyns, H.C., 2010. Geochemistry of oceanic anoxic events. Geochemistry, Geophysics,
1992     Geosystems, 11(3).
1993 Ke, C., Meng, W., 2009. Constraints of sedimentary records on Cretaceous paleoclimate
1994     simulation in China mainland. Earth Science Frontiers, 16(5), pp.29-36.
1995 Kim, J.Y., Lockley, M.G., 2012. New sauropod tracks (Brontopodus pentadactylus ichnosp. nov.)
1996     from the Early Cretaceous Haman Formation of Jinju Area, Korea: implications for
1997     sauropods manus morphology. Ichnos, 19(1-2), pp.84-92.
1998 Kirkland, J., Suarez, M., Suarez, C., Hunt-Foster, R., 2016. The Lower Cretaceous in east-central
1999     Utah—the Cedar Mountain Formation., its bounding strata. Geology of the Intermountain
2000     West, 3, pp.101-228.
2001 Klein, H., Gierliński, G.D., Oukassou, M., Saber, H., Lallensack, J.N., Lagnaoui, A., Hminna, A.,
2002     Charrière, A., 2023. Theropod and ornithischian dinosaur track assemblages from Middle to?
2003     Late Jurassic deposits of the Central High Atlas, Morocco. Historical Biology, 35(3),
2004     pp.320-346.
2005 Kubo, T., Kubo, M.O., Sakamoto, M., Winkler, D.E., Shibata, M., Zheng, W., Jin, X., You, H.L.,
2006     2023. Dental microwear texture analysis reveals a likely dietary shift within Late
2007     Cretaceous ornithopod dinosaurs. Palaeontology, 66(6), p.e12681.
2008 Lallensack, J.N., van Heteren, A.H., Wings, O., 2016. Geometric morphometric analysis of
2009     intratrackway variability: a case study on theropod and ornithopod dinosaur trackways from
2010     Münchehagen (Lower Cretaceous, Germany). PeerJ, 4, p.e2059.
2011 Lallensack, J.N., Ishigaki, S., Lagnaoui, A., Buchwitz, M., Wings, O., 2018. Forelimb
2012     orientation., locomotion of sauropod dinosaurs: insights from the? Middle Jurassic
2013     Tafaytour tracksites (Argana Basin, Morocco). Journal of Vertebrate Paleontology, 38(5),
2014     p.e1512501.
2015 Lallensack, J.N., Engler, T., Barthel, H.J., 2020. Shape variability in tridactyl dinosaur footprints:
2016     the significance of size and function. Palaeontology, 63(2), pp.203-228.
2017 Lallensack, J.N., Falkingham, P.L., 2022. A new method to calculate limb phase from trackways
2018     reveals gaits of sauropod dinosaurs. Current Biology, 32(7), pp.1635-1640.
2019 Lamanna, M.C., Casal, G.A., Martínez, R.D., Ibiricu, L.M., 2020. Megaraptorid (Theropoda:
2020     Tetanurae) partial skeletons from the Upper Cretaceous Bajo Barreal Formation of central
2021     Patagonia, Argentina: implications for the evolution of large body size in Gondwanan
2022     megaraptorans. Annals of Carnegie Museum, 86(3), pp.255-294.
2023 Leonardi, G., Carvalho, I., 2021. Dinosaur tracks from Brazil: a lost world of Gondwana.
2024     Indiana University Press.
2025 Leonardi, G., 1984. Le impronte fossili di Dinosauri. In: Bonaparte, J.F., Colbert, E.H., Currie,
2026     P.J., de Ricqlès, A.J., Keilan-Jaworowska, Z., Leonardi, G., Morello, F. (Eds.), Sulle Orme
2027     dei Dinosauri. Erizzo Editrice, Venice, pp. 164e186.

2028 Leonardi, G., 1987. Glossary and Manual of Tetrapod Footprint Ichnology. Ministry of Mines
2029     and Energy, Brasilia, Brazil, p. 75.

2030 Li, J., 1997. Stratigraphy (Lithostratic) of Fujian province. Wuhan: China University of
2031     Geosciences Press, 216.

2032 Li, J., Zhang, Y., Dong, S., Johnston, S.T., 2014. Cretaceous tectonic evolution of South China:
2033     A preliminary synthesis. Earth-Science Reviews, 134, pp.98-136.

2034 Li, X., Chen, S., Cao, K., Chen, Y., Xu, B., Ji, Y., 2009. Paleosols of the mid-cretaceous: a
2035     report from Zhejiang., Fujian, SE China. Earth Science Frontiers, 16(5), pp.63-70.

2036 Li, X., Xu, W., Liu, W., Zhou, Y., Wang, Y., Sun, Y., Liu, L., 2013. Climatic and environmental
2037     indications of carbon and oxygen isotopes from the Lower Cretaceous calcrete and
2038     lacustrine carbonates in Southeast and Northwest China. Palaeogeography,
2039     Palaeoclimatology, Palaeoecology, 385, pp.171-189.

2040 Liang, S., Cao, B., Ma, A., 1992. On the chronogensis and correlation of Cretaceous red beds in
2041     Fujian province. Geology of Fujian, 11(4), 263-282.

2042 Lim, J.D., Kim, K.S., Gierlinski, G., 2014. A bonanza of new tetrapod tracksites from the
2043     Cretaceous Dakota Group, western Colorado: implications for paleoecology. Fossil
2044     Footprints of Western North America: Bulletin 62, 62, p.393.

2045 Lockley, M.G., Xing, L., 2015. Flattened fossil footprints: implications for paleobiology.
2046     Palaeogeography, Palaeoclimatology, Palaeoecology, 426, pp.85-94.

2047 Lockley, M.G., Xing, L., 2021. A review of the non-avian theropod track record and the
2048     implications for the Ontogenetic Niche Shift model. Earth-Science Reviews, 220, p.103715.

2049 Lockley, M.G., Hunt, A., Holbrook, J., Matsukawa, M., Meyer, C., 1992. The dinosaur freeway:
2050     a preliminary report on the Cretaceous megatracksite, Dakota Group, Rocky Mountain front
2051     range, and high plains, Colorado, Oklahoma and New Mexico. Rocky Mountain Section
2052     (SEPM).

2053 Lockley, M.G., Farlow, J.O., Meyer, C.A., 1994. *Brontopodus* and *Parabrontopodus* ichnogen.
2054     nov., the significance of wide-and narrow-gauge sauropod trackways. Gaia, 10, 135–145.

2055 Lockley, M.G., Meyer, C., dos Santos, V.F., 1998a. *Megalosauripus* and the problematic concept
2056     of megalosaur footprints. GAIA: revista de geociências, 15, p.313.

2057 Lockley, M.G., Meyer, C., Moratalla, J.J., 1998b. *Therangospodus*: trackway evidence for the
2058     widespread distribution of a Late Jurassic theropod with well-padded feet. Gaia: revista de
2059     Geociencias, (15), p.339.

2060 Lockley, M.G., Wright, J., White, D., Matsukawa, M., Jianjun, L., Lu, F., Hong, L., 2002. The
2061     first sauropod trackways from China. Cretaceous Research, 23(3), pp.363-381.

2062 Lockley, M.G., Wright, J.L., Thies, D., 2004. Some observations on the dinosaur tracks at
2063     Münchehagen (Lower Cretaceous), Germany. Ichnos, 11(3-4), pp.261-274.

2064 Lockley, M.G., Lires, J., García-Ramos, J.C., Pinuela, L., Avanzini, M., 2007. Shrinking the
2065     world's largest dinosaur tracks: Observations on the ichnotaxonomy of Gigantosauropus
2066     asturiensis and *Hispanosauropus* hauboldi from the Upper Jurassic of Asturias, Spain.
2067     Ichnos, 14(3-4), pp.247-255.

2068  Lockley, M.G., Cart, K., Martin, J., Milner, A.R., 2011a. New theropod tracksites from the
2069      Upper Cretaceous "Mesaverde" Group, western Colorado: implications for
2070      ornithomimosaur track morphology. New Mexico Museum of Natural History and Science
2071      Bulletin, 53, pp.321-329.
2072  Lockley, M.G., Gierlinski, G.D.,Lucas, S.G., 2011b. *Kayentapus* Revisited: Notes on the Type
2073      Materialand the Importance of This Theropod Footprintichnogenus. Fossil Record 3:
2074      Bulletin 53, 53, P.330.
2075  Lockley, M.G., Gierlinski, G.D., Dubicka, Z., Breithaupt, B.H., Matthews, N.A., 2014b. A
2076      preliminary report on a new dinosaur tracksite in the Cedar Mountain Formation
2077      (Cretaceous) of eastern Utah. New Mexico Museum of Natural History and Science,
2078      Bulletin, 62, pp.279-285.
2079  Lockley, M.G., Xing, L., Kim, J.Y., Matsukawa, M., 2014a. Tracking Lower Cretaceous
2080      dinosaurs in China: a new database for comparison with ichnofaunal data from Korea, the
2081      Americas, Europe, Africa and Australia. Biological Journal of the Linnean Society, 113(3),
2082      pp.770-789.
2083  Lockley, M.G., Xing, L., Lockwood, J.A., Pond, S., 2014c. A review of large Cretaceous
2084      ornithopod tracks, with special reference to their ichnotaxonomy. Biological Journal of the
2085      Linnean Society, 113(3), pp.721-736.
2086  Lockley, M.G., Li, J., Xing, L., Guo, B., Matsukawa, M., 2018. Large theropod and small
2087      sauropod trackmakers from the Lower Cretaceous Jingchuan Formation, Inner Mongolia,
2088      China. Cretaceous Research, 92, pp.150-167.
2089  Lockley, M.G., Breithaupt, B., Matthews, N., Shibata, K., Hunt-Foster, R., 2021. A preliminary
2090      report on an Early Jurassic *Eubrontes*-dominated tracksite in the Navajo formation at the
2091      Mail Station Dinosaur Tracksite,eastern Utah. New Mexico Museum of Natural History and
2092      Science Bulletin, 82: 195–208.
2093  Lü, B., Liu, X., Guo, H., Zheng, X., Chen, Z., He, M., Zhao, G., 2014. The cretaceous strata in
2094      Danxia of Yong'an in Fujian province. Journal of Shandong Normal University (Natural
2095      Science), 29(4), 78-84.
2096  Lü, B., Liu, X.M., Guo, H., 2019. Magnetic properties of the cretaceous Shaxian formation
2097      stratum in Fujian province and their environmental significance. Acta Sedimentologica
2098      Sinica, 37(03), pp.519-531.
2099  Lü, J., Azuma, Y., Chen, R., Zheng, W., Jin, X., 2008. A new titanosauriform sauropod from the
2100      early Late Cretaceous of Dongyang, Zhejiang Province. Acta Geologica Sinica-English
2101      Edition, 82(2), pp.225-235.
2102  Lü, J., Chen, R., Brusatte, S.L., Zhu, Y., Shen, C., 2016. A Late Cretaceous diversification of
2103      Asian oviraptorid dinosaurs: evidence from a new species preserved in an unusual posture.
2104      Scientific Reports, 6(1), p.35780.
2105  Lü, J., Jin, X., Sheng, Y., Li, Y., Wang, G., Azuma, Y., 2007. New nodosaurid dinosaur from the
2106      late cretaceous of Lishui, Zhejiang Province, China. Acta Geologica Sinica-English Edition,
2107      81(3), pp.344-350.

2108 Maidment, S.C., Bates, K.T., Falkingham, P.L., VanBuren, C., Arbour, V., Barrett, P.M., 2014.
2109     Locomotion in ornithischian dinosaurs: an assessment using three-dimensional
2110     computational modelling. Biological Reviews, 89(3), pp.588-617.
2111 Mannion, P.D., Barrett, P.M., 2013. Additions to the sauropod dinosaur fauna of the Cenomanian
2112     (early Late Cretaceous) Kem Kem beds of Morocco: palaeobiogeographical implications of
2113     the mid-Cretaceous African sauropod fossil record. Cretaceous Research, 45, pp.49-59.
2114 Mannion, P.D., Upchurch, P., 2010. A quantitative analysis of environmental associations in
2115     sauropod dinosaurs. Paleobiology, 36(2), pp.253-282.
2116 Marchetti, L., Belvedere, M., Voigt, S., Klein, H., Castanera, D., Díaz-Martínez, I., Marty, D.,
2117     Xing, L., Feola, S., Melchor, R.N., Farlow, J.O., 2019. Defining the morphological quality
2118     of fossil footprints. Problems and principles of preservation in tetrapod ichnology with
2119     examples from the Palaeozoic to the present. Earth-Science Reviews, 193, pp.109-145.
2120 Marty D. 2008. Sedimentology, taphonomy, and ichnology of Late Jurassic dinosaur tracks from
2121     the Jura carbonate platform (Chevenez–Combe Ronde tracksite, NW Switzerland): insights
2122     into the tidal-flat palaeoenvironment and dinosaur diversity, locomotion, and palaeoecology
2123     [dissertation]. [Fribourg (Switzerland)]: University of Fribourg. GeoFocus 21.
2124 Marty, D., Belvedere, M., Meyer, C.A., Mietto, P., Paratte, G., Lovis, C., Thuering, B., 2010.
2125     Comparative analysis of Late Jurassic sauropod trackways from the Jura Mountains (NW
2126     Switzerland) and the central High Atlas Mountains (Morocco): implications for sauropod
2127     ichnotaxonomy. Historical Biology, 22(1-3), pp.109-137.
2128 Marty, D., Belvedere, M., Razzolini, N.L., Lockley, M.G., Paratte, G., Cattin, M., Lovis, C.,
2129     Meyer, C.A., 2018. The tracks of giant theropods (*Jurabrontes* curtedulensis ichnogen. &
2130     ichnosp. nov.) from the Late Jurassic of NW Switzerland: palaeoecological &
2131     palaeogeographical implications. Historical Biology, 30(7), pp.928-956.
2132 Masrour, M., Lkebir, N., Pérez-Lorente, F., 2017. Anza palaeoichnological site. Late Cretaceous.
2133     Morocco. Part II. Problems of large dinosaur trackways and the first African
2134     Macropodosaurus trackway. Journal of African Earth Sciences, 134, pp.776-793.
2135 Matsukawa, M., Lockley, M., Jianjun, L., 2006. Cretaceous terrestrial biotas of East Asia, with
2136     special reference to dinosaur-dominated ichnofaunas: towards a synthesis. Cretaceous
2137     Research, 27(1), pp.3-21.
2138 Mazin, J.M., Hantzpergue, P., Olivier, N., 2017. The dinosaur tracksite of Plagne (early
2139     Tithonian, Late Jurassic; Jura Mountains, France): the longest known sauropod trackway.
2140     Geobios, 50(4), pp.279-301.
2141 McAllister, J.A., Kirby, J., 1998. An occurrence of reptile subaqueous traces in the Moenkopi
2142     Formation (Triassic) of Capitol Reef National Park, south central Utah, USA. National Park
2143     Service, Technical Report, 98(1), pp.45-49.
2144 Melchor, R.N., Rivarola, D.L., Umazano, A.M., Moyano, M.N., Belmontes, F.R.M., 2019.
2145     Elusive Cretaceous Gondwanan theropods: The footprint evidence from central Argentina.
2146     Cretaceous Research, 97, pp.125-142.
2147 Meyer, C.A., Marty, D., Belvedere, M., 2018. Titanosaur trackways from the late cretaceous el

2148        molino Formation of Bolivia (Cal orck'o, sucre). In Annales Societatis Geologorum
2149        Poloniae (Vol. 88).
2150  Meyer, C.A., Belvedere, M., Englich, B., Lockley, M.G., 2021a. A reevaluation of the Late
2151        Jurassic dinosaur tracksite Barkhausen (Wiehengebirge, Northern Germany). PalZ, 95(3),
2152        pp.537-558.
2153  Meyer, C.A., Marty, D., Thüring, B., Thüring, S., Belvedere, M., 2021b. The Late Cretaceous
2154        dinosaur track record of Bolivia–Review and perspective. Journal of South American Earth
2155        Sciences, 106, p.102992.
2156  Milàn, J., 2006. Variations in the morphology of emu (Dromaius novaehollandiae) tracks
2157        reflecting differences in walking pattern and substrate consistency: ichnotaxonomic
2158        implications. Palaeontology, 49(2), pp.405-420.
2159  Molina-Pérez, R., Larramendi, A., Connolly, D., Cruz, G.Á.R., 2019. Dinosaur facts., figures:
2160        The theropods and other dinosauriformes. Princeton University Press.
2161  Moreau, J.D., Trincal, V., Fara, E., Baret, L., Jacquet, A., Barbini, C., Flament, R., Wienin, M.,
2162        Bourel, B., Jean, A., 2019. Middle Jurassic tracks of sauropod dinosaurs in a deep karst
2163        cave in France. Journal of Vertebrate Paleontology, 39(6), p.e1728286.
2164  Moreno, K., Benton, M.J., 2005. Occurrence of sauropod dinosaur tracks in the Upper Jurassic of
2165        Chile (redescription of Iguanodonichnus frenki). Journal of South American Earth Sciences,
2166        20(3), pp.253-257.
2167  Navarro, B.A., Giaretta, A.A., Fernandes, M.A., Carvalho, A.B., Zaher, H., 2025. First dinosaur
2168        ichnofauna from the Bauru Group indicates Cenomanian–Turonian events led to an
2169        'Ornithischian Hiatus' in the Upper Cretaceous of Southeast Brazil. Cretaceous Research,
2170        168, p.106075.
2171  Navarro-Lorbés, P., Díaz-Martínez, I., Valle-Melón, J.M., Rodriguez-Miranda, A., Moratalla,
2172        J.J., Ferrer-Ventura, M., San Juan-Palacios, R., Torices, A., 2023. Dinosaur swim tracks
2173        from the Lower Cretaceous of La Rioja, Spain: An ichnological approach to non-common
2174        behaviours. Cretaceous Research, 147, p.105516.
2175  Niedźwiedzki, G., Pieńkowski, G., 2016. A dinosaur track assemblage from the Upper
2176        Hettangian (Lower Jurassic) marginal-marine deposits of Zapniów, Holy Cross Mountains,
2177        Poland. Geological Quarterly, 60(4), pp.840-856.
2178  Niu, K., Xing, L., 2023. The first dinosaur track assemblages from the Upper Cretaceous
2179        Shaxian Formation, Fujian Province, southeastern China. Cretaceous Research, 146,
2180        p.105486.
2181  Noè, L.F., Gómez–Pérez, M., Rodríguez, J.V., Corrales–García, A., Caranton–Mateus, W.G.,
2182        2020. Dinosaur footprints from the Lower Cretaceous, Batá Formation, Colombia (South
2183        America), the possible interchange of large ornithopods between southern Laurasia.,
2184        northern Gondwana. The Geology of Colombia, 2, pp.375-401.
2185  Noto, C.R., D'Amore, D.C., Drumheller, S.K., Adams, T.L., 2022. A newly recognized theropod
2186        assemblage from the Lewisville Formation (Woodbine Group; Cenomanian) and its
2187        implications for understanding Late Cretaceous Appalachian terrestrial ecosystems. PeerJ,

2188        10, p.e12782.

2189    Novas, F.E., Agnolín, F.L., Ezcurra, M.D., Porfiri, J., Canale, J.I., 2013. Evolution of the
2190        carnivorous dinosaurs during the Cretaceous: the evidence from Patagonia. Cretaceous
2191        Research, 45, pp.174-215.

2192    Novas, F.E., Pol, D., Canale, J.I., Porfiri, J.D., Calvo, J.O., 2009. A bizarre Cretaceous theropod
2193        dinosaur from Patagonia and the evolution of Gondwanan dromaeosaurids. Proceedings of
2194        the Royal Society B: Biological Sciences, 276(1659), pp.1101-1107.

2195    O'Connor, L.K., Jenkyns, H.C., Robinson, S.A., Remmelzwaal, S.R., Batenburg, S.J., Parkinson,
2196        I.J., Gale, A.S., 2020. A re-evaluation of the Plenus Cold Event, and the links between CO2,
2197        temperature, and seawater chemistry during OAE 2. Paleoceanography and
2198        Paleoclimatology, 35(4), p.e2019PA003631.

2199    Olsen, P.E., Smith, J.B., McDonald, N.G., 1998. Type material of the type species of the classic
2200        theropod footprint genera *Eubrontes*, Anchisauripus, and *Grallator* (Early Jurassic, Hartford
2201        and Deerfield basins, Connecticut and Massachusetts, USA). Journal of vertebrate
2202        Paleontology, 18(3), pp.586-601.

2203    Paul, G.S., 2024. The Princeton Field Guide to Dinosaurs (Princeton Field Guides). Princeton
2204        University Press.

2205    Pearson, D.A., Schaefer, T., Johnson, K.R., Nichols, D.J., Hunter, J.P., 2002. Vertebrate
2206        biostratigraphy of the Hell Creek formation in southwestern North Dakota and northwestern
2207        South Dakota. Geological society of America special paper, 361(145), p.e167.

2208    Perle, A., 1999. A new maniraptoran theropod, Achillobator giganticus (Dromaeosauridae), from
2209        the Upper Cretaceous of Burkhant, Mongolia. Ulan Bator: National University of Mongolia,
2210        104 pp.

2211    Pol, D., Gomez, K., Holwerda, F.M., Rauhut, O.W., Carballido, J.L., 2022. Sauropods from the
2212        Early Jurassic of South America and the Radiation of Eusauropoda. In South American
2213        Sauropodomorph Dinosaurs: Record, Diversity and Evolution (pp. 131-163). Cham:
2214        Springer International Publishing.

2215    Pol, D., Leardi, J.M., 2015. Diversity patterns of Notosuchia (Crocodyliformes,
2216        mesoeucrocodylia) during the cretaceous of Gondwana.

2217    Qian, M., Zhang, Z., Jiang, Y., Jiang, Y., Zhang, Y., Chen, R., Xing, G., 2012. Cretaceous
2218        therizinosaur dinosaurs in Zhejiang, China. Journal of Geology, 36(4), pp.337-348.

2219    Razzolini, N.L., Belvedere, M., Marty, D., Paratte, G., Lovis, C., Cattin, M., Meyer, C.A., 2017.
2220        *Megalosauripus* transjuranicus ichnosp. nov. A new Late Jurassic theropod ichnotaxon from
2221        NW Switzerland and implications for tridactyl dinosaur ichnology and ichnotaxonomy. Plos
2222        one, 12(7), p.e0180289.

2223    Rolando, M.A., Cerroni, M.A., Marsà, J.A.G., Motta, M.J., Rozadilla, S., Eglí, F.B., Novas, F.E.,
2224        2021. A new medium-sized abelisaurid (Theropoda, Dinosauria) from the late cretaceous
2225        (Maastrichtian) Allen Formation of Northern Patagonia, Argentina. Journal of South
2226        American Earth Sciences, 105, p.102915.

2227    Romilio, A. 2020. An Instructional Guide to Visualising Dinosaur Tracks. Columbia, South

2228     Carolina, USA. Amazon; p. 36.

2229 Salisbury, S.W., Romilio, A., Herne, M.C., Tucker, R.T., Nair, J.P., 2016. The dinosaurian

2230     ichnofauna of the lower cretaceous (Valanginian–Barremian) broome sandstone of the

2231     Walmadany area (James Price Point), Dampier Peninsula, Western Australia. Journal of

2232     Vertebrate Paleontology, 36(sup1), pp.1-152.

2233 Sánchez-Fenollosa, S., Verdú, F.J., Cobos, A., 2023. The largest ornithopod (Dinosauria:

2234     Ornithischia) from the Upper Jurassic of Europe sheds light on the evolutionary history of

2235     basal ankylopollexians. Zoological Journal of the Linnean Society, 199(4), pp.1013-1033.

2236 Santos, V.F., Moratalla, J.J., Royo-Torres, R., 2009. New sauropod trackways from the Middle

2237     Jurassic of Portugal. Acta Palaeontologica Polonica, 54(3), pp.409-422.

2238 Santos, V.F., Moratalla, J.J., Royo-Torres, R., Belvedere, M., Castanera, D., Ceríaco, L.M.,

2239     Mocho, P., Merino, M., Meyer, C.A., Sciscio, L., 2024. A revised name and new insights

2240     into the Middle Jurassic sauropod trackways from Portugal. A correction of Santos et al.

2241     2009. Acta Palaeontologica Polonica, 69, p.587.

2242 Schlanger, S.O., Jenkyns, H., 1976. Cretaceous oceanic anoxic events: causes and consequences.

2243     Geologie en mijnbouw, 55(3-4).

2244 Schroeder, K., Lyons, S.K., Smith, F.A., 2021. The influence of juvenile dinosaurs on

2245     community structure and diversity. Science, 371(6532), pp.941-944.

2246 Scotese, C.R., Vérard, C., Burgener, L., Elling, R.P., Kocsis, A.T., 2025. The Cretaceous world:

2247     plate tectonics, palaeogeography and palaeoclimate. Geological Society, London, Special

2248     Publications, 544(1), pp.SP544-2024.

2249 Stevens, K.A., Ernst, S., Marty, D., 2016. Uncertainty and ambiguity in the interpretation of

2250     sauropod trackways (pp. 226-243). Bloomington: Indiana University Press.

2251 Stevens, K.A., Ernst, S., Marty, D., 2022. Coupling length: a generalized gleno-acetabular

2252     distance measurement for interpreting the size and gait of quadrupedal trackmakers. Swiss

2253     Journal of Geosciences, 115(1), p.18.

2254 Stommel, H., 1957. A survey of ocean current theory. Deep Sea Research (1953), 4, pp.149-184.

2255 Strickson, E.C., 2020. Underfoot Pressure Equalisation as an Explanation for Extreme

2256     Heteropody. Liverpool John Moores University (United Kingdom).

2257 Tanaka, I., 2021. Morphological variability of Ciconia boyciana (Aves: Ciconiidae) tracks in

2258     homogeneous sediment. Palaios, 36(4), pp.141-154.

2259 Tanaka, K., Anvarov, O.U.O., Zelenitsky, D.K., Ahmedshaev, A.S., Kobayashi, Y., 2021. A new

2260     carcharodontosaurian theropod dinosaur occupies apex predator niche in the early Late

2261     Cretaceous of Uzbekistan. Royal Society Open Science, 8(9), p.210923.

2262 Tang, F., Kang, X., Jin, X., Wei, F., Wu, W., 2001. A new sauropod dinosaur of Cretaceous from

2263     Jiangshan, Zhejiang Province. Vertebrata PalAsiatica, 39(04), p.272.

2264 Tomaselli, M.B., David, L.D.O., Riga, B.J.G., 2021. Paleoenvironmental contexts of South

2265     American Cretaceous sauropod tracks. Journal of South American Earth Sciences, 110,

2266     p.103393.

2267 Tomaselli, M.B., David, L.D.O., Riga, B.J.G., Coria, J.P., Mercado, C.R., Guerra, M., Tiviroli,

2268   G.S., 2022. New titanosaurian sauropod tracks with exceptionally well-preserved claw
2269   impressions from the Upper Cretaceous of Argentina. Cretaceous Research, 129, p.104990.
2270   Torcida Fernández-Baldor, F., Díaz-Martínez, I., Huerta, P., Montero Huerta, D., Castanera, D.,
2271   2021. Enigmatic tracks of solitary sauropods roaming an extensive lacustrine megatracksite
2272   in Iberia. Scientific Reports, 11(1), p.16939.
2273   Tsuihiji, T. Watabe, M., Tsogtbaatar, K., Barsbold, R., Suzuki, S., 2012. A tyrannosauroid
2274   frontal from the Upper Cretaceous (Cenomanian-Santonian) of the Gobi Desert, Mongolia.
2275   Vertebrata PalAsiatica. 50 (2), 102−110.
2276   Turner, M.L., Falkingham, P.L., Gatesy, S.M., 2020. It's in the loop: shared sub-surface foot
2277   kinematics in birds And other dinosaurs shed light on a new dimension of fossil track
2278   diversity. Biology Letters, 16(7), p.20200309.
2279   Unwin, D.M., Lü, J., 1997. On Zhejiangopterus and the relationships of pterodactyloid
2280   pterosaurs. Historical Biology, 12(3-4), pp.199-210.
2281   Van den Heever, A., Mhlongo, R., Benadie, K., Thomas, I., 2024. Tracker Manual: A practical
2282   guide to animal tracking in southern Africa. Penguin Random House South Africa.
2283   Vermeij, G.J., 2016. Gigantism and its implications for the history of life. PLoS One, 11(1),
2284   p.e0146092.
2285   Vila, B., Oms, O., Galobart, À., Bates, K.T., Egerton, V.M., Manning, P.L., 2013. Dynamic
2286   similarity in titanosaur sauropods: ichnological evidence from the Fumanya dinosaur
2287   tracksite (southern Pyrenees). PLoS One, 8(2), p.e57408.
2288   Wan, X.Q., Chen, P.J., Wei, M.J. 2007. The cretaceous system in China. Acta Geologica
2289   Sinica-English Edition, 81(6), pp.957-983.
2290   Wang, J.Y., Li, X.H., Li, L.Q., Wang, Y.D., 2022. Cretaceous climate variations indicated by
2291   palynoflora in South China. Palaeoworld, 31(3), pp.507-520.
2292   Weems. R. E. 2006. Locomotor speeds and patterns of running behavior in non-maniraptoriform
2293   theropod dinosaurs. In J. D. Harris, S. G. Lucas, J. A. Spielmann, M. G. Lockley, A. R. C.
2294   Milner, & J. I. Kirkland (eds.), The Triassic-Jurassic Terrestrial Transition. New Mexico
2295   Museum of Natural History and Science Bulletin 37:379-389
2296   Wilson, J.A., Carrano, M.T., 1999. Titanosaurs., the origin of "wide-gauge" trackways: a
2297   biomechanical and systematic perspective on sauropod locomotion. Paleobiology, 25(2),
2298   pp.252-267.
2299   Wroblewski, A.F.J., Gulas-Wroblewski, B.E., 2021. Earliest evidence of marine habitat use by
2300   mammals. Scientific Reports, 11(1), p.8846.
2301   Wu, H., Jin, X., Du, T., Huang, M., Zheng, W., Sheng, Y., 2018. New findings and preliminary
2302   study of tetrapod track assemblages from Guanyintang Village, Yiwu City, Zhejiang
2303   Province. Earth, 8, 82-87.
2304   Wyenberg-Henzler, T., Patterson, R.T., Mallon, J.C., 2022. Ontogenetic dietary shifts in North
2305   American hadrosaurids (Dinosauria: Ornithischia). Cretaceous Research, 135, p.105177.
2306   Xi, D., Wan, X., Li, G., Li, G., 2019. Cretaceous integrative stratigraphy and timescale of China.
2307   Science China Earth Sciences, 62, pp.256-286.

2308 Xing, L., Lockley, M.G., 2016. Early Cretaceous dinosaur and other tetrapod tracks of
2309     southwestern China. Science Bulletin 61(13): 1044–1051.
2310 Xing, L., Li, D., Harris, J.D., Bell, P.R., Azuma, Y., Fujita, M., Lee, Y.N., Currie, P.J., 2013. A
2311     new deinonychosaurian track from the Lower Cretaceous Hekou group, Gansu Province,
2312     China. Acta Palaeontologica Polonica, 58(4), pp.723-730.
2313 Xing, L., Klein, H., Lockley, M.G., Wetzel, A., Li, Z.D., Li, J.J., Gierliński, G.D., Zhang, J.P.,
2314     Matsukawa, M., Divay, J.D., Zhou, L., 2014c. *Changpeipus* (theropod) tracks from the
2315     Middle Jurassic of the Turpan Basin, Xinjiang, Northwest China: review, new discoveries,
2316     ichnotaxonomy, preservation and paleoecology. Vertebrata PalasiAtica. 52(2), 233–259
2317 Xing, L., Lockley, M.G., Klein, H., Gierliński, G.D., Divay, J.D., Hu, S.M., Zhang, J.P., Ye, Y.,
2318     He, Y.P., 2014b. The non-avian theropod track *Jialingpus* from the Cretaceous of the Ordos
2319     Basin, China, with a revision of the type material: implications for ichnotaxonomy and
2320     trackmaker morphology. Palaeoworld, 23(2), pp.187-199.
2321 Xing, L., Lockley, M.G., Zhang, J.P., Klein, H., Persons, W.S.IV., Dai, H., 2014a. Diverse
2322     sauropod–, theropod–, ornithopod–track assemblages and a new ichnotaxon Siamopodus
2323     xui ichnosp. nov. from the Feitianshan Formation, Lower Cretaceous of Sichuan Province,
2324     southwest China. Palaeogeography, Palaeoclimatology, Palaeoecology 414: 79–97.
2325 Xing, L., Lockley, M.G., Marty, D., Zhang, J.P., Wang, Y., Klein, H., McCrea, R.T., Buckley,
2326     L.G., Belvedere, M., Mateus, O., Gierliński, G.D., Piñuela, L., Persons, W.S.IV, Wang, F.P.,
2327     Ran, H., Dai, H., Xie, X.M., 2015. An ornithopod-dominated tracksite from the Lower
2328     Cretaceous Jiaguan Formation (Barremian–Albian) of Qijiang, South-Central China: new
2329     discoveries, ichnotaxonomy, preservation and palaeoecology. PLOS ONE 10(10):
2330     e0141059
2331 Xing, L., Lockley, M.G., Klein, H., Peng, G.Z., Ye, Y., Jiang, S., Zhang, J.P., Persons, W.S.IV.,
2332     Xu, T., 2016. A theropod track assemblage including large deinonychosaur tracks from the
2333     Lower Cretaceous of Asia. Cretaceous Research 65: 213–222.
2334 Xing, L., Lockley, M.G., Li, D.L., Klein, H., Persons, W.S IV, Ye, Y., Zhang, J.P., Ran, H.,
2335     2017. Late Cretaceous Ornithopod-dominated, theropod, pterosaur track assemblages from
2336     the Nanxiong Basin, China: new discoveries, ichnotaxonomy, palaeoecology.
2337     Palaeogeography, Palaeoclimatology, Palaeoecology, 466: 303–313. DOI:
2338     10.1016/j.palaeo.2016.11.035
2339 Xing, L., Ba, J., Lockley, M.G., Klein, H., Yan, S.W., Romilio, A., Chou, C.Y., Persons, W.S.IV.
2340     2018b. Late Triassic sauropodomorph and Middle Jurassic theropod tracks from the
2341     Xichang Basin, southwestern China: a first Chinese report for ichnogenus Carmelopodus.
2342     Journal of Palaeogeography 7(1): 1–13.
2343 Xing, L., Lockley, M.G., Klein, H., Zeng, R., Cai, S., Luo, X., Li, C., 2018a. Theropod
2344     assemblages and a new ichnotaxon Gigandipus chiappei ichnosp. nov. from the Jiaguan
2345     Formation, Lower Cretaceous of Guizhou Province, China. Geoscience Frontiers, 9(6),
2346     pp.1745-1754.
2347 Xing, L., Lockley, M.G., Tang, Y., Romilio, A., Xu, T., Li, X., Tang, Y., Li, Y., 2018c. Tetrapod

track assemblages from Lower Cretaceous desert facies in the Ordos Basin, Shaanxi Province, China and their implications for Mesozoic paleoecology. Palaeogeography, Palaeoclimatology, Palaeoecology, 507, pp.1-14.

Xing, L., Niu, K., Lockley, M.G., Klein, H., Romilio, A., Persons, W.S.IV., Brusatte, S L. 2019. A probable tyrannosaurid track from the Upper Cretaceous of Southern China. Science Bulletin 64(16): 1136–1139

Xing, L., Niu, K., Wang, D.H., Prieto-Marquez, A. 2020. A partial articulated hadrosaurid skeleton from the Maastrichtian (Upper Cretaceous) of the Ganzhou area, Jiangxi Province, China. Historical Biology DOI: 10.1080/08912963.2020.1782397

Xing, L., Lockley, M.G., Jiang, Z., Klein, H., Persons IV, W.S., Zhang, P., Wan, X., 2021b. Variation in sauropod trackway pattern from the Tuchengzi Formation (Jurassic-Cretaceous boundary) in western Liaoning, China. Cretaceous Research, 118, p.104662.

Xing, L., Lockley, M.G., Klein, H., Chou, C.Y., Wang, D.H., Persons, W.S., 2021a. A mid-Cretaceous dinosaur track assemblage from the Hengshan Formation in central Zhejiang, China. Historical Biology, 33(7), 973–980.

Xing, L., Lockley, M.G., Klein, H., Zhang, L.J., Romilio, A., Scott Persons, W., Peng, G.Z., Ye, Y., Wang, M.Y., 2021. The new ichnotaxon *Eubrontes* nobitai ichnosp. nov., other saurischian tracks from the Lower Cretaceous of Sichuan Province and a review of Chinese *Eubrontes*-type tracks. Journal of Palaeogeography, 10, pp.1-19.

Xing, L., Lockley, M.G., Mao, Z., Klein, H., Gu, Z., Bai, C., Qiu, L., Liu, Y., Romilio, A., Persons IV, W.S., Wan, X., 2021d. A new dinosaur track site from the earliest Cretaceous (Berriasian) part of the Tuchengzi Formation, Hebei Province, China: Implications for morphology, ontogeny and paleocommunity structure. Palaeogeography, Palaeoclimatology, Palaeoecology, 580, p.110619.

Xing, L., Lockley, M.G., Romilio, A., 2021f. An unusual dinosaur track assemblage from the Jurassic–Cretaceous boundary, Anning formation, Lufeng Basin, China. Historical Biology, 33(4), pp.514-526.

Xing, L., Dai, H., Wei, G., Lockley, M.G., Klein, H., Persons, W.S., Wang, M., Jing, S. and Hu, H., 2021e. The early jurassic *kayentapus* dominated tracks from Chongqing, China. Historical Biology, 33(10), pp.2067-2073.

Xing, L., Niu, K., Mallon, J., Miyashita, T., 2023. A new armored dinosaur with double cheek horns from the early Late Cretaceous of southeastern China. Vertebrate Anatomy Morphology Palaeontology, 11.

Xing, L., Díaz-Martínez, I., Lallensack, J.N., Kim, K.S., Buckley, L.G., Romilio, A., Piñuela, L., Wang, D.H., Chen, Q.Y., Yang, Q., Chou, C.Y., Yin, H., Jin, Y.F. 2024b. Cretaceous vertebrate tracks. In: Lucas, S.G., Hunt, P.A., Klein, H. (Eds). Vertebrate Ichnology: the Fossil Record of Prehistoric Behavior. Elsevier. ISBN: 9780443138379

Xing, L., Lockley, M.G., Klein, H., Romilio, A, Persons, W.S.IV, Wan, X.Q. 2024c. First *Grallator* ichnospecies from the Tuchengzi Formation in North China: Review and new observations on grallatorid footprint in China. New Mexico Museum of Natural History and

2388        Science Bulletin 95: 403-433

2389    Xing, L., Niu, K., Lockley, M.G., Romilio, A., Deng, K., Persons, W.S., 2024a. Deinonychosaur
2390        trackways in southeastern China record a possible giant troodontid. Iscience, 27(5).

2391    Xu, X., Tan, Q., Gao, Y., Bao, Z., Yin, Z., Guo, B., Wang, J., Tan, L., Zhang, Y., Xing, H., 2018.
2392        A large-sized basal ankylopollexian from East Asia, shedding light on early biogeographic
2393        history of Iguanodontia. Science Bulletin, 63(9), pp.556-563.

2394    You, H., Luo, Z., Shubin, N.H., Witmer, L.M., Tang, Z., Tang, F., 2003. The earliest-known
2395        duck-billed dinosaur from deposits of late Early Cretaceous age in northwest China and
2396        hadrosaur evolution. Cretaceous Research, 24(3), pp.347-355.

2397    You, H., Ji, Q., Li, D., 2005. Lanzhousaurus magnidens gen. Et sp. Nov. From Gansu Province,
2398        China: the largest-toothed herbivorous dinosaur in the world. Geological Bulletin of China,
2399        24(9), 785-794.

2400    Yu, F.M. 2013. Dinosaurs in Zhejiang — The Investigation and Research of Dinosaur Fossils
2401        from Zhejiang Province. Hangzhou: Zhejiang People's Publishing House, 254 pp.

2402    Zhang, J., Liu, Y., Flögel, S., Zhang, T., Wang, C., Fang, X., 2021. Altitude of the East Asian
2403        coast mountains., their influence on Asian climate during early Late Cretaceous. Journal of
2404        Geophysical Research: Atmospheres, 126(22), p.e2020JD034413.

2405    Zheng, D., Wang, H., Li, S., Wang, B., Jarzembowski, E.A., Dong, C., Fang, Y., Teng, X., Yu,
2406        T., Yang, L., Li, Y., 2021. Synthesis of a chrono-and biostratigraphical framework for the
2407        Lower Cretaceous of Jiuquan, NW China: implications for major evolutionary events.
2408        Earth-Science Reviews, 213, p.103474.

2409    Zheng, F., Li, W.B., 1986. Cretaceous miospore assemblages of Fujian. Acta Palaeontologica
2410        Sinica, 25(2), pp.201-210.

2411    Zheng, W., Jin, X., Shibata, M., Azuma, Y., Yu, F., 2012. A new ornithischian dinosaur from the
2412        cretaceous Liangtoutang formation of Tiantai, Zhejiang Province, China. Cretaceous
2413        Research, 34, pp.208-219.

2414    Zheng, W., Jin, X., Azuma, Y., Wang, Q., Miyata, K., Xu, X., 2018. The most basal
2415        ankylosaurine dinosaur from the Albian–Cenomanian of China, with implications for the
2416        evolution of the tail club. Scientific Reports, 8(1), p.3711.

2417    Zhou, X., 2007. Petrogenesis of the Late Mesozoic Granitoids in the Nanling Range and
2418        Geodynamic Evolution of Lithosphere. Beijing: Science Press, pp. 691.

2419    Zhou, Z., Wang, Y., Xu, X., Ren, D., 2018. The Jehol Biota: an exceptional window into Early
2420        Cretaceous terrestrial ecosystems. Terrestrial Conservation Lagerstatten: Windows into the
2421        Evolution of Life on Land, p.169.

2422

## Supplementary Information

2424    **Supplementary information 1.** The raw measurements (in cm and degrees) of all the newly
2425    discovered or re-described trackways and the relatively well-preserved isolated tracks from LXIs
2426    and LXIII tracksites.
2427    **Supplementary information 2.** Complete raw data of close-up photographs and interpretive line

2428  drawings of tracks from LXID and LXIU partially presented in Figures 15 and 16.

2429  **Supplementary information 3.** The photographs and interpretive line drawings of the

2430  ornithopod trackways from LXIN without detailed descriptions.

2431  **Supplementary information 4.** The complete version of ichnofauna composition and their size

2432  distribution of the LXI tracksites. Both track length and width values in this table represent the

2433  mean value of the trackway or the sole isolated track from a certain type, which could better

2434  represent the size of a single trackmaker.

2435

2436  *Supplementary files 2-3 can be found in Dryad: https://doi.org/10.5061/dryad.rjdfn2znd.

2437

# Figure 1

Location of the Longxiang sites in Fujian Province, southwestern China (from Niu and Xing, 2023) .
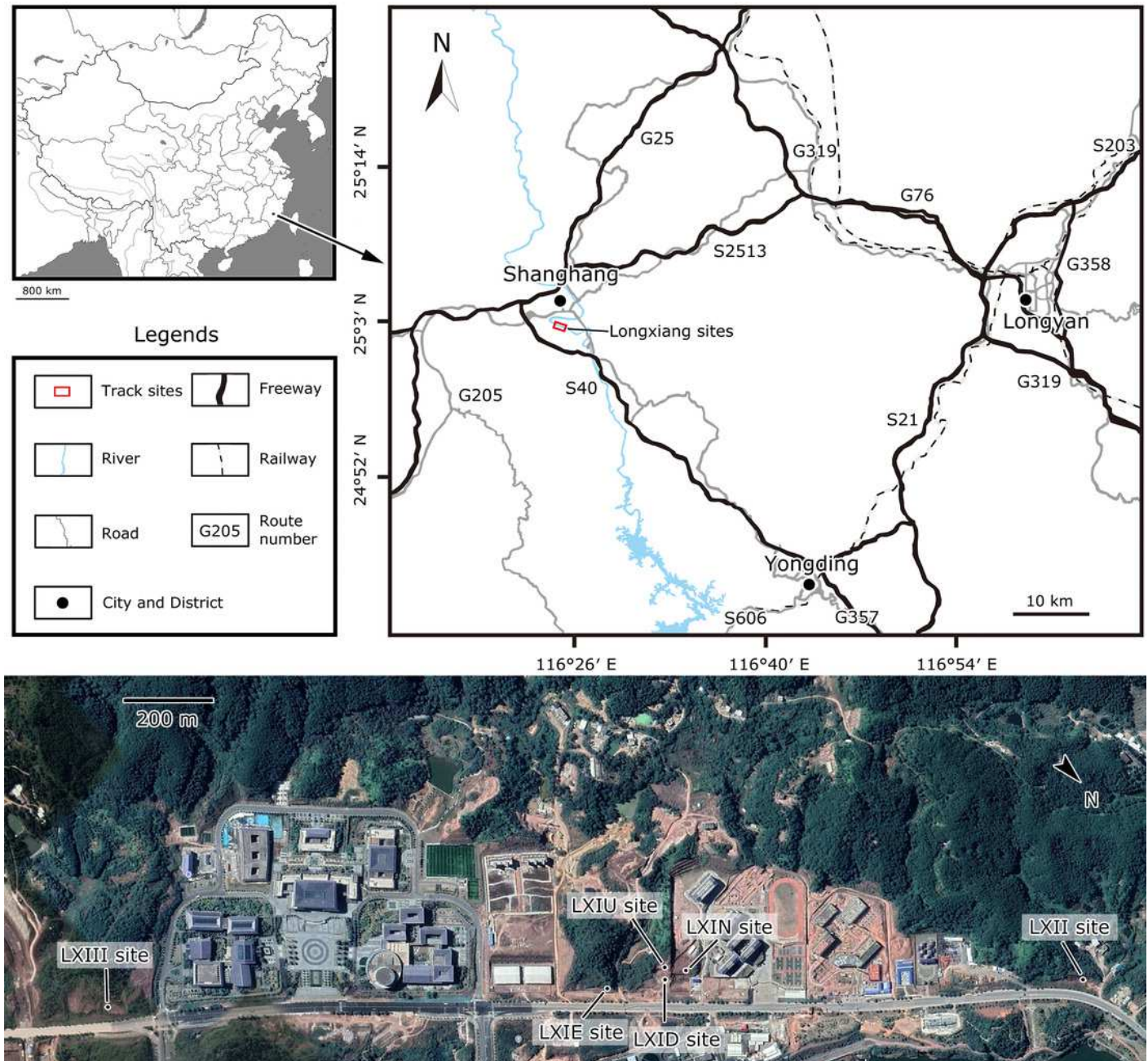
# Figure 2

Distribution of Cretaceous deposits in southeastern China.

HF, Hefei Basin; HY, Hengyang Basin; JH, Jianghan Basin; NHB, South China Basin; NX, Nanxiong Basin; NY, Nanyang Basin; SB, Subei Basin (modified after Cao, 2018; Xi et al., 2019 and Wang et al., 2022).

# Figure 3

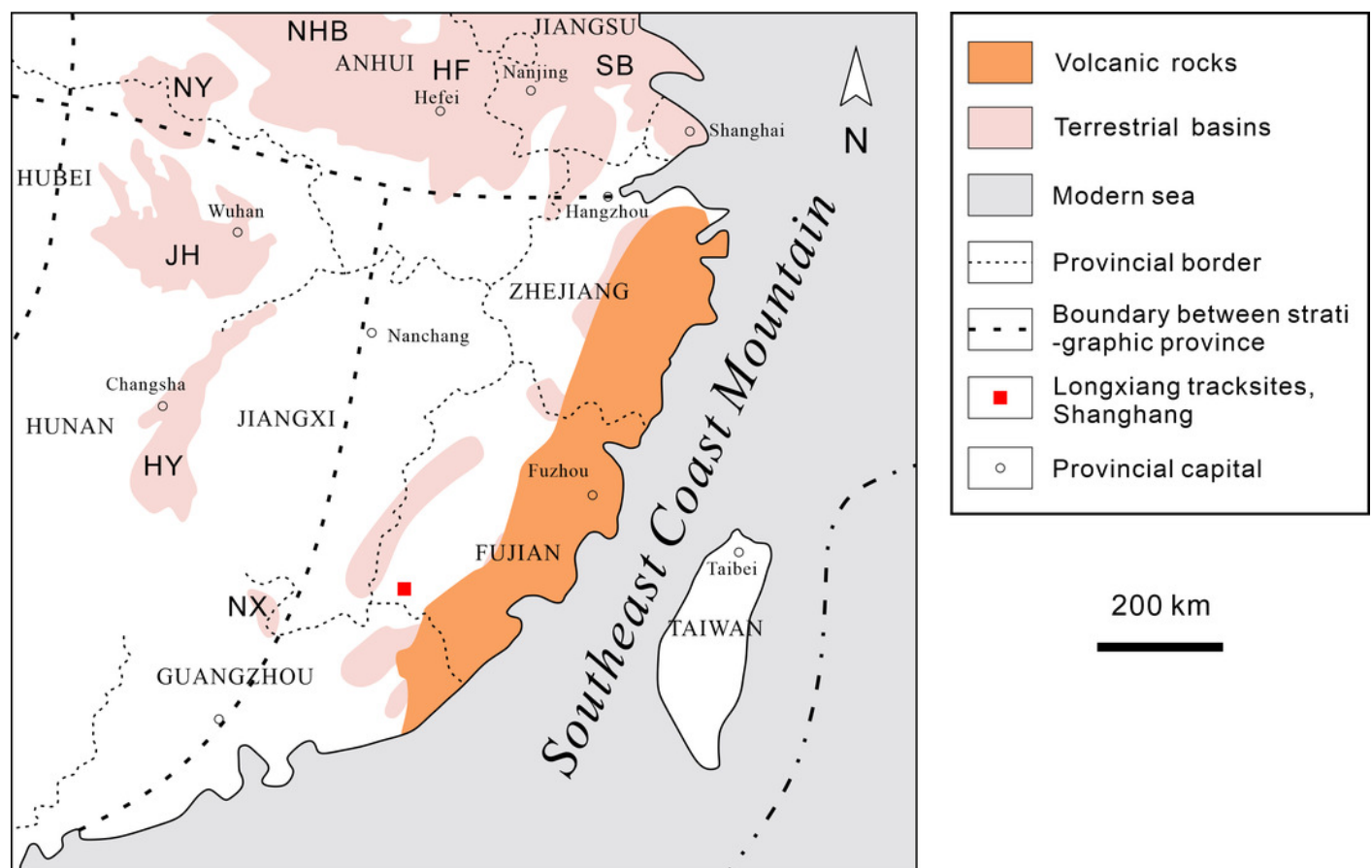Stratigraphic subdivision and correlation of Cretaceous strata in the typical stratigraphic provinces of southeastern, south-central and northwestern China (modified after Xi et al., 2019).
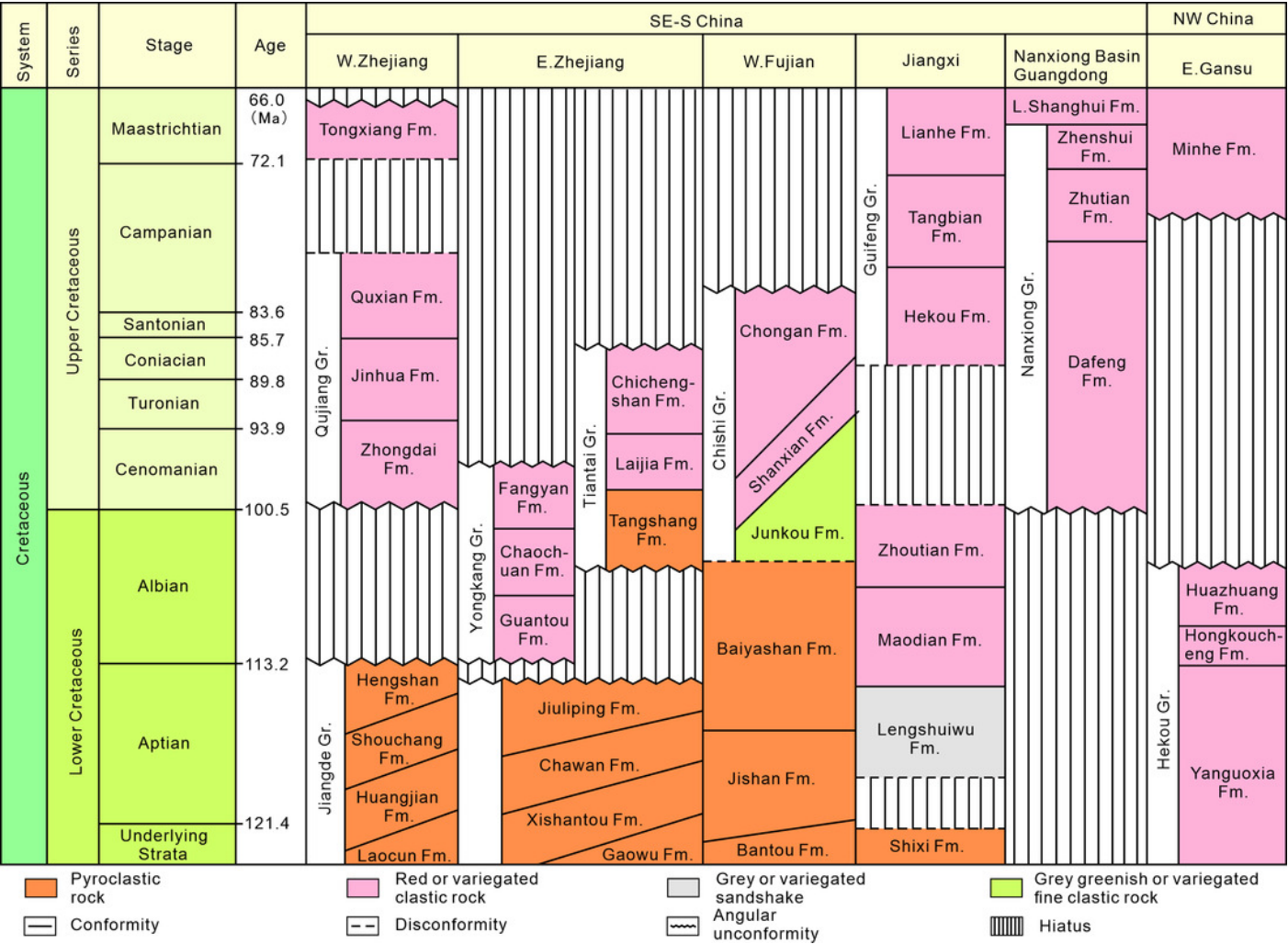
# Figure 4

The track-bearing layer of Longxiang tracksite in the Cretaceous Shaxian Formation from Shanghang Basin, Fujian, China.

The upper part of Shaxian Formation is not exposed at the Longxiang site.

| Age | Formation | Layer | Thickness (cm) | Lithology sequence |
|---|---|---|---|---|
| Lower Cretaceous | Shaxian Formation | 6 | 290.0 | |
| | | 5 | 275.3 | |
| | | 4 | 125.0 | |
| | | 3 | 126.0 | |
| | | 2 | 130.5 | |
| | | 1 | 60.2 | |

**Legends**

| | |
|---|---|
| | Pebbly argillaceous siltstone |
| | Argillaceous siltstone |
| | Mud shales |
| | Calcareous siltstone |
| | Silty mudstone |
| | Gypsum |
| | Burrow |
| | Ripple marks |
| | Tracks |
| | Algal mats |

1 m
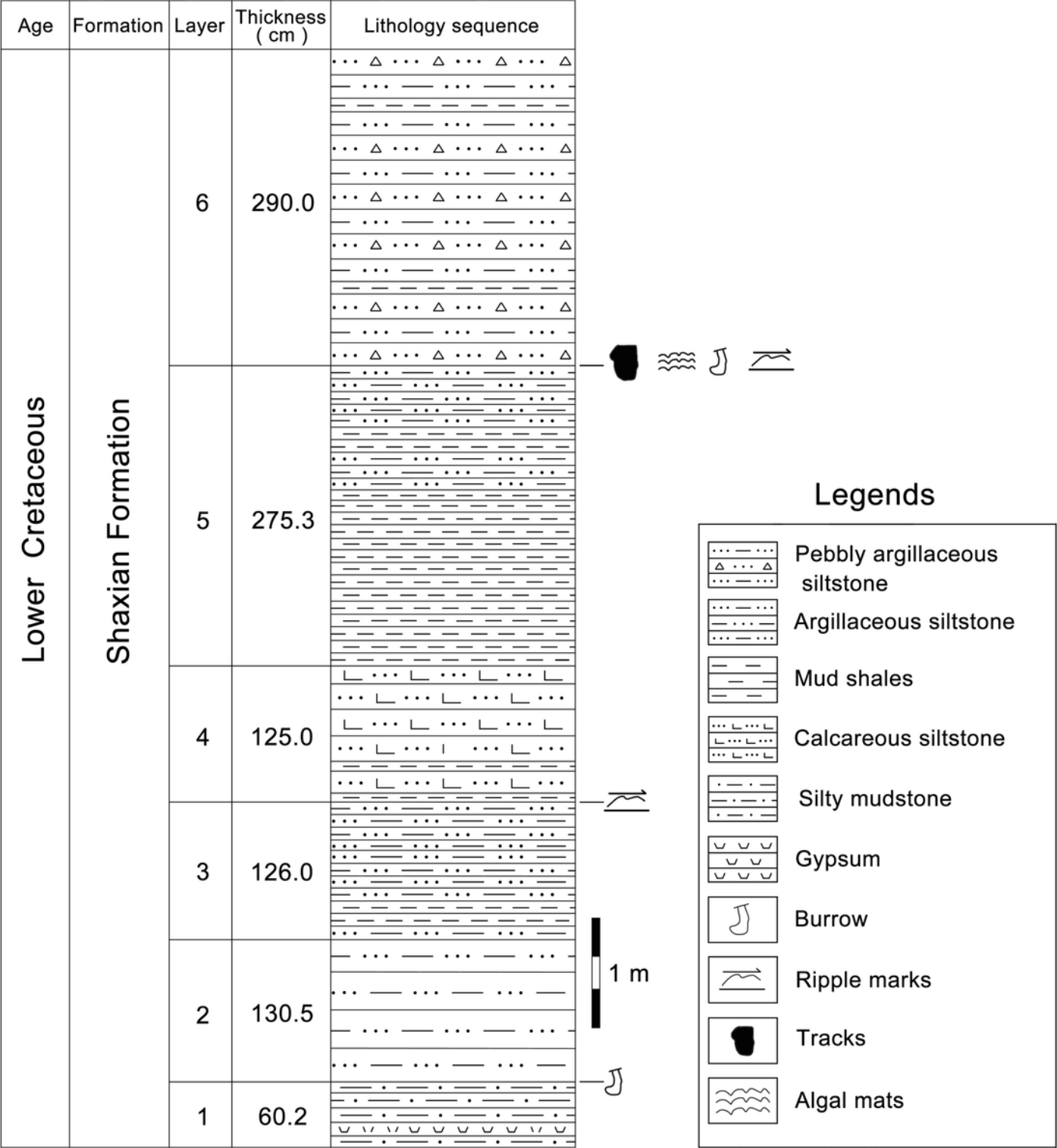
# Figure 5

Mapping of the Longxiang IU (LXIU) tracksite and the related trackway orientation rose diagrams.
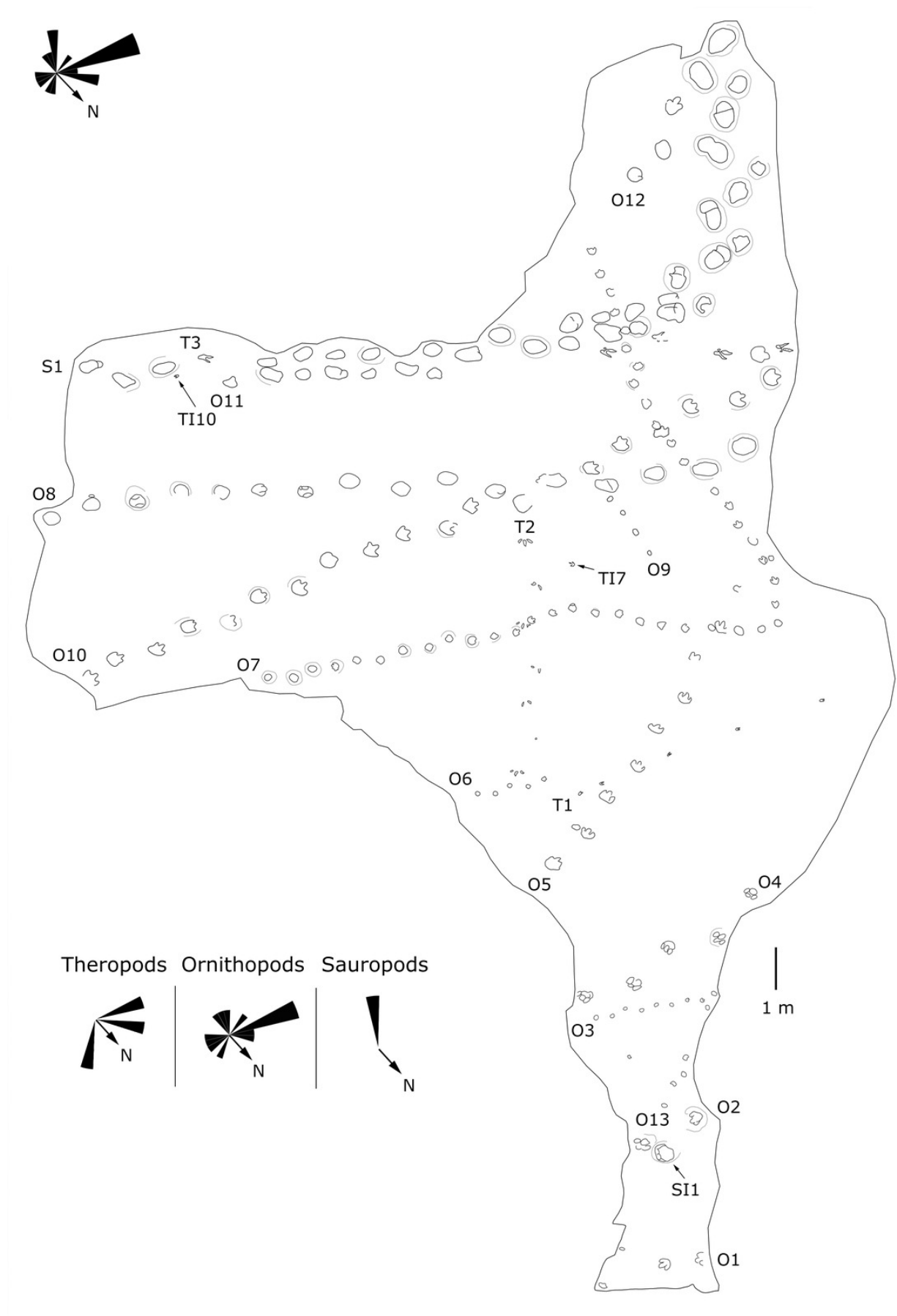
# Figure 6

Mapping of the Longxiang ID (LXID) tracksite and the related trackway orientation rose diagrams.
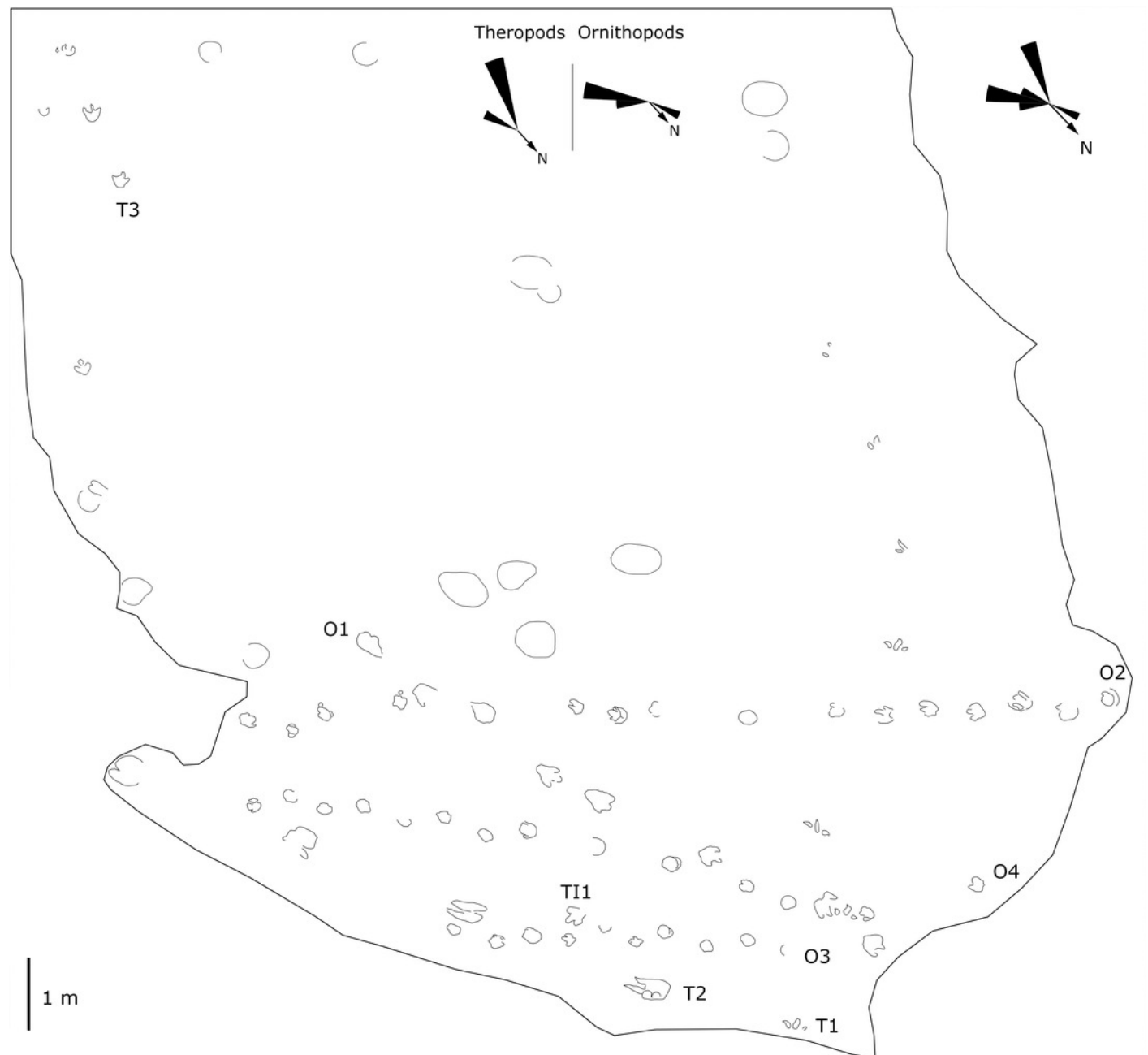
# Figure 7

Mapping of the Longxiang IN (LXIN) tracksite and the related trackway orientation rose diagrams.

# Figure 8

Photographs and interpretive line drawings of the dinosaur tracks from Longxiang II (LXII) tracksite and mapping of Longxiang III (LXIII) tracksite.
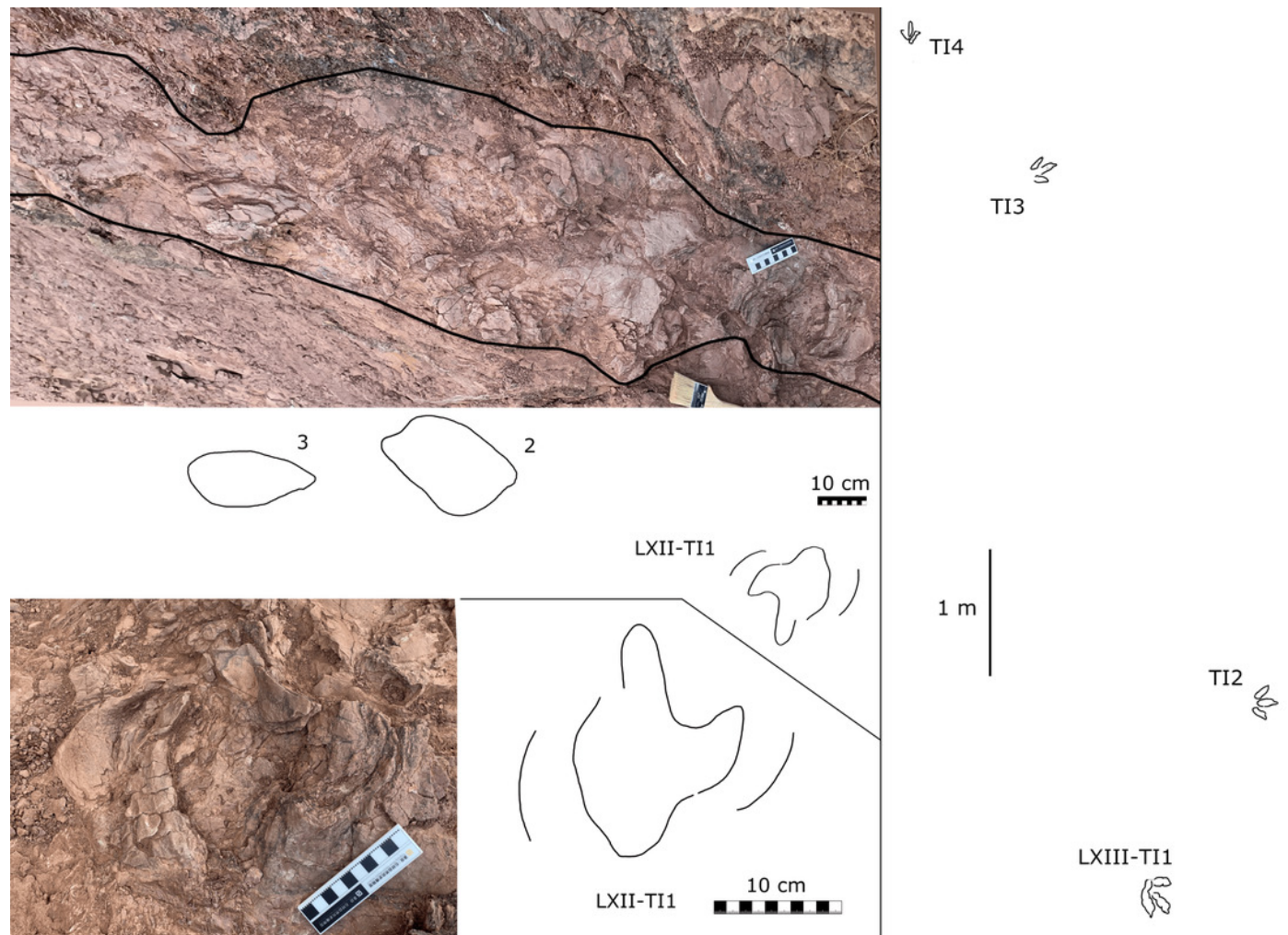
# Figure 9

Close-up photographs and interpretive line drawings of tracks from *cf. Brontopodus* trackway LXIU-S1.
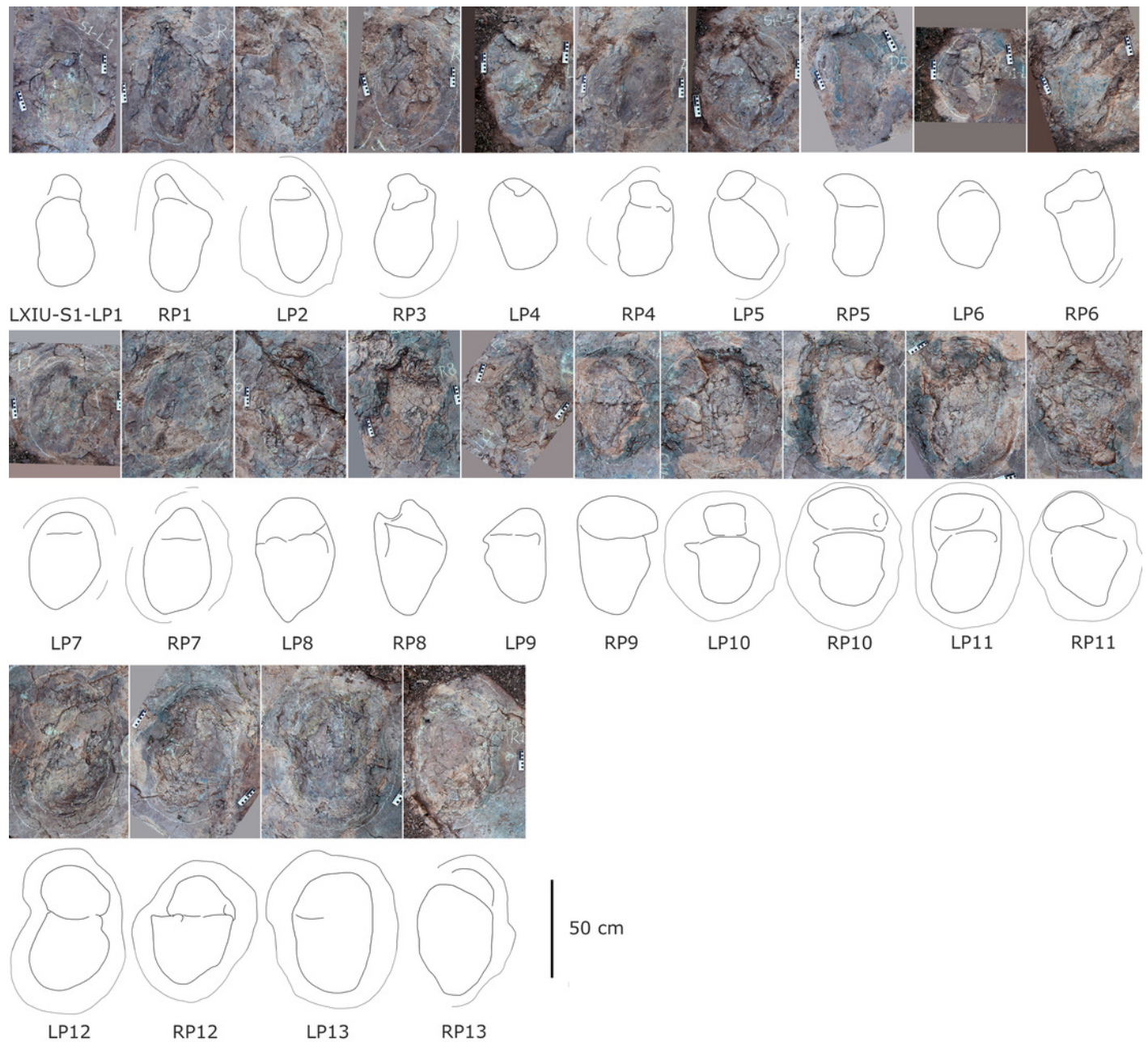
# Figure 10

Other photographs and interpretive line drawings of *cf. Brontopodus* from LXI tracksites.

A, Trackway LXIN-S1; B, Relatively well-preserved tracks in LXIN-S1; C-D, Isolated sauropod tracks from LXIU and LXIII.
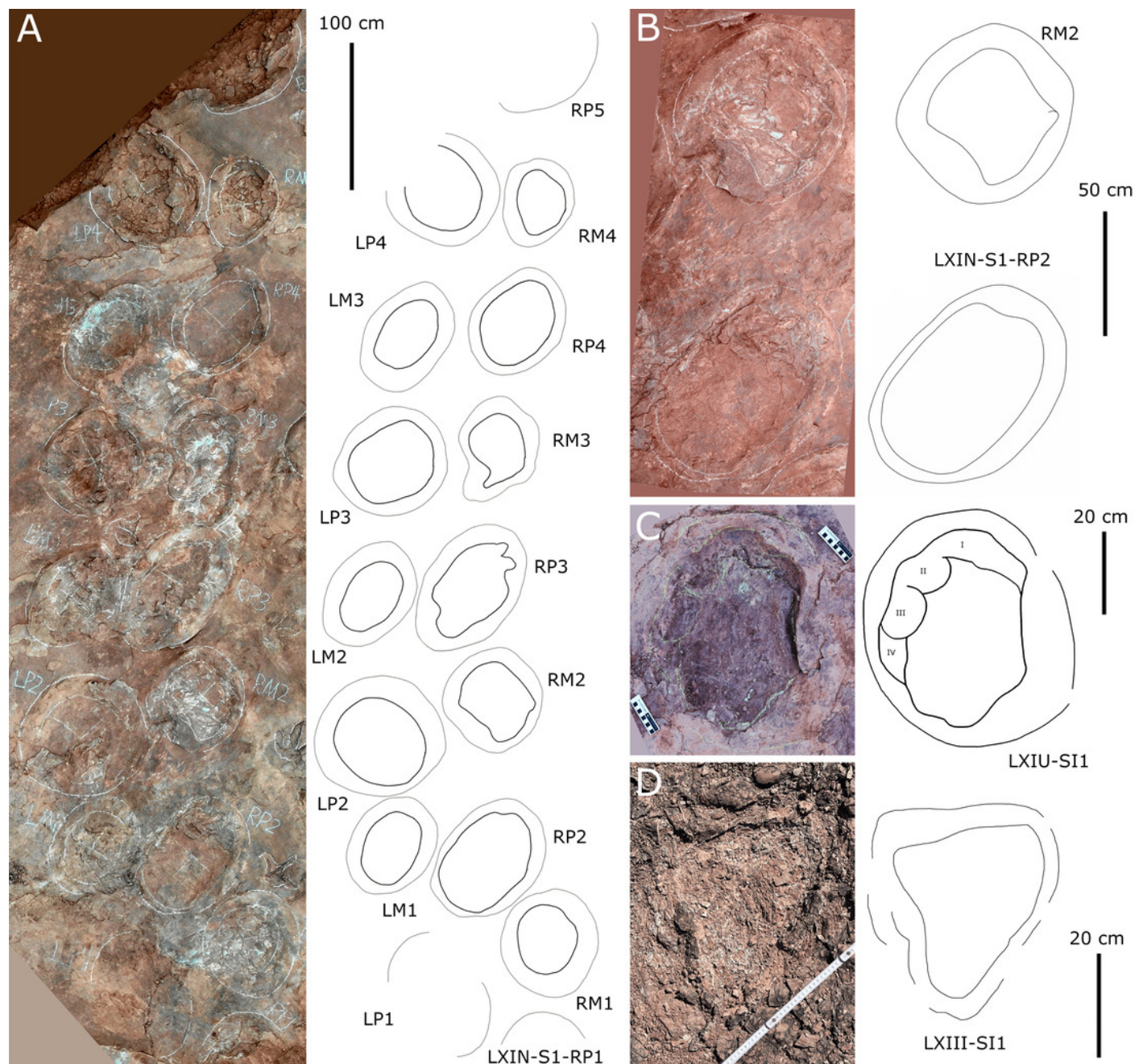
# Figure 11

Photographs and interpretive line drawings of isolated theropod tracks from LXIs and LXIII.

The tracks posited in the same row or from the same tracksite share the similar scale bar.

10 cm

LXIU-TI0    TI1    TI5    TI7    TI9    TI10

LXIU-TI8

20 cm

LXIII-TI1    TI2    TI3    TI4    LXID-TI1    LXIII-OI1

LXIN-TI1    TI2    TI3    TI4    TI5    TI16  TI17    TI11  TI10

20 cm

TI12    TI13    TI14    TI15    TI16
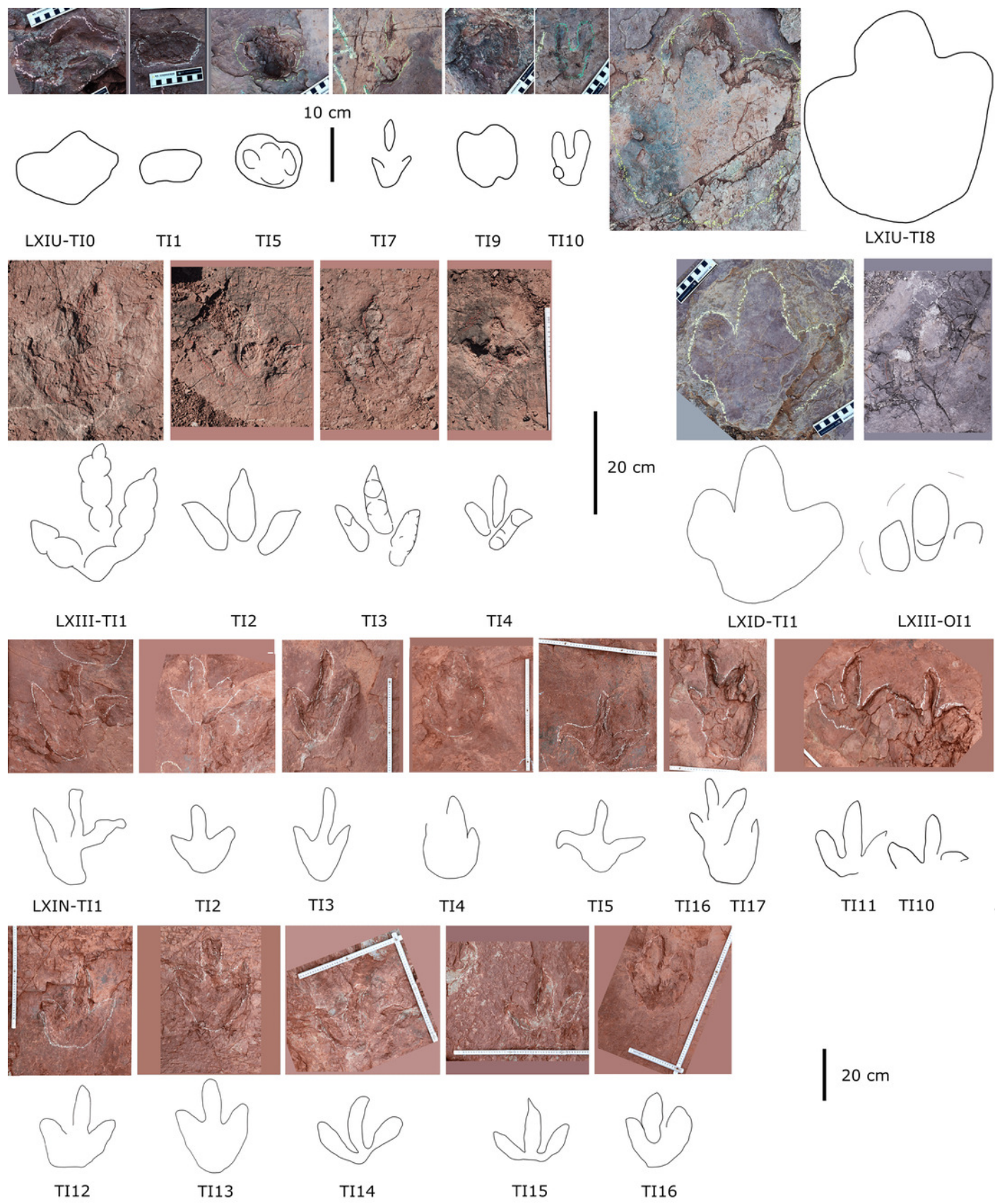
# Figure 12

P h otographs and interpretive line drawings of theropod morphotype A trackways from LXIN.

LXIN-T2 (A, left) and the other trackways (B–D, right) share the similar scale bar separately.
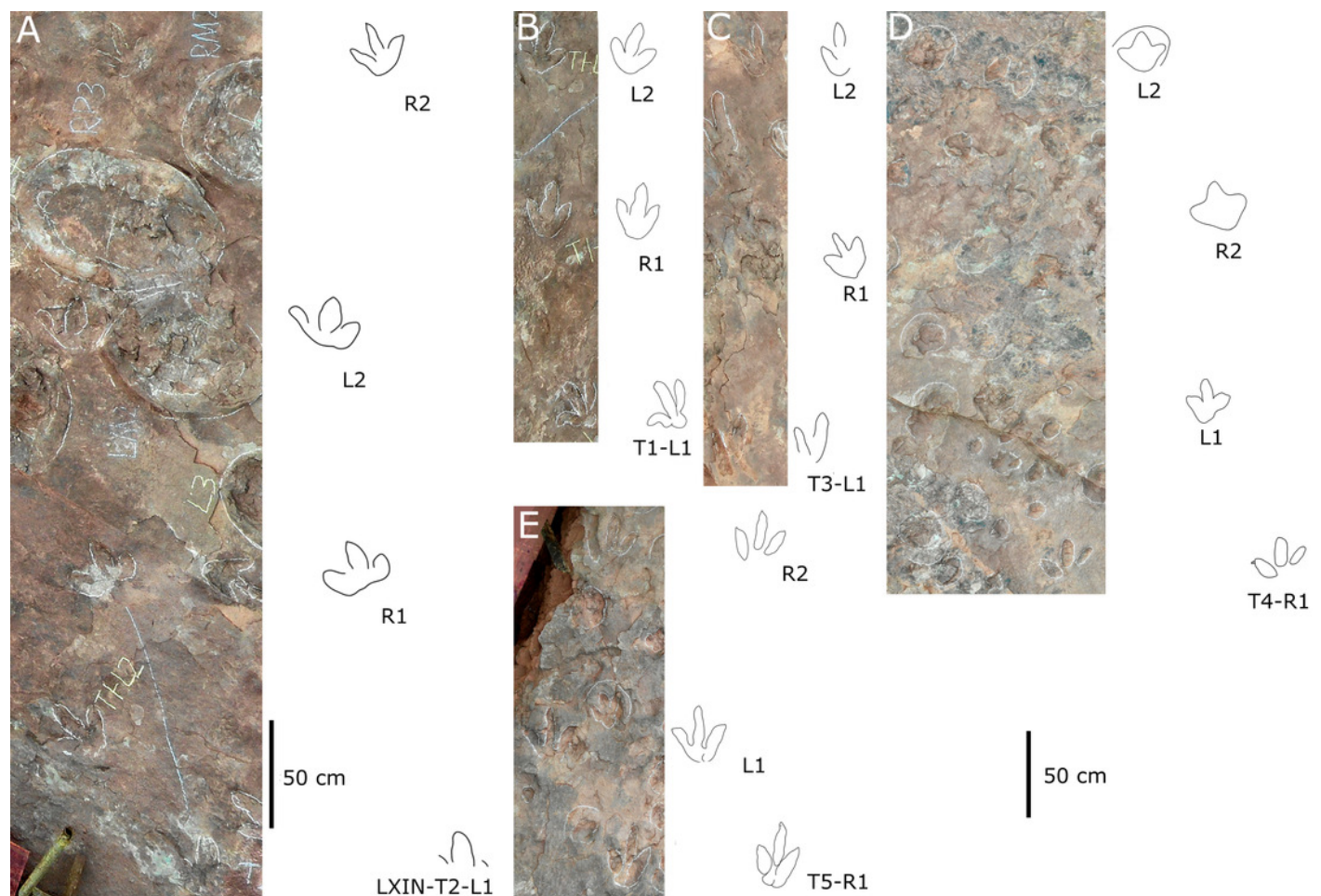
# Figure 13

Close-up p hotographs and interpretive line drawings of theropod morphotype A&B tracks from trackways in LXI sites.

All the tracks share the similar scale bar.

LXIN-T1-L1   R1   L2   T2-R1   L2   R2   T4-R1   L1   R2

T5-R1   L1   R2   LXID-T3-R1   L1   R2

20 cm

Morphotype A

LXIU-T2-R1   L1   R2   L2   R3   L3   R4

LXID-T1-L1   R1   L2   L3   R3   L4   R4

Morphotype B

# Figure 14

Box plot of ornithopod tracks size distribution from all the LXI tracksites.

The ornithopod track size is represented by the track length (in cm), for no anomalous length/width ratios are observed.
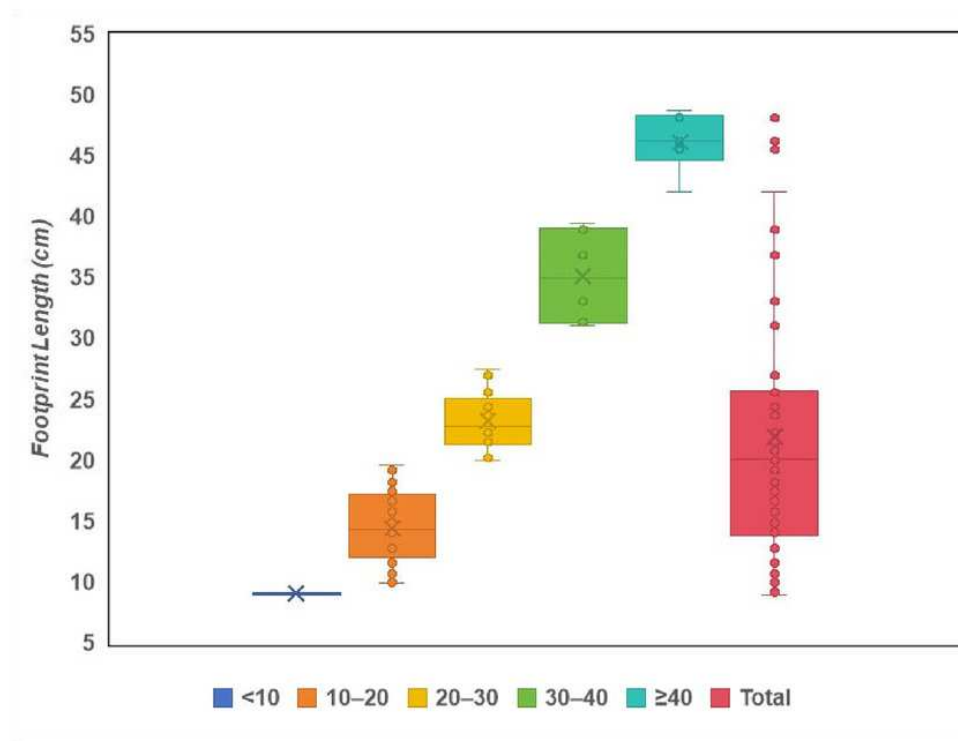
# Figure 15

Close-up p hotographs and interpretive line drawings of relative larger *Caririchnium* morphotype tracks from trackways in LXID and LXIU.

All the tracks share the similar scale bar.



20 cm
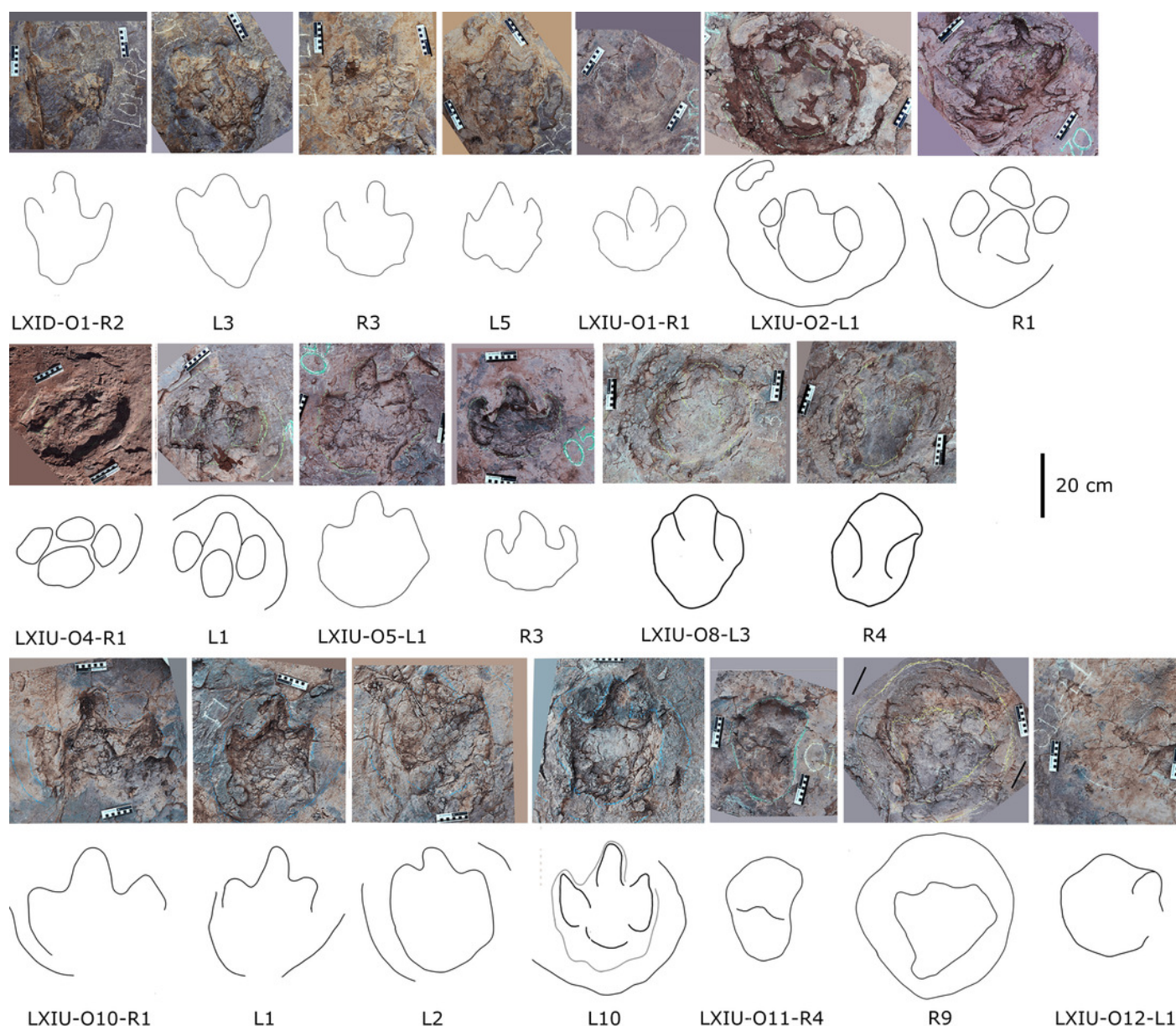
# Figure 16

Close-up p hotographs and interpretive line drawings of relative smaller *Caririchnium* morphotype tracks from trackways in LXID and LXIU.

All the tracks share the similar scale bar.



20 cm

LXIU-O3-L4    R4    LXIU-O6-L3    LXIU-O9-L4    LXIU-O13-L1

LXID-O2-L2    R3    LXID-O3-L4    R4    LXID-O4-R1    R5

LXIU-O7-R6    L7    R13    L14    L22    R22
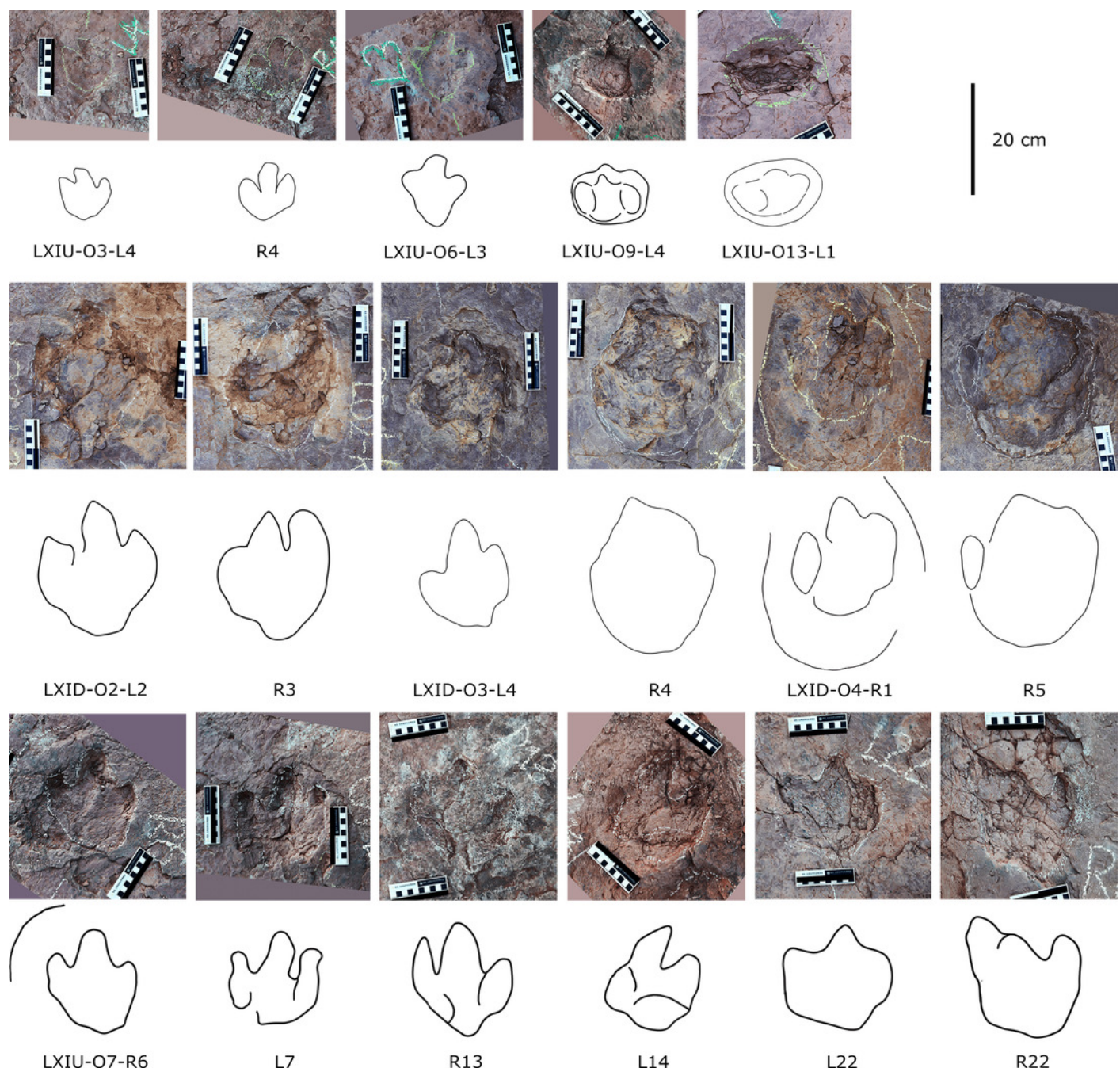
# Figure 17

Close-up photographs, 3D models & depth maps and interpretive line drawings of representative ornithopod tracks in trackways of different sizes from LXIU site.

With the comparison with theropod morphotype B (LXIU-T2-R1).

LXIU-O5-R3

L7

LXIU-O7-R6

LXIU-O10-L10

LXIU-T2-R1
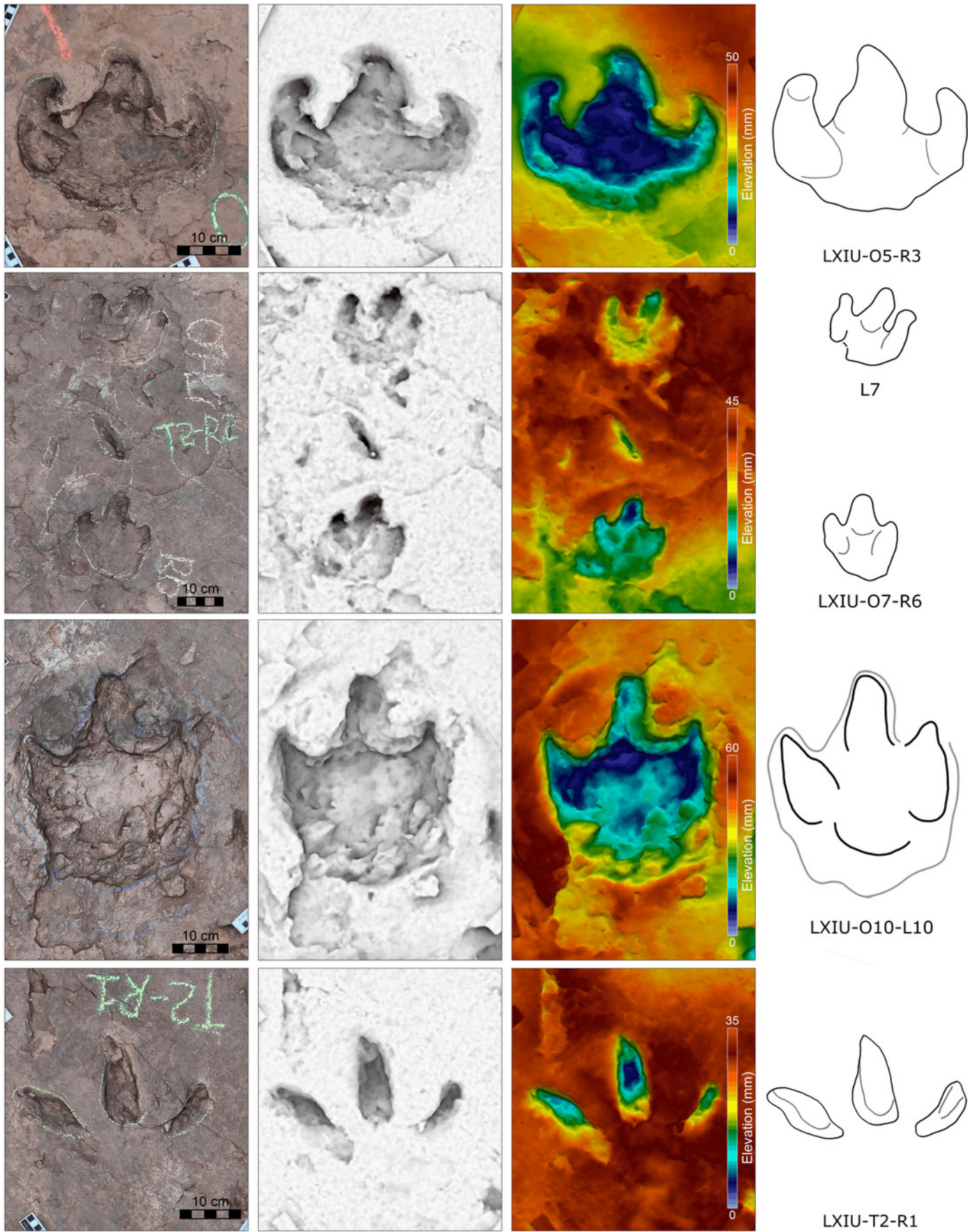
# Figure 18

P h otographs and interpretive line drawings of typical *Caririchnium* morphotype trackways from LXIN.
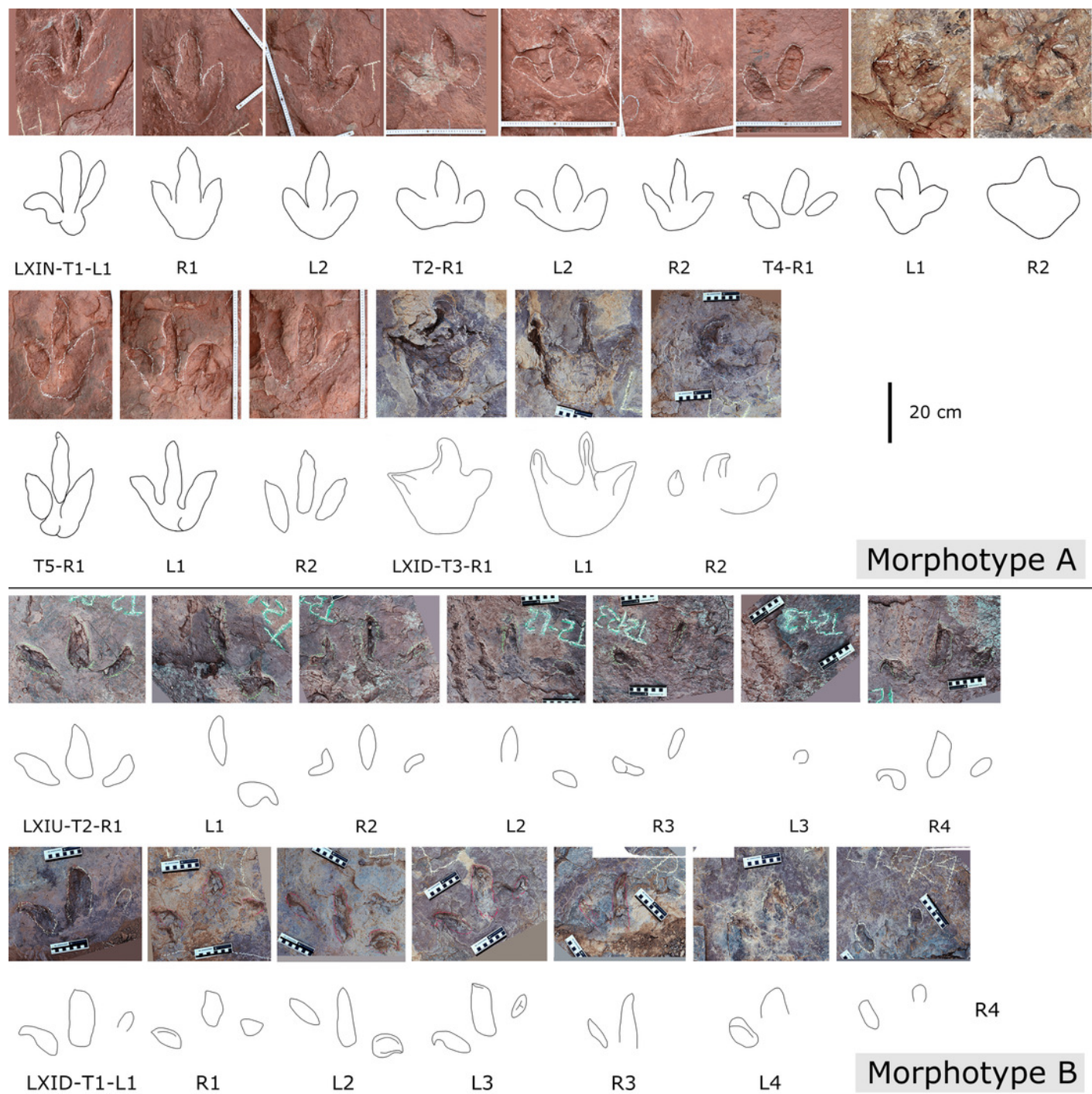
LXIN-O1 (A, left) and the other trackways (B–F, right) share the similar scale bar separately.
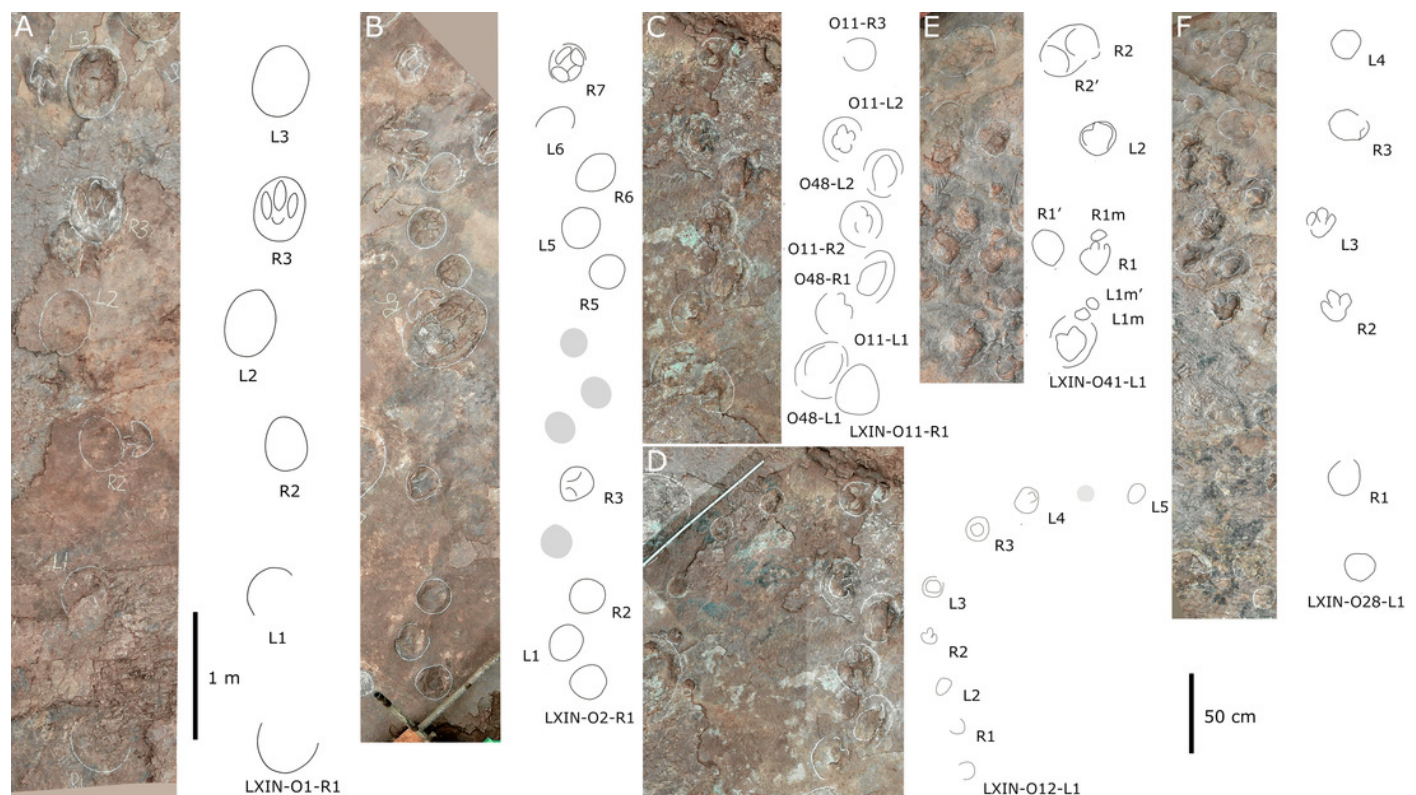
# Figure 19

Close-up p hotographs and interpretive line drawings of *Caririchnium* morphotype tracks from trackways in LXIN, and an isolated track from LXIE.
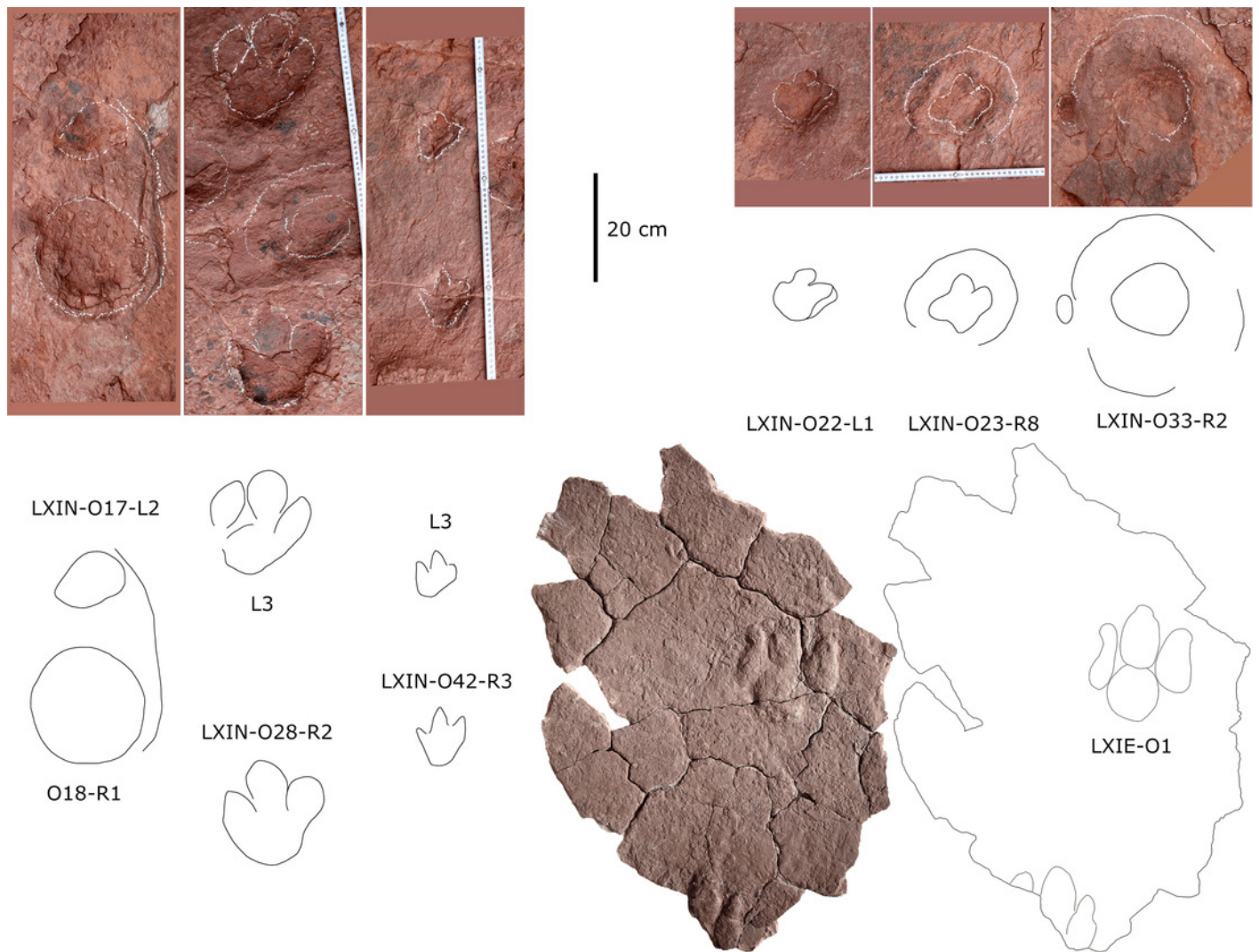
# Figure 20

Close-up p hotographs and interpretive line drawings of *Velociraptorichnus* and *Fujianipus* trackways from LXIU .
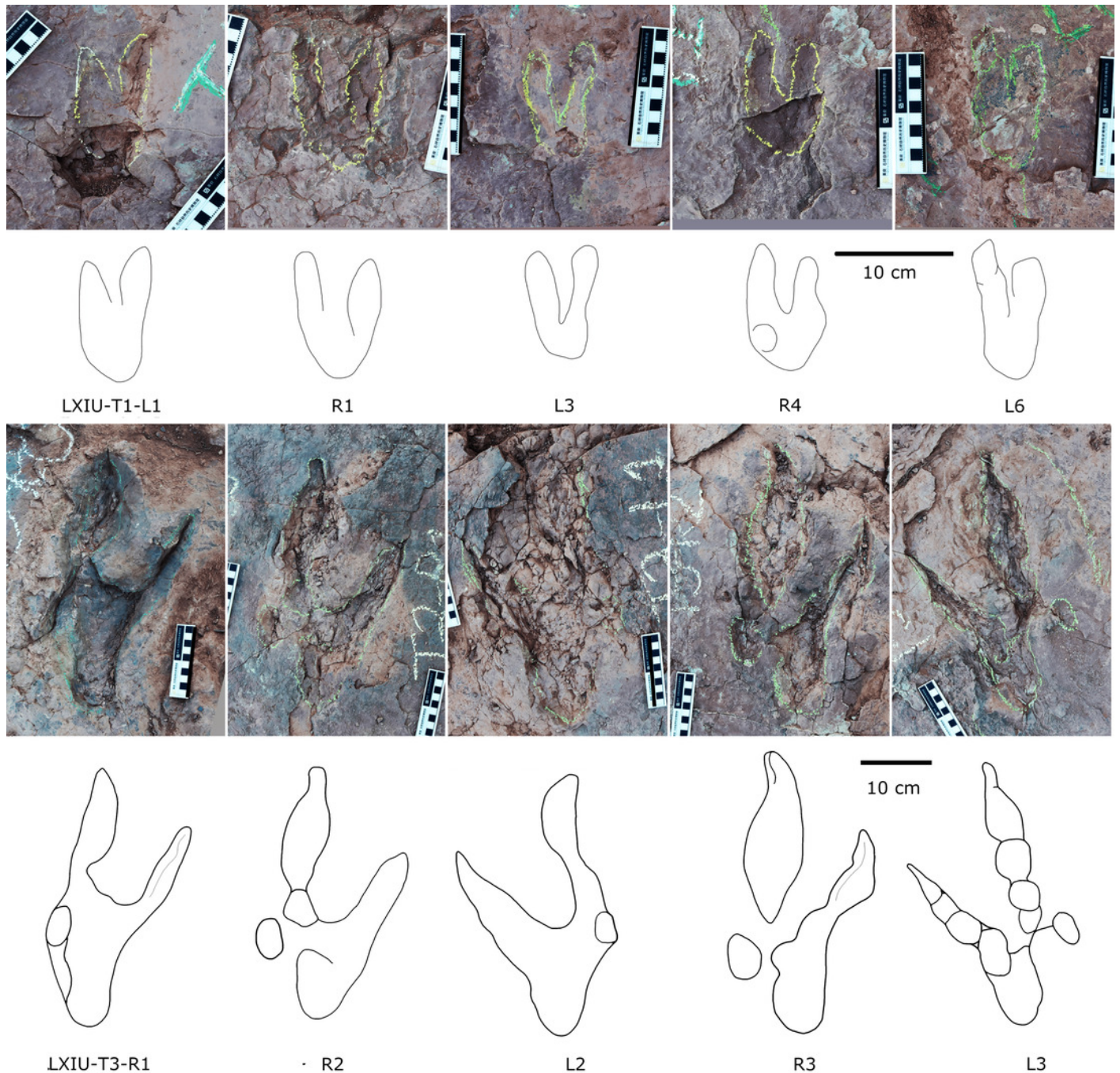
# Figure 21

Close-up photographs and interpretive line drawings of tracks from possible large
didactyl theropod trackway LXID-T2.
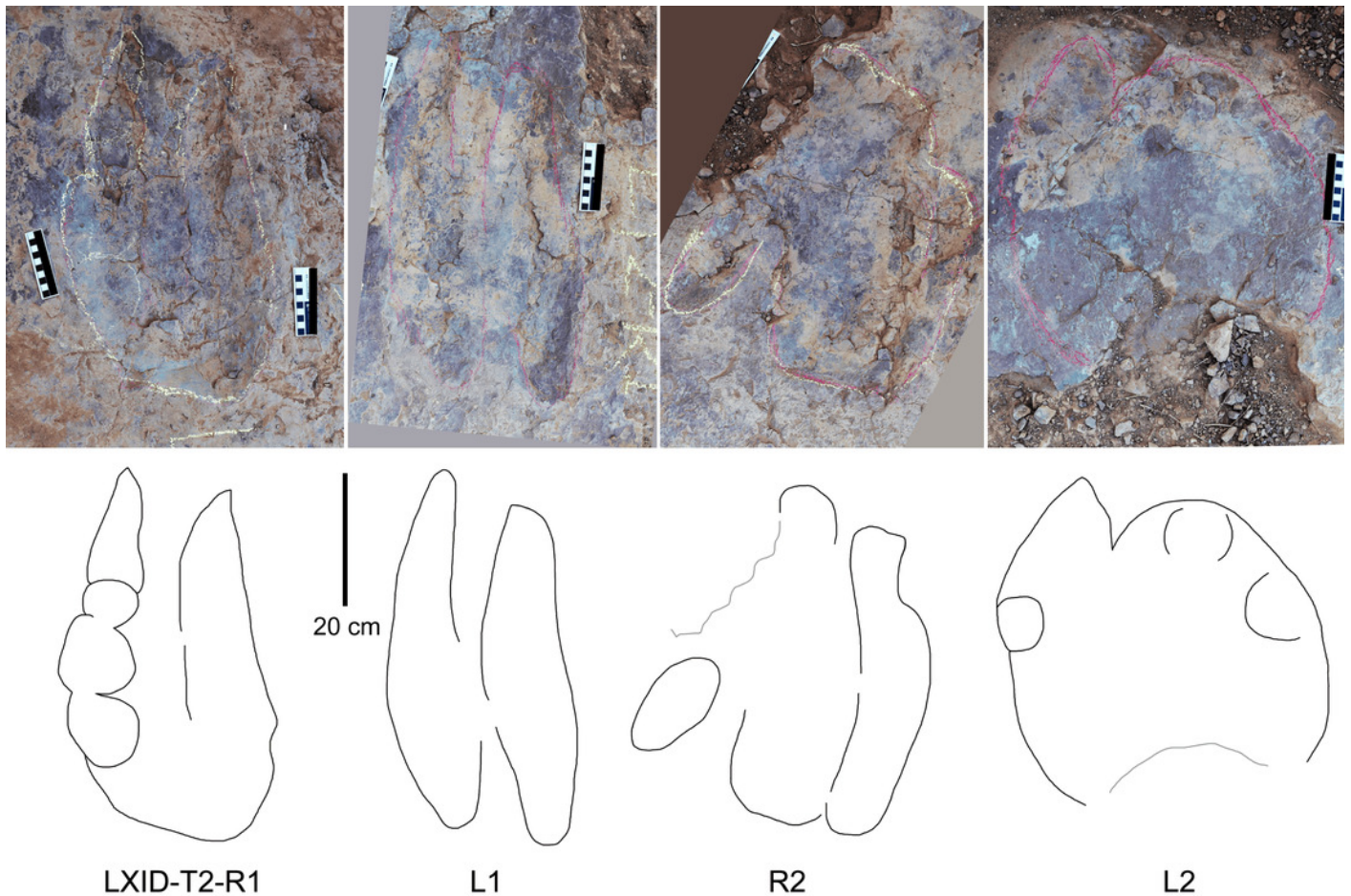
# Figure 22

Size frequency of tridactyl trackways from LXIs sites. Only the average length is
considered.

A, Considering track length, only the ornithopod trackways exhibit relatively lower axial
deformation are included; B, Considering track width, both theropod and ornithopod
trackways are included.
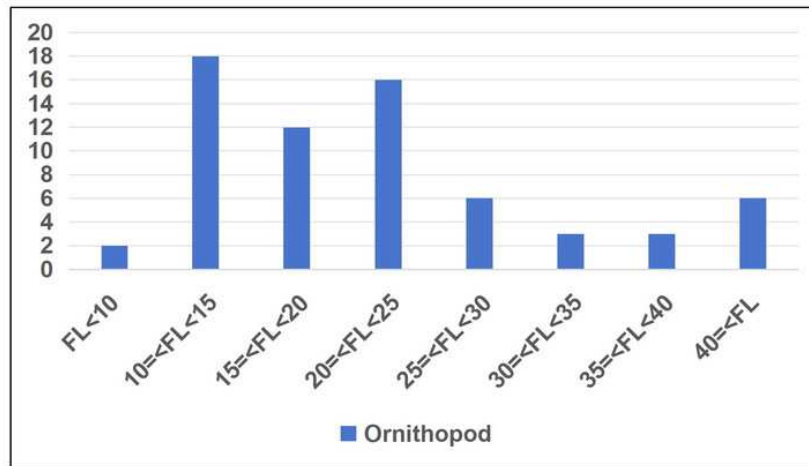
(A)
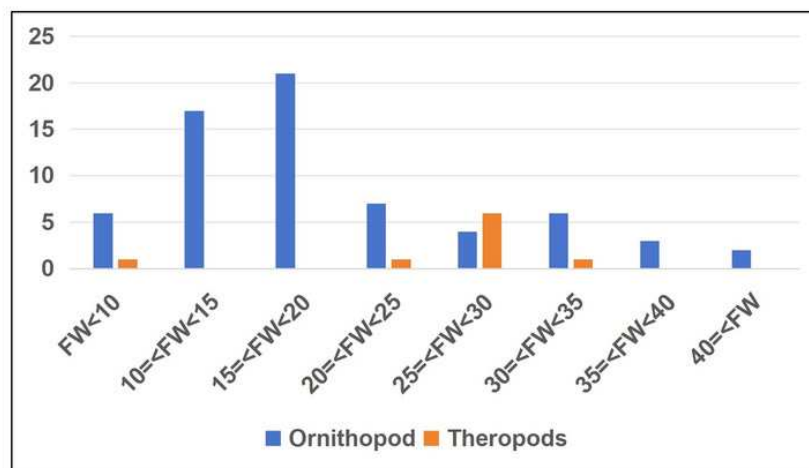


(B)

# Table 1(on next page)

The ichnofanua composition of the LXI tracksites.

The frequency of each trackmaker type is represented by the number of trackways, and it should be noted that the sole isolated track from the *Grallator* morphotype is the only trackway counted as such due to its uniqueness. The interval of large ornithopod includes all the trackways with a mean track length of ≥ 25 cm.

1  **Table 1.** The ichnofanua composition of the LXI tracksites. The frequency of each trackmaker
2  type is represented by the number of trackways, and it should be noted that the sole isolated track
3  from the *Grallator* morphotype is the only trackway counted as such due to its uniqueness. The
4  interval of large ornithopod includes all the trackways with a mean track length of ≥25 cm.
5

| | Frequency | Probability | large/total, ornithopod |
|---|---|---|---|
| Total (LXIs included) | | | |
| Total | 79 | | |
| Ornithopods | 66 | 0.84 | 0.27 |
| Sauropods | 2 | 0.03 | |
| Theropods | 11 | 0.14 | |
| LXIN | | | |
| Total | 54 | | |
| Ornithopods | 48 | 0.89 | 0.19 |
| Sauropods | 1 | 0.02 | |
| Theropods | 5 | 0.09 | |
| LXID | | | |
| Total | 7 | | |
| Ornithopods | 4 | 0.57 | 0.25 |
| Sauropods | 0 | 0 | |
| Theropods | 3 | 0.43 | |
| LXIU | | | |
| Total | 17 | | |
| Ornithopods | 13 | 0.76 | 0.62 |
| Sauropods | 1 | 0.06 | |
| Theropods | 3 | 0.18 | |
| LXIE | | | |
| Total | 1 | | |
| Ornithopods | 1 | 1 | 0 |
| Sauropods | 0 | 0 | |
| Theropods | 0 | 0 | |

6
7

**Table 2**(on next page)

Measurement s (in cm and degrees) comparison of *Brontopodus* morphotype trackway s from Cretaceous Longxiang site I , Fujian , southwestern China .

1 **Table 2.** Measurements (in cm and degrees) comparison of *Brontopodus* morphotype trackways

2 from Cretaceous Longxiang site I, Fujian, southwestern China.

3

| | L | W | R | L/W | PL | SL | PA | A | H | WAP | WAP/P'ML | TL* |
|---|---|---|---|---|---|---|---|---|---|---|---|---|
| LXIU-S1p | 40.78 | 33.22 | \|26\| | 1.25 | 91.24 | 161.99 | 127 | 1079.72 | 4.40 | 39.88 | 1.04 | 55.37 |
| LXIU-S1m | 16.62 | 25.91 | \|27\| | 0.70 | 99.81 | 162.58 | 111 | 358.88 | — | 56.59 | | |
| LXIN-S1p | 65.30 | 51.22 | 43 | 1.29 | 114.31 | 187.58 | 108 | 2578.26 | 1.82 | 67.58 | 0.97 | 81.20 |
| LXIN-S1m | 36.63 | 48.82 | 61 | 0.75 | 120.51 | 172.63 | 92 | 1452.94 | — | 81.56 | — | 59.74 |

4

5 **Abbreviations:** L, Track Length; W, Track width; R, Rotation angle; L/W, Length/width ratio; PL, Pace

6 length; SL, Stride length; PA, Pace angulation; A, Area of the track; H, Heteropody; WAP, width of angulation

7 pattern (=Gauge width); WAP/P'ML, the ratio of WAP and P'ML; TL*, Total length of pes and manus; —, no

8 measurement available.

9 *All data are averaged within precise trackway, and *Sxp* and *Sxm* are the mean values of pes and manus

10 respectively within the same trackway.

11

**Table 3**(on next page)

The comparison of the track depth of the worldwide sauropod ichnogenera .

1 **Table 3.** The comparison of the track depth of the worldwide sauropod ichnogenera.

2

| Region | | Age | | Ichnotaxa | PL (cm) | PW (cm) | ML (cm) | MW (cm) | PD (cm) | MD (cm) | H | Manus /Pes set | ref |
|---|---|---|---|---|---|---|---|---|---|---|---|---|---|
| North America | Texas, USA | K1 | Albian | *Brontopodus birdi* | 86.50 | ? | ? | 43.70 | ? | ? | >3 | loose | Farlow (1989) |
| | Corolado, USA | J3 | Kimmeridgian | *Parabrontopodus mcintochi* | 78.00 | 56.00 | 38.00 | 24.00 | ? | ? | (pronounced) | packed | Lockley et al. (1994) |
| East Asia | South Korea | K1 —2 | Albian — Cenomanian | *Gyeongsangsaurop us* ("Brontopodus") | 50.39 | 44.33 | 32.46 | 41.36 | (particularly shallow) | ? | ~2 | very loose | Kim and Lockley (2012) |
| | | | | *Brontopodus* (*cf. Gyeongsangsaurop us*) | 39.54 | 36.43 | 25.18 | ~34.79 | (particularly shallow) | ? | ~2 | very loose | Kim and Lockley (2012) |
| | Yunnan, China | K2 | Turonian – Coniacian | *Brontopodus changlingensis* | 38.30 | 32.00 | 14.67 | 26.67 | ? | ? | 2.5 | packed | Lockley et al. (2002) |
| | Shandong, China | K1 —2 | Albian — Cenomanian | *Parvieouspodus* holotype | 27.10 | 25.20 | 13.70 | 19.10 | 8~10# | 8~10# | ~3.5 | very loose | Xing et al. (2013) |
| | | | | *Parvieouspodus* paratype | 27.00 | 20.70 | 8.50 | 13.90 | ~4 | ~4 | ~3.5 | very loose | Xing et al. (2013) |
| Europe | Switzerland | J3 | Kimmeridgian | *Brontopodus* | 30.00 | 23.90 | 9.60 | 19.10 | 4.3 | 3.3 | 1.8 | packed | Marty et al. (2010) |
| | | | | *Parabrontopodus* | 46.90 | 41.00 | 12.30 | 23.30 | 3.3 | 2.6 | 2.4 | packed | Marty et al. (2010) |
| | Germany | J3 | Kimmeridgian | *Parabrontopodus* ("Elephantopoides") | 35.5 | 25.00 | 12.00 | 24.00 | ~8?# | ~8?# | 3.2 | packed | Meyer et al. (2021a) |
| | | K1 | Berriasian | "Rotundichnus" | ? | ~60 | ? | ~40 | ? | ? | ? | packed | Hendricks (1981); Lockley et al. (2004) |

| | Country | | Stage | Ichnotaxon | | | | | | | | | Reference |
|---|---|---|---|---|---|---|---|---|---|---|---|---|---|
| | France | J2 | Bathonian | *Occitanopodus* | 85.00 | 102.00 | 34.00 | 62.00 | ? | ? | 4~6 | packed | Moreau et al. (2019) |
| | | | | Sauropoda indet. | 77.00 | 103.00 | 27.00 | 65.00 | ? | ? | 3~4 | packed | Moreau et al. (2019) |
| | | | | Sauropoda indet. | 122.00 | 100.00 | — | — | ? | ? | — | — | Moreau et al. (2019) |
| | | J3 | Tithonian | *Brontopodus plagnensis* | 97.80 | 74.90 | 48.40 | 71.00 | ~10 | ~10 | 1.9 | loose | Mazin et al. (2017) |
| | Portugal | J2 | Bajocian – Bathonian | *Galinhapodus* ("Polyonyx") | 90.00 | 60.00 | 38.00 | 58.00 | ~6? | ~6? | 2.0 | loose | Santos et al. (2009); Santos et al. (2024) |
| | Spain | J3 — K1 | Tithonian – Berriasian | *Iniestapodus* ("Polyonyx" assosiated) | 63.00 | 43.00 | 28.00 | 31.00 | >11? | ~5? | 2.5 | loose | Torcida Fernández—Baldor et al. (2021) |
| | | | | *Iniestapodus* ("Polyonyx" assosiated) | 60.00 | 43.00 | 29.00 | 40.00 | ~8? | >7? | 2.5 | loose | Torcida Fernández—Baldor et al. (2021) |
| | | | | *Iniestapodus* ("Polyonyx" assosiated) | 55.00 | 41.00 | 23.00 | 39.00 | ~10# | ~10# | 2.7 | loose | Torcida Fernández—Baldor et al. (2021) |
| Africa | Morroco | J3 | Oxfordian — Kimmeridgian | *Breviparopus* | 110.70 | 99.00 | 29.70 | 55.40 | 13.0 | 4.9 | 2.4 | packed | Marty et al. (2010) |
| | | J3 | Tithonian | *Parabrontopodus frenki* | 62.00 | 35.00 | — | — | ? | ? | — | — | Moreno and Benton (2005) |
| South America | Neuquen, Argentina | K2 | Cenomanian | *Brontopodus* ("Sauropodichnus") | 70.00 | 60.00 | 25.00 | 40.00 | ? | ? | ? | very loose | Calvo and Mazzetta (2004) |
| | Mendoza, Argentina | K2 | Campanian | *Teratopodus* | 41.00 | 37.00 | 20.00 | 26.10 | ~5? | ~5? | 2.3 | loose | Tomaselli et al. (2021) |
| | Mendoza, Argentina | K2 | Campanian | *Titanopodus* | 46.00 | 42.40 | 19.60 | 32.20 | ? | ? | 3.1 | very loose | Gonzalez Riga and Calvo (2009) |
| | Croatia | K1 | Albian | *Titanosaurimanus* | ? | ? | 20/24. | 19/21? | ? | ? | — | — | Dalla Vecchia (2000) |

| | | | | | PL | PW | PD | ML | MW | MD | H | | |
|---|---|---|---|---|---|---|---|---|---|---|---|---|---|
| | | | | holotype | | | 5? | | | | | | |
| | | | | *Titanosaurimanus* | 21.5/27? | 21.0/27? | ? | ? | ? | ? | ? | loose? | Dalla Vecchia (2000) |
| | | | | *Titanosaurimanus* | 29/30.0 | 26.5/27.5 | ? | ? | ? | ? | — | — | Dalla Vecchia (2000) |
| | Bolivia | K2 | Maastrichtian | *Calorckosauripus* | [49] | [42] | [34] | [29] | 5.7#? | 8.8#? | [1.85] | loose | Meyer et al. (2018); Meyer et al. (2021b) |
| Oceania | Western Australia | K1 | Valanginian–Barremian | *Oobardjidama* | 75.30 | 61.00 | 41.00 | 48.00 | ~10# | ~10# | 2.9 | very loose | Salisbury et al. (2016) |

3

4 **Abbreviations:** PL, pes length; PW, pes width; PD, pes depth; ML, manus length ;MW, manus width ; MD, manus depth; H,
5 Heteropody (=the ratio of the manus/pes track area);?, no recorded data (measurable); —, no measurement available.

6

7 * measurements without displacement rims.
8 # maximum depth.
9 ? estimated from partial specimens of the trackway.
10 [] the average data of the morphotype from the presice site.

**Table 4**(on next page)

Measurement s (in cm and degrees) comparison of t heropod morphotype A and B trackways from Longxiang sites .

1 **Table 4.** Measurements (in cm and degrees) comparison of theropod morphotype A and B

2 trackways from Longxiang sites.

3

| | L | W | L/W | II-III | III-IV | II-IV | PL | SL | PA | R | WAP |
|---|---|---|---|---|---|---|---|---|---|---|---|
| **Theropod morphotype A** | | | | | | | | | | | |
| LXIN-T1 | 31.48 | 27.03 | 1.19 | 40 | 31 | 70 | 103.43 | 206.70 | 176 | 27 | 0.46 |
| LXIN-T5 | 30.71 | 24.82 | 1.23 | 37 | 29 | 66 | 108.37 | 216.70 | 177 | 27 | 0.44 |
| LXIN-T3 | 29.95 | 22.60 | 1.27 | 34 | 28 | 62 | 113.30 | 226.70 | 177 | |6| | 0.41 |
| | | | | | | | | | | | |
| LXIN-T2 | 23.67 | 28.27 | 0.85 | 42 | 49 | 91 | 128.53 | 247.85 | 166 | |15| | 0.35 |
| LXIN-T4 | 24.30 | 28.66 | 0.85 | 43 | 42 | 85 | 104.08 | 207.39 | 152 | |11| | 0.37 |
| LXID-T3 | 23.55 | 27.20 | 0.86 | 37 | 44 | 80 | 96.49 | 192.43 | 171 | 36 | 0.26 |
| | | | | | | | | | | | |
| LXIU-T2 | 14.73 | 29.35 | 0.50 | 62 | 45 | 107 | 99.07 | 179.79 | 133 | |9| | 0.30 |
| LXID-T1 | 14.01 | 30.68 | 0.46 | 63 | 46 | 109 | 144.69 | 279.63 | 156 | |28| | 0.29 |
| | | | | | | | | | | | |
| **Theropod morphotype B** | | | | | | | | | | | |
| LXIU-T2 | 14.73 | 29.35 | 0.50 | 62 | 45 | 107 | 99.07 | 179.79 | 133 | |9| | 0.30 |
| LXID-T1 | 14.01 | 30.68 | 0.46 | 63 | 46 | 109 | 144.69 | 279.63 | 156 | |28| | 0.29 |

4

5 **Abbreviations:** L, Track Length; W, Track width; L/W, Length/width ratio; II-III, III-IV and II-IV, the

6 divarication angle between digit II-III, III-IV and II-IV; PL, Pace length; SL, Stride length; PA, Pace

7 angulation; R, Rotation angle; M, Mesaxony (=AT, anterior triangle length/width ratio); —, no measurement

8 available.

9 *All data are averaged within precise trackway.

10

**Table 5**(on next page)

Measurement s (in cm and degrees) comparison of the isolated theropod tracks from Longxiang sites .

1    **Table 5.** Measurements (in cm and degrees) comparison of the isolated theropod tracks from

2    Longxiang sites.

3

|  | L | W | L/W | II-III | III-IV | II-IV | M |
|---|---|---|---|---|---|---|---|
| **Tridactyl** | | | | | | | |
| LXIU-TI7 | 12.9 | 7.2 | 1.8 | 31 | 35 | 66 | 0.99 |
| LXIN-TI1 | 37.9 | 36.9 | 1.0 | 29 | 37 | 66 | 0.27 |
| LXIN-TI2 | 26.4 | 21.7 | 1.2 | 34 | 33 | 67 | 0.45 |
| LXIN-TI3 | 36.8 | 23.0 | 1.6 | 31 | 25 | 56 | 0.67 |
| LXIN-TI4 | 33.4 | 18.1 | 1.8 | — | 21 | — | 0.68 |
| LXIN-TI5 | 30.5 | 36.6 | 0.8 | 61 | 53 | 114 | 0.50 |
| LXIN-TI6 | 19.7 | 19.9 | 1.0 | 32 | 49 | 80 | 0.36 |
| LXIN-TI11 | 27.3 | 25.3 | 1.1 | 43 | 34 | 77 | 0.45 |
| LXIN-TI12 | 31.4 | 28.3 | 1.1 | 41 | 33 | 75 | 0.49 |
| LXIN-TI13 | 36.6 | 36.7 | 1.0 | 36 | 37 | 73 | 0.32 |
| LXIN-TI14 | 25.2 | 31.4 | 0.8 | 47 | 39 | 86 | 0.28 |
| LXIN-TI15 | 24.1 | 28.4 | 0.8 | 48 | 27 | 74 | 0.40 |
| LXIN-TI16 | 26.1 | 23.5 | 1.1 | 34 | 35 | 69 | 0.40 |
| LXIII-TI1 | 28.9 | 28.3 | 1.0 | 50 | 24 | 74 | 0.31 |
| LXIII-TI2 | >17.5 | 25.1 | — | 33 | 46 | 79 | 0.32 |
| LXIII-TI3 | 21.1 | 17.6 | 1.2 | 32 | 31 | 62 | 0.50 |
| LXIII-TI4 | 15.8 | 14.0 | 1.1 | 37 | 39 | 76 | 0.53 |
| **Didactyl** | | | | | | | |
| LXIN-TI10 | — | 30.0 | — | 47 | 88 | 135 | 0.48 |

4

5    **Abbreviations:** L, Track Length; W, Track width; L/W, Length/width ratio; II-III, III-IV and II-IV, the

6    divarication angle between digit II-III, III-IV and II-IV; M, Mesaxony (=AT, anterior triangle length/width

7    ratio); —, no measurement available.

8

**Table 6**(on next page)

Measurement s (in cm and degrees) comparison of *Caririchnium* trackways from multiple area of Longxiang site I .

1 **Table 6.** Measurements (in cm and degrees) comparison of *Caririchnium* trackways from
2 multiple area of Longxiang site I.

3

| | L | W | W' | L/W | L/W' | II-IV | II-III | III-IV | PL | SL | PA | R | M |
|---|---|---|---|---|---|---|---|---|---|---|---|---|---|
| **LXID** | | | | | | | | | | | | | |
| LXID-O1 | 33.11 | 24.18 | 28.35 | 1.33 | 1.20 | 49 | 24 | 25 | 91.47 | 186.08 | 161 | \|7\| | 0.32 |
| LXID-O2p | 22.80 | 17.19 | 20.27 | 1.40 | 1.10 | 49 | 28 | 21 | 60.37 | 120.41 | 154 | \|10\| | 0.27 |
| LXID-O2m | 6.78 | 4.97 | — | 1.37 | — | — | — | — | — | — | — | — | — |
| LXID-O3 | 20.77 | 16.62 | 16.17 | 1.29 | 1.26 | 61 | 38 | 24 | 54.11 | 101.40 | 144 | \|11\| | 0.49 |
| LXID-O4 | 21.86 | 17.17 | 19.82 | 1.34 | 1.09 | 46 | 22 | 21 | 64.79 | 122.65 | 146 | \|12\| | 0.28 |
| **LXIU** | | | | | | | | | | | | | |
| LXIU-O1 | 27.50 | 20.65 | 31.81 | 1.24 | 0.90 | 59 | 30 | 29 | 87.00 | — | — | — | 0.33 |
| LXIU-O2p | 31.10 | 26.05 | 34.89 | 1.20 | 0.89 | 59 | 31 | 28 | 141.00 | — | — | — | 0.24 |
| LXIU-O2-L1m | 14.04 | — | 5.96 | — | 2.36 | — | — | — | — | — | — | — | — |
| LXIU-O3 | 9.98 | 7.60 | 9.15 | 1.24 | 1.10 | 55 | 23 | 32 | 36.39 | 71.16 | 153 | 6 | 0.25 |
| LXIU-O4p | 27.21 | 21.11 | 30.99 | 1.29 | 0.89 | 51 | 26 | 25 | 121.83 | 227.33 | 141 | \|8\| | 0.14 |
| LXIU-O4-R3m | 12.69 | — | 8.66 | — | 1.47 | — | — | — | — | — | — | — | — |
| LXIU-O5 | 26.99 | 25.33 | 33.73 | 1.07 | 0.80 | 63 | 34 | 28 | 97.89 | 192.47 | 160 | \|5\| | 0.21 |
| LXIU-O6 | 11.10 | 8.86 | 10.71 | 1.39 | 1.04 | 52 | 28 | 24 | 40.98 | 79.77 | 154 | — | 0.34 |
| LXIU-O7 | 18.27 | 15.12 | 17.57 | 1.21 | 1.05 | 55 | 24 | 32 | 52.26 | 102.33 | 161 | \|12\| | 0.24 |
| LXIU-O8p | 44.54 | — | 33.30 | — | 1.38 | — | — | — | 112.01 | 221.23 | 160 | \|3\| | — |
| LXIU-O8-L1m | 13.00 | — | 7.88 | — | 1.65 | — | — | — | — | — | — | — | — |
| LXIU-O9 | 9.99 | 9.01 | 10.15 | 0.91 | 1.01 | — | — | — | 52.57 | 104.15 | 162 | — | — |
| LXIU-O10 | 35.86 | 25.71 | 32.09 | 1.48 | 1.13 | 46 | 23 | 23 | 93.02 | 184.88 | 155 | \|8\| | 0.28 |
| LXIU-O11 | 36.90 | 21.70 | 25.96 | 1.34 | 1.43 | 60 | 35 | 25 | 92.70 | 168.75 | 124 | 12 | 0.42 |
| LXIU-O12 | 39.50 | 27.08 | 32.80 | 1.50 | 1.21 | 45 | 25 | 20 | 100.25 | 194.60 | 152 | 29 | 0.37 |
| LXIU-O13 | 12.23 | 14.03 | 14.39 | 0.87 | 0.82 | 97 | 60 | 37 | 36.46 | 60.79 | 129 | \|14\| | 0.18 |
| **LXIE** | | | | | | | | | | | | | |
| LXIE-O1 | 21.46 | 13.45 | 17.01 | 1.46 | 1.26 | 20 | 21 | 46 | 50.68 | — | PA | — | 0.26 |

4

5 **Abbreviations:** L, Track Length; W, Track width; W', track width with the inclusion of deformation rim; L/W
6 and L/W', Length/width ratio with different width measurements; II-III, III-IV and II-IV, the divarication
7 angle between digit II-III, III-IV and II-IV; PL, Pace length; SL, Stride length; PA, Pace angulation; R,
8 Rotation angle; M, Mesaxony (=AT, anterior triangle length/width ratio); —, no measurement available.
9 *All data are averaged within precise trackway, and O*xp* and O*xm* are the mean values of pes and manus
10 respectively within the same trackway. In trackway LXIU-O2, 4 and 8, only one manus track can be identified
11 in the trackway.
12
13

**Table 7**(on next page)

Speed estimation (m and km/h) of *Caririchnium* trackways from Longxiang site I .

1 **Table 7.** Speed estimation (m and km/h) of *Caririchnium* trackways from Longxiang site I.

2

| Small ornithopods (L≤ 0.25 cm) | | | | | | | | Large ornithopods (L > 0.25 cm) | | | |
|---|---|---|---|---|---|---|---|---|---|---|---|
| Trackway | L | SL/h | speed | Trackway | L | SL/h | speed | Trackway | L | SL/h | speed |
| LXID-O2 | 0.228 | 1.10 | 3.46 | LXIN-O25 | 0.202 | 1.09 | 3.20 | LXID-O1 | 0.331 | 0.95 | 3.64 |
| LXID-O3 | 0.208 | 1.02 | 2.88 | LXIN-O26 | 0.145 | 1.45 | 4.36 | LXIU-O4 | 0.260 | 1.48 | 6.73 |
| LXID-O4 | 0.219 | 1.15 | 3.64 | LXIN-O27 | 0.129 | 1.07 | 2.48 | LXIU-O5 | 0.270 | 1.21 | 4.90 |
| LXIU-O3 | 0.100 | 1.48 | 3.74 | LXIN-O28 | 0.186 | 1.25 | 3.85 | LXIU-O8 | 0.456 | 0.82 | 3.35 |
| LXIU-O6 | 0.111 | 1.50 | 4.03 | LXIN-O29 | 0.090 | 1.02 | 1.91 | LXIU-O10 | 0.390 | 0.80 | 2.95 |
| LXIU-O7 | 0.183 | 1.16 | 3.42 | LXIN-O30 | 0.128 | 1.38 | 3.82 | LXIU-O11 | 0.369 | 0.78 | 2.74 |
| LXIU-O9 | 0.100 | 2.17 | 7.13 | LXIN-O31 | 0.107 | 1.51 | 4.00 | LXIU-O12 | 0.395 | 0.84 | 3.17 |
| LXIU-O13 | 0.122 | 1.04 | 2.30 | LXIN-O32 | 0.182 | 1.15 | 3.31 | LXIN-O1 | 0.463 | 0.77 | 2.99 |
| LXIN-O2 | 0.229 | 0.60 | 1.26 | LXIN-O33 | 0.122 | 1.75 | 5.51 | LXIN-O8 | 0.488 | 0.79 | 3.24 |
| LXIN-O4 | 0.205 | 1.76 | 7.16 | LXIN-O34 | 0.129 | 1.42 | 3.96 | LXIN-O9 | 0.262 | 0.82 | 2.52 |
| LXIN-O5 | 0.246 | 1.65 | 7.06 | LXIN-O35 | 0.141 | 1.18 | 3.06 | LXIN-O13 | 0.421 | 0.82 | 3.20 |
| LXIN-O6 | 0.244 | 2.09 | 10.44 | LXIN-O36 | 0.193 | 0.95 | 2.48 | LXIN-O14 | 0.462 | 0.67 | 2.41 |
| LXIN-O10 | 0.208 | 1.13 | 3.46 | LXIN-O37 | 0.225 | 1.23 | 4.14 | LXIN-O16 | 0.314 | 0.70 | 2.12 |
| LXIN-O11 | 0.223 | 0.97 | 2.77 | LXIN-O39 | 0.158 | 1.23 | 3.49 | LXIN-O20 | 0.256 | 0.88 | 2.81 |
| LXIN-O12 | 0.109 | 1.28 | 3.06 | LXIN-O40 | 0.175 | 1.17 | 3.35 | LXIN-O41 | 0.250 | 0.89 | 2.84 |
| LXIN-O15 | 0.149 | 1.47 | 4.54 | LXIN-O42 | 0.092 | 2.00 | 5.94 | | | | |
| LXIN-O17 | 0.153 | 1.50 | 4.79 | LXIN-O43 | 0.192 | 0.89 | 2.23 | | | | |
| LXIN-O18 | 0.220 | 1.04 | 3.10 | LXIN-O44 | 0.167 | 1.30 | 3.89 | | | | |
| LXIN-O19 | 0.200 | 1.19 | 3.71 | LXIN-O45 | 0.237 | 0.94 | 2.74 | | | | |
| LXIN-O21 | 0.196 | 1.31 | 4.28 | LXIN-O46 | 0.172 | 0.86 | 2.02 | | | | |
| LXIN-O22 | 0.116 | 2.06 | 7.02 | LXIN-O47 | 0.128 | 1.24 | 3.13 | | | | |
| LXIN-O23 | 0.101 | 1.40 | 3.46 | LXIN-O48 | 0.238 | 1.13 | 3.71 | | | | |
| LXIN-O24 | 0.146 | 1.38 | 4.03 | | | | | | | | |

3

4 **Abbreviations:** L, Track Length (in m); SL/h, The ratio of stride length/estimated hip height.

5 *All data are averaged within precise trackway.

6

7

**Table 8**(on next page)

Measurement s (in cm and degrees) comparison of p ossible large didactyl tracks from Longxiang site ID .

1　**Table 8.** Measurements (in cm and degrees) comparison of possible large didactyl tracks　from

2　Longxiang site ID.

3

| | L | L-II | L-III | L-IV | W | W-max III-IV | W-max II-IV | L/W | III-IV | PL | SL | PA | R |
|---|---|---|---|---|---|---|---|---|---|---|---|---|---|
| LXID-T2-R1 | 56.0 | — | 51.9 | 52.1 | 15.8 | 32.9 | — | 3.5 | 17 | 292.2 | 552.3 | 178 | \|3\| |
| LXID-T2-L1 | 56.3 | — | 50.8 | 53.6 | 13.5 | 28.3 | — | 4.2 | 13 | 260.1 | 532.4 | 180 | 6 |
| LXID-T2-R2 | 52.1 | 17.6 | 50.3 | 45.5 | 14.6 | 28.4 | 43.8 | 3.6 | 16 | 272.2 | — | — | — |
| LXID-T2-L2 | 49.1 | — | — | — | — | — | 48.1 | — | — | — | — | — | — |
| Mean | 53.4 | 17.6 | 51.0 | 50.4 | 14.7 | 29.9 | 45.9 | 3.8 | 15 | 274.9 | 542.3 | 179 | \|5\| |

4

5　**Abbreviations:** L, Track Length; L-II, III and IV, Length of digit II, III and IV; W, Track width between the

6　claw tip of digit III and IV; W-max III-IV and II-IV, Maximum width between digit III-IV and II-IV; L/W,

7　Length/width ratio; III-IV, the divarication angle between digit III-IV; PL, Pace length; SL, Stride length; PA,

8　Pace angulation; R, Rotation angle; —, no measurement available.

9